

Article

On the Evolution of the Hubble Constant with the SNe Ia Pantheon Sample and Baryon Acoustic Oscillations: A Feasibility Study for GRB-Cosmology in 2030

Maria Giovanna Dainotti^{1,2,3,*}, Biagio De Simone^{4,5}, Tiziano Schiavone^{6,7}, Giovanni Montani^{8,9}, Enrico Rinaldi^{10,11,12}, Gaetano Lambiase^{4,5}, Malgorzata Bogdan^{13,14} and Sahil Ugale¹⁵

- ¹ National Astronomical Observatory of Japan, 2 Chome-21-1 Osawa, Mitaka, Tokyo 181-8588, Japan
- ² The Graduate University for Advanced Studies, SOKENDAI, School of Physical Sciences, Shonankokusaimura, Hayama 240-0193, Japan
- ³ Space Science Institute, Boulder, CO 80301, USA
- ⁴ Department of Physics “E.R. Caianiello”, University of Salerno, Via Giovanni Paolo II, 132, Fisciano, I-84084 Salerno, Italy; bdesimone@unisa.it (B.D.S.); glambiase@unisa.it (G.L.)
- ⁵ INFN Gruppo Collegato di Salerno—Sezione di Napoli—c/o Dipartimento di Fisica “E.R. Caianiello”, Ed. F, Università di Salerno—Via Giovanni Paolo II, 132, Fisciano, I-84084 Salerno, Italy
- ⁶ Department of Physics “E. Fermi”, University of Pisa, Polo Fibonacci, Largo B. Pontecorvo 3, I-56127 Pisa, Italy; tiziano.schiavone@phd.unipi.it
- ⁷ INFN, Istituto Nazionale di Fisica Nucleare, Sezione di Pisa, Polo Fibonacci, Largo B. Pontecorvo 3, I-56127 Pisa, Italy
- ⁸ ENEA, Fusion and Nuclear Safety Department, C.R. Frascati, Via E. Fermi 45, Frascati, I-00044 Rome, Italy; giovanni.montani@enea.it
- ⁹ Physics Department, “Sapienza” University of Rome, P.le Aldo Moro 5, I-00185 Rome, Italy
- ¹⁰ Physics Department, University of Michigan, Ann Arbor, MI 48109, USA; erinaldi.work@gmail.com
- ¹¹ Theoretical Quantum Physics Laboratory, Center for Pioneering Research, RIKEN, 2-1 Hirosawa, Wako, Saitama 351-0198, Japan
- ¹² Interdisciplinary Theoretical & Mathematical Science Program, RIKEN (iTHEMS), 2-1 Hirosawa, Wako, Saitama 351-0198, Japan
- ¹³ Department of Mathematics, University of Wroclaw, plac Uniwersytecki 1, 50-137 Wroclaw, Poland; malgorzata.bogdan@uwr.edu.pl
- ¹⁴ Department of Statistics, Lund University, Box 117, SE-221 00 Lund, Sweden
- ¹⁵ Department of Physics, Mithibai College, Mumbai 400056, India; sahil.ugale@svkmmumbai.onmicrosoft.com
- * Correspondence: maria.dainotti@nao.ac.jp



Citation: Dainotti, M.G.; De Simone, B.; Schiavone, T.; Montani, G.; Rinaldi, E.; Lambiase, G.; Bogdan, M.; Ugale, S. On the Evolution of the Hubble Constant with the SNe Ia Pantheon Sample and Baryon Acoustic Oscillations: A Feasibility Study for GRB-Cosmology in 2030. *Galaxies* **2022**, *10*, 24. <https://doi.org/10.3390/galaxies10010024>

Academic Editor: Elena Moretti and Francesco Longo

Received: 5 November 2021

Accepted: 25 January 2022

Published: 29 January 2022

Publisher’s Note: MDPI stays neutral with regard to jurisdictional claims in published maps and institutional affiliations.



Copyright: © 2022 by the authors. Licensee MDPI, Basel, Switzerland. This article is an open access article distributed under the terms and conditions of the Creative Commons Attribution (CC BY) license (<https://creativecommons.org/licenses/by/4.0/>).

Abstract: The difference from 4 to 6 σ in the Hubble constant (H_0) between the values observed with the local (Cepheids and Supernovae Ia, SNe Ia) and the high- z probes (Cosmic Microwave Background obtained by the Planck data) still challenges the astrophysics and cosmology community. Previous analysis has shown that there is an evolution in the Hubble constant that scales as $f(z) = \mathcal{H}_0 / (1+z)^\eta$, where \mathcal{H}_0 is $H_0(z=0)$ and η is the evolutionary parameter. Here, we investigate if this evolution still holds by using the SNe Ia gathered in the Pantheon sample and the Baryon Acoustic Oscillations. We assume $H_0 = 70 \text{ km s}^{-1} \text{ Mpc}^{-1}$ as the local value and divide the Pantheon into three bins ordered in increasing values of redshift. Similar to our previous analysis but varying two cosmological parameters contemporaneously (H_0, Ω_{0m} in the Λ CDM model and H_0, w_a in the w_0w_a CDM model), for each bin we implement a Markov-Chain Monte Carlo analysis (MCMC) obtaining the value of H_0 assuming Gaussian priors to restrict the parameters spaces to values we expect from our prior knowledge of the current cosmological models and to avoid phantom Dark Energy models with $w < -1$. Subsequently, the values of H_0 are fitted with the model $f(z)$. Our results show that a decreasing trend with $\eta \sim 10^{-2}$ is still visible in this sample. The η coefficient reaches zero in 2.0 σ for the Λ CDM model up to 5.8 σ for w_0w_a CDM model. This trend, if not due to statistical fluctuations, could be explained through a hidden astrophysical bias, such as the effect of stretch evolution, or it requires new theoretical models, a possible proposition is

arXiv:2201.09848v3 [astro-ph.CO] 29 Jan 2022

the modified gravity theories, $f(R)$. This analysis is meant to further cast light on the evolution of H_0 and it does not specifically focus on constraining the other parameters. This work is also a preparatory to understand how the combined probes still show an evolution of the H_0 by redshift and what is the current status of simulations on GRB cosmology to obtain the uncertainties on the Ω_{0m} comparable with the ones achieved through SNe Ia.

Keywords: supernovae; Ia; cosmology; Hubble; tension; Λ CDM; evolution; modified; gravity; theories

1. Introduction

The Λ CDM model is one of the most accredited models, which implies an accelerated expansion phase [1,2]. Although it represents the favored paradigm, it is affected by great challenges: the fine-tuning, the coincidence [3,4], and the Dark Energy nature's problems.

More importantly, the H_0 tension represents a big challenge for modern cosmology. Indeed, the 4.4 up to 6.2 σ discrepancy, depending on the sample used [5–7], between the local value of H_0 obtained with Cepheids observations and SNe Ia, $H_0 = 74.03 \pm 1.42 \text{ km s}^{-1} \text{ Mpc}^{-1}$ [8,9], and the Planck data of Cosmic Microwave background radiation (CMB), $H_0 = 67.4 \pm 0.5 \text{ km s}^{-1} \text{ Mpc}^{-1}$ from the Planck Collaboration [10] requires further investigation. From now on, H_0 will be in the units $\text{km s}^{-1} \text{ Mpc}^{-1}$.

We stress that other probes report values of $H_0 \approx 72 \pm 2$, similar to the value obtained with the SNe Ia. Surely, to solve the Hubble tension it is necessary to use probes that are standard candles. SNe Ia, considered one of the best standard candles, are observed only up to a low redshift range: the farthest so far discovered is at $z = 2.26$ [11].

It is important for studying the evolution of the cosmological parameters to investigate probes at high redshift. One of the best candidates in this regard is represented by the Gamma-ray Bursts (GRBs).

GRBs are observed up to cosmological redshifts (the actual record is of $z = 9.4$ [12]) and surpassed even the quasars (the most distant being at $z = 7.64$ [13]). Due to their detectability at high redshift, GRBs allow extending the current Hubble diagram to new redshift ranges [14–18].

Indeed, it is important to stress that once we have established if the Hubble constant undergoes redshift evolution, the Pantheon sample can safely be combined with other probes. Surely the advantage of the use of the SNe Ia is that their emission mechanism is pretty clear, namely they originate from the thermonuclear explosion of carbon–oxygen white dwarfs (C/O WDs).

For GRBs, more investigation about their progenitor mechanism is needed. We here stress that this work can be also preparatory to the work of future application of GRBs as cosmological tools together with SNe Ia and Baryon Acoustic Oscillations (BAOs) through well-established correlations among the prompt variables, such as: the Amati relation [19], which connects the peak in the νF_ν spectrum to the isotropic energy in the prompt emission (E_{iso}), the Yonetoku relation [20,21] between E_{peak} and the peak luminosity of the prompt emission, L_{peak} , the Liang and Zhang relation [22] between E_{iso} , the rest-frame break time of the GRB t'_b and the peak energy spectrum in the rest frame E'_p , the Ghirlanda relation ($E_{peak} - E_{jet} = E_{iso} \times (1 - \cos\theta)$) [23], and the prompt-afterglow relations for the GRBs with the plateau emission investigated in [24–38], which have as common emission mechanism most likely the magnetar model, where a neutron star with an intense magnetic field undergoes a fast-spinning down [39–43].

A feasibility study shows that GRBs can give relevant constraints on the cosmological parameters [17,44]. We here give a list of examples of other probes used for measuring the Hubble constant tension. One of them is the use of data from time-delay measurements and

strong lens systems [45,46]. On the contrary, additional probes carry similar values of H_0 to the ones of Planck, based on the Cosmic Chronometers (CC) ($H_0 = 67.06 \pm 1.68$) in [8]. Besides, there is a series of independent probes, such as quasars [47], the Tip of the Red-Giant Branch (TRGB) calibration through SNe Ia [48], and also GRBs [14,15,17,18,49,50], which bring estimates of H_0 ranging between the values obtained with local measurements (SNe Ia and Cepheids) and Baryon Acoustic Oscillations (BAO)+CMB. [51] discuss possible reasons behind the H_0 tension in the Pantheon sample: selection biases of parameters of the SNe Ia, unknown systematics, internal inconsistencies in the Planck data, or alternative theoretical interpretations compared to the standard cosmological model. Furthermore, the use of type 1 Active Galactic Nuclei (AGN) represents another promising cosmological probe given the peculiarity of their spectral emission [52].

To date, a wide range of different solutions to the Hubble constant tension has been provided by several groups [53–86]. Concerning the observational solutions, we here detail a series of proposals [87–130]. In [131], the simulations of data taken from the anomalously fast-colliding El Gordo galaxy clusters allow discussing the probability of observing such a scenario in a Λ CDM framework. Ref. [132] perform a re-calibration of Cepheids in NGC 5584, thus obtaining a relation between the periods of Cepheids and their amplitude ratios (tighter than the one obtained in SH0ES [9]) which could be useful to better estimate the value of H_0 . In [133], the UV and X-ray data coming from quasars are used to constrain H_0 in the Finslerian cosmology. Ref. [123] demonstrate that the Planetary Nebula Luminosity Function (PNLF) can be extended beyond the Cepheid distances, thus promoting it to be an additive probe for constraining H_0 . In [134], the analysis of Pan-STARRS telescope SNe Ia data provides a value of H_0 which lies between the SH0ES and Planck values.

Ref. [135] investigated how the H_0 measurements can depend on the choice of different probes (SNe, BAO, Cepheid, CC, etc.), showing also that through the set of filters on cosmological models, such as fiducial values for cosmological parameters ($w = -1$, with w parameter for the equation of state, or $\Omega_k = 0$, namely the curvature parameter set to zero), the tension can be alleviated.

Ref. [136] extended a Hubble diagram up to redshift $z \sim 8$ combining galaxies and high-redshift quasars to test the late-time cosmic expansion history, giving a constraint on the upper-value of H_0 which is only marginally consistent with the results obtained by the Cepheids.

Ref. [137] further tests the w CDM (with varying parameters of the equation of state), and o CDM models (with varying curvature) through the merging of BAOs, SNe Ia, CC, GRBs, and quasars data, after the analysis of the standard Λ CDM model.

In [138], the combination of strongly lensed quasars and SNe Ia led the authors to conclude that the solution to the tension should be found outside of the Friedmann–Lemaître–Robertson–Walker metric.

Ref. [125,139] detect in the Stochastic Gravitational Wave Background a new method to alleviate the tension, while [140,141] focuses on the gravitational-wave signals from compact star mergers as probes that can give constraints on the H_0 value.

Ref. [142] combine the SNe Ia and the VLT-KMOS HII galaxies data to put new constraints on the cosmokinetic parameters. The proposed solutions deal also with models that are alternative to the standard Λ CDM or, in other cases, that can extend it.

Ref. [143] constrain the Brans–Dicke (BD) theory through CMB and BAOs. The TRGB method, combined with SNe Ia, gives a value of H_0 compatible with the one from CMB [144].

Ref. [145] obtain an 8%-precise value of H_0 through the Fast Radio Bursts (FRB).

In [146], the Cepheids calibration parameters are allowed to vary, thus leading to an estimated value of H_0 which is compatible with the CMB one. The possibility that the Solar system's proper motion may induce a bias in the measurement of H_0 has been subject to study

in [147], finding out that there is no degeneracy between the cosmological parameters and the parameters of the Solar system motion.

Ref. [148] measure H_0 through the galaxies parallax having as reference the CMB rest-frame, being this parallax caused by the peculiar motions.

Ref. [149] verified through the measurements on GRBs and quasars that the Hubble constant has a bigger value in the sky directions aligned with the CMB dipole polarization, suggesting that a detachment from the FLRW should be considered.

Ref. [150–153] investigate how the dark sirens producing gravitational waves could help to probe H_0 . Despite being a promising method, the incompleteness of galaxy catalogs may hinder the outcome of this method, thus [154] proposes a pixelated-sky approach to overcome the issue of event redshifts which are missing but may be retrieved through the galaxies present on the line of sight.

A review of the most promising emerging probes to measure the Hubble constant can be found in [155].

Recent results on the measurements of the Hubble parameter and constant through the Third LIGO-Virgo-KAGRA Gravitational-Wave Transient Catalog (GWTC-3) can be found in [156]. An evolving trend for H_0 may be naturally predicted in Teleparallelism [157–161], as well as in modified gravity theories [162–167]. Refs. [168–170] study the $f(Q, T)$ models in Teleparallel Gravity through CC and SNe Ia, thus obtaining a value of H_0 compatible in 1σ with the SH0ES result. The linear theory of perturbation for the $f(Q, T)$ theory is investigated in [171], allowing the future tests of this model through CMB data.

In [172], the Unimodular Gravity model is constrained with Planck 2018 [10], SH0ES, SNe Ia, and H0LiCOW collaboration [7]. Furthermore, the Axi-Higgs model is tested with CMB, BAO, Weak Lensing data (WL), and SNe [173]: in another paper, it is shown how this model relaxes the Hubble tension [173]. Ref. [174] describe the modified inflationary models considering constant-roll inflation. Ref. [175] give boundaries on the Hubble constant value with the gravitino mass conjecture.

Ref. [176–180] show the role of cosmological second-order perturbations of the flat Λ CDM model in the H_0 tension. Ref. [181] discuss how Dark Energy may be generated by quantum fluctuations of an inflating field and how the Hubble tension may be reduced by the spatial correlations induced by this effect. The Dark Energy itself may be subject to evolution, as pointed out in [182]. Ref. [183] show how a modification of the Friedmann equation may naturally explain the inconsistency between the local and the cosmological measurements of the Hubble constant.

Ref. [184] explain how the search for low-frequency gravitational waves (GWs) justifies the Hubble tension's solution through the assumption of neutrino-dark sector interactions. Ref. [185] show how the $R_K^{(*)}$ anomalies (namely, the discrepancy between the theoretical ratio of the fractions $B \rightarrow K^* \mu^+ \mu^- / B \rightarrow K^* e^+ e^-$ for the dilepton invariant mass bins from the Standard Model and the observed one, see [186]) and the H_0 tension can be solved by Dirac neutrinos in a two-Higgs-doublet theory.

The introduction of models where the cosmological axio-dilation is present may lead to a solution of the Hubble tension [187].

Ref. [188–191] discuss how the Early Dark Energy models (EDE) can be used to alleviate the H_0 tension. Ref. [192] analyze how the phantom Dark Energy models can give a limited reduction of the H_0 tension, while [193] explore how the Kaniadakis holographic Dark Energy model alleviates the H_0 tension.

In [194], the Viscous Generalized Chaplygin Gas (VGCG) model is used to diminish the Hubble tension. The holographic Dark Energy models are pointed as a possible solution through the study of unparticle cosmology [195].

Ref. [196] test seven cosmological models through the constraints of SNe Ia, BAO, CMB, Planck lensing, and Cosmic Chronometers with the outcome that in the Λ CDM scenario a flat universe is favored.

Ref. [197] discuss how the new physical scenarios before the recombination epoch imply the shift of cosmological parameters and how these shifts are related to the discrepancy between the local and non-local values of H_0 .

Ref. [198] proposes that the H_0 tension may be solved if the speed of light is treated as a function of the scale factor (as in [199]), and applies this scenario to SNe Ia data.

Ref. [200,201] discuss the implementation of the alternative Phenomenologically Emergent Dark Energy model (PEDE), which can be also extended to a Generalized Emergent Dark Energy model (GEDE) with the addition of an extra free parameter. This shows the possibility of obtaining the PEDE or the Λ CDM cosmology as sub-cases of the GEDE scenario.

Ref. [202] consider a scenario of modified gravity predicting the increase of the expansion rate in the late-universe, thus proving that in this scenario the Hubble tension reduces significantly.

Ref. [203] study the Λ CDM model constrained, at the early-time universe, by the presence of the early Integrated Sachs–Wolfe (eISW) effect, proving that the early-time models aimed at attenuating the Hubble tension should be able to reproduce the same eISW effect just like the Λ CDM does. The observations of a locally higher value for H_0 led to the discussion of local measurements, constraints, and modeling. In this regards, the assumption of a local void [204–206] may produce locally an increased value for H_0 .

The Universe appears locally inhomogeneous below a scale of roughly 100 Mpc. The question some cosmologists are attempting to solve is whether local inhomogeneities have impact on cosmological measurements and the Hubble diagram. Many observables are related to photons paths, which may be directly affected by the matter distribution. Many theoretical attempts were made during the last few decades to develop the necessary average prescription to evaluate the photon propagation on the observer's past light cone based on covariant and gauge-invariant observables [207–210]. Local inhomogeneities and cosmic structure cause scattering and bias effects in the Hubble diagram, which are due to peculiar velocities, selection effects, and gravitational lensing, but also to non-linear relativistic corrections [210–212]. This question was addressed in [213] utilising the N-body simulation of cosmic structure formation through the numerical code *gevolution*. This non-perturbative approach pointed out discrepancies in the luminosity distance between a homogeneous and inhomogeneous scenario, showing, in particular, the presence of non-Gaussian effects at higher redshifts. These studies related to distance indicators will become even more significant considering the large number of the forthcoming surveys designed to the observations on the Large Scale Structure of the Universe in the next decade (for instance, the Euclid survey [214,215] and the Vera C. Rubin Observatory's LSST [216]). The effect of local structures in an inhomogeneous universe should be considered in the locally measured value of H_0 [217,218]. The local under-density interpretation was also studied in Milgromian dynamics [131,219,220], but in [221] it is shown how this interpretation does not solve the tension. Ref. [219] study the KBC local void which is in contrast with the Λ CDM, thus proposing the Milgromian dynamics as an alternative to standard cosmology. Milgromian dynamics are studied also in [222] where, through the galactic structures and clusters, it is shown how this model can be consistent at different scales and alleviate the Hubble tension.

Ref. [223] describe the late time approaches and their effect on the Hubble parameter. The bulk viscosity of the universe is also considered the link between the early and late universe values of H_0 [224].

Ref. [225] explain how the local measurements over-constrain the cosmological models and propose the graphical analysis of the impact that these constraints have on the H_0 estimation through ad hoc triangular plots.

Ref. [220,226,227] describes the effects of inhomogeneities at small scales in the baryon density. Ref. [228] find out that the late time modifications can solve the tension between the H_0 SH0ES and CMB values through a parametrization of the comoving distance.

Ref. [229] propose to alleviate the Hubble tension considering an abrupt modification of the effective gravitational constant at redshift $z \approx 0.01$.

Other proposals are focused on the existence of different approaches.

Ref. [230,231] show how H_0 evolves with redshift at local scales.

Ref. [232] discuss how the breakdown of Friedmann–Lemaître–Robertson–Walker (FLRW [233]) may be a plausible assumption to alleviate the Hubble tension. Ref. [234] investigate the binary neutron stars mergers and, with the analysis of simulated catalogs, show their potential to help to alleviate the H_0 tension.

Ref. [235] explain how Gaussian process (GP) and locally weighted scatter plot smoothing are used in conjunction with simulation and extrapolation (LOESS-Simex) methods can reproduce different sets of data with a high level of precision, thus giving new perspectives on the Hubble tension through the simulation of Cosmic Chronometers, SNe Ia, and BAOs data sets.

Ref. [236] focus on the GP and state the necessity of lower and upper bounds on the hyperparameters to obtain a reliable estimation of H_0 .

On the other hand, Ref. [237] suggested a novel approach to measure H_0 based on the distance duality relation, namely a method that connects the luminosity distance of a source to its angular diameter. In this case, data do not require a calibration phase and the relative constraints are not dependent on the underlying cosmological model.

Ref. [238] showed how the tension can be solved with a modified weak-field General Relativity theory, thus defining a local H_0 and a global H_0 value.

Ref. [239] investigated how a specific Dark Energy model in the generalized Proca theory can alleviate the tension.

In [240], the Horndeski model can describe with significantly good precision the late expansion of the universe thanks to the Hubble parameter data. The same model is considered promising for the solution of the H_0 tension in [241].

Ref. [242] described how the transition observed in Tully–Fisher data could imply an evolving gravitational strength and explain the tension.

Ref. [197] explain how the physical models of the pre-recombination era could cause the observed H_0 values discrepancy and suggest that if the local H_0 measurements are consistent then a scale-invariant Harrison–Zeldovich spectrum should be considered to solve the H_0 issue. The Dynamical Dark Energy (DDE) models are the object of study in [243,244]: in the former, the DDE is proposed as an alternative to Λ CDM, while in the latter it is shown how the Chevallier–Polarski–Linder (CPL) parametrization [245,246] is insensitive to Dark Energy at low redshift scales.

Ref. [247,248] propose Dark Radiation as a new surrogate of the Standard Model.

In [249], the scalar field cosmological model is used, together with the parametrization of the equation of state, to obtain H_0 and investigate the nature of Dark Energy. The possibility of a scalar field non minimally coupled to gravity as a probable solution to the H_0 tension is investigated in [250].

Ref. [251] highlight the advantage of the braneworld models to predict the local higher values of H_0 and, contemporaneously, respect the CMB constraints. Another approach is to solve the H_0 tension by allowing variations in the fundamental constants [252].

Ref. [253] propose a non-singular Einstein–Cartan cosmological model with a simple parametrization of spacetime torsion to alleviate the tension, while [254] propose a model where the Dark Matter is annihilated to produce Dark Radiation.

Ref. [255] introduce a hidden sector of atomic Dark Matter in a realistic model that avoids the fine-tuning problem. The observed weak effect of primordial magnetic fields can create clustering at small scales for baryons and this could explain the H_0 tension [256].

Ref. [257] test the General Relativity at galactic scales through Strong Gravitational Lensing. The Strong Lensing is a promising probe for obtaining new constraints on H_0 , thanks to the next generation DECIGO and B-DECIGO space interferometers [258].

In [259], the cosmological constant Λ is considered a dynamical quantity in the context of the running vacuum models and this assumption could tackle the H_0 tension. [260] show the singlet Majoron model to explain the acceleration of the expansion at later times and prove that this is consistent with large-scale data: this model has been subsequently discussed in other works [261]. The vacuum energy density value is affected by the Hubble tension as well and its measurement may cast more light on this topic [262].

Ref. [263] discuss the outcomes of the Oscillatory Tracker Model with an H_0 value that agrees with the CMB measurements. In [264], it is explained how the Generalized Uncertainty Principle and the Extended Uncertainty Principle can modify the Hubble parameter. [265] explore the implication of the Mirror Twin Higgs model and the need for future measurements to alleviate the tension.

The artificial neural networks can be applied to reconstruct the behavior of large scale structure cosmological parameters [266].

Another alternative is given by the gravitational transitions at low redshift which can solve the H_0 tension better than the late-time $H(z)$ smooth deformations [84,229].

Another comparison between the late-time gravitational transition models and other models which predict a smooth deformation of the Hubble parameter can be found in [267].

Ref. [268], as modifications to the Λ CDM model, consider as plausible scenarios or a Dark Matter component with negative pressure or the decay of Dark Energy into Dark Matter.

Ref. [269] does not observe the H_0 tension through the Effective Field Theory of Large Scale Structure and the Baryon Oscillation Spectroscopic Survey (BOSS) Correlation Function.

Considering the Dark Matter particles with two new charges, Ref. [270] reproduce a repulsive force which has similar effects to the Λ cosmological constant. Furthermore, the models where interaction between Dark Matter and Dark Energy is present are promising for a solution of the Hubble constant tensions, see [271].

In [272], it is shown how two independent sets of cosmological parameters, the background (geometrical) and the matter density (growth) component parameters, respectively, give consistent results and how the preference for high values of H_0 is less significant in their analysis.

Ref. [273] introduce a global parametrization based on the cosmic age which rules out the early-time and the late-time frameworks.

Ref. [274] point out, through the use of non-parametric methods, how the cosmological models may induce biases in the cosmological parameters. In the same way, the statistical analysis of galaxies' redshift value and distance estimations may be affected by biases which could, in turn, affect the estimation of H_0

Ref. [275]. This consideration holds also for the quadruply lensed quasars which are another method to measure H_0 [276].

Ref. [277] use the machine learning techniques to measure time delays in lensed SNe Ia, these being an independent method to measure H_0 .

Additionally, in [231] it is explained how an evolution of H_0 with the redshift is to be expected. If a statistical approach on the different H_0 values is used instead, together with the

assumption of an alternative cosmology, another solution to the tension could be naturally implied [278].

Ref. [279] use data to reconstruct the $f(T)$ gravity function without assuming any cosmological model: this $f(T)$ could in turn represent a solution to the H_0 tension.

Ref. [124] discuss how the addition of scalar fields with particle physics motivation to the cosmological model which predicts Dark Matter can retrieve the observed abundances of the Big Bang Nucleosynthesis.

In [280], a Dark Matter production mechanism is proposed to alleviate the H_0 tension. A general review of the perspectives and proposals concerning the H_0 tension can be found in [281] and [282,283].

SNe Ia represents a very good example of standard candles. Here we consider also the contribution of geometrical probes, the so-called *standard rulers*: while standard candles show a constant intrinsic luminosity (or obey an intrinsic relation between their luminosity and other physical parameters independent of luminosity), standard rulers are characterized by a typical scale dimension. This property allows estimating their distance according to the apparent angular size. Among the possible standard rulers, the BAOs assume great importance for cosmological purposes.

We here investigate the H_0 tension in the Pantheon sample (hereafter PS) from [284] and we add the contribution of BAOs to the cosmological computations to check if the trend of H_0 found in [36] is present also with the addition of other probes. We here point out that the current analysis is not meant to constrain Ω_{0m} or any other cosmological parameters, but it is focused to study the reliability of the trend of H_0 as a function of the redshift.

We here point out that this analysis is not meant to constrain Ω_{0m} or any other cosmological parameters, but it is focused to study the reliability of the trend of H_0 as a function of the redshift. The range of redshift in the PS goes from $z = 0.01$ to $z = 2.26$. We tackle the problem with a redshift binning approach of H_0 , the same used in [51], but here we adopt a starting value of $H_0 = 70$ instead of 73.5: if a trend with redshift exists, it should be independent on the initial value for H_0 . The systematic contributions for the PS are calibrated through a reference cosmological model, where H_0 is 70.0 [284]. In the current paper, the aforementioned systematic uncertainties are considered for the analysis. Our approach has a two-fold advantage: on the one hand, it is relatively simple and on the other hand, it avoids the re-estimation of the SNe Ia uncertainties and may be able to highlight a residual dependence on the SNe Ia parameters with redshift.

While a slow varying Einstein constant with the redshift, as it emerges in a modified $f(R)$ gravity, appears as the most natural explanation for a trend $H_0(z)$, the analysis of Section 7 seems to indicate that such effect is not necessarily related with the Dark Energy contribution of the late universe. Since the Hu–Sawicki gravity lacks of reproducing the correct profile $H_0(z)$ shows that a Dark Energy model in the late Universe may not be enough to explain the observed effect since the scalar mode dynamics can not easily conciliate the Dark Energy contribution with the decreasing trend of $H_0(z)$. Thus, it may be necessary a modified gravity scenario more general than a Dark Energy model in the late Universe.

The current paper is composed as expressed in the following: in Section 2 the Λ CDM and w_0w_a CDM models are briefly introduced together with SNe Ia properties; Section 3 describes the use of BAOs as cosmological rulers; Section 4 contains our binned analysis results, after slicing the PS in 3 redshift bins for the aforementioned models, and assuming locally $H_0 = 70$; in Section 5, we investigate, through simulated events, how the GRBs will be contributing to cosmological investigations by 2030; in Section 6 we discuss the results; in Section 7 we test the Hu–Sawicki model through a binning approach; in Section 8 we report an overview on the requirements that a suitable $f(R)$ model should have to properly describe the observed trend of H_0 and in Section 9 our conclusions are reported.

2. SNe Ia Cosmology

SNe Ia are characterized by an intrinsic luminosity that is almost uniform. Because of this, SNe Ia are considered reliable *standard candles*. We compare the theoretical distance moduli μ_{th} with the observed distance moduli μ_{obs} of SNe Ia belonging to the PS. The theoretical distance moduli are defined through the luminosity distance $d_L(z)$ which we need to define based on the cosmological model of interest. We here show the CPL parametrization which describes the w parameter as a function of redshift ($w(z) = w_0 + w_a \times z/(1+z)$) in the w_0w_a CDM model. In the usual assumptions $w_0 \sim -1$ and $w_a \sim 0$, and $d_L(z)$ is defined as the following [285]:

$$d_L(z, H_0, \dots) = \frac{c(1+z)}{H_0} \int_0^z \frac{dz^*}{\sqrt{\Omega_{0m}(1+z^*)^3 + \Omega_{0\Lambda}(1+z^*)^{3(w_0+w_a+1)} e^{-3w_a \frac{z^*}{1+z^*}}}}, \quad (1)$$

where $\Omega_{0\Lambda}$ is the Dark Energy component, c is the speed of light, and z is the redshift. We stress that in this context the relativistic components are ignored. Moreover, since in the present universe the radiation density parameter $\Omega_{0r} \approx 10^{-5}$, this contribution can be neglected. If we substitute $w_a = 0$, $w_0 = -1$ in Equation (1) the luminosity distance expression for Λ CDM model is automatically retrieved. According to the distance luminosity expression, the theoretical distance modulus can be written in the following form:

$$\mu_{th} = 5 \log_{10} d_L(z, H_0, \dots) + 25, \quad (2)$$

which is usually expressed in Megaparsec (Mpc). The observed distance modulus, $\mu_{obs} = m'_B - M$, taken from PS contains the apparent magnitude in the B-band corrected for statistical and systematic effects (m'_B) and the absolute in the B-band for a fiducial SN Ia with a null value of stretch and color corrections (M). Considering the color and stretch population models for SNe Ia, in our approach we average the distance moduli given by the [286] (G2010) and [287] (C2011) models. We here remind the reader that H_0 and M are degenerate parameters: in the PS release, $M = -19.35$ such that $H_0 = 70.0$.

Ref. [51] obtain information on H_0 by comparing μ_{obs} in [284]¹ with μ_{th} for each SN. Moreover, they fix Ω_{0m} to a fiducial value to better constrain the H_0 parameter. Furthermore, according to [288], we consider the correction of the luminosity distance keeping into account the peculiar velocities of the host galaxies which contain the SNe Ia. To perform our analysis, we define the χ^2 for SNe:

$$\chi_{SN}^2 = \Delta\mu^T \cdot \mathcal{C}^{-1} \cdot \Delta\mu. \quad (3)$$

Here $\Delta\mu = \mu_{obs} - \mu_{th}$, and \mathcal{C} denotes the 1048×1048 covariance matrix, given by [284]. As for the μ_{obs} values of G2010 and C2011, the systematic uncertainty matrices of the two models have been averaged. After building the \mathcal{C} total matrix from Equation (16) in [51], we slice the PS in redshift bins, and then we divide \mathcal{C} into submatrices considering the order in redshift. More in detail, starting from the 1048 SNe Ia redshift-ordering, we divide the SNe Ia into 3 equally populated bins made up of ≈ 349 SNe Ia. Concerning only D_{stat} , it is trivial to build its submatrices considering that the statistical matrix is diagonal. Hence, a single matrix element is related to a given SN of the PS. On the other hand, if the non-diagonal matrix C_{sys} is included, a customized code will be used² to build the submatrices. Our code was developed to select only the total covariance matrix elements related to SNe Ia having redshift within the considered bin.

The choice of three bins is justified by the high number of SNe Ia (around hundreds of SNe per bin) that can still constitute statistically illustrative subsamples of the PS and that can properly consider the contribution of systematic uncertainties. Subsequently to the bins

division, we focus on the optimal values of H_0 to minimize the χ^2 in Equation (3). H_0 is regarded as a nuisance parameter, which is free to vary, to better analyze a possible redshift function of H_0 . We follow the assumptions on the fiducial value of $M = -19.35$: while in [51] M was estimated assuming a local ($z = 0$) value of $H_0 = 73.5$, we here consider the conventional H_0 value of the PS release, namely $H_0 = 70.0$ for three bins. Our choice of a starting value of $H_0 = 70$ is dictated by the presence in the current literature of more than 50 papers that are using the PS in combination with other probes to estimate the value of H_0 , see [172,198,204,205,288–307,307–339]. Thus, if an evolutionary effect is present, it is necessary to investigate to which extent this can affect current and future results largely based on the PS sample. Conversely, we fix $\Omega_{0m} = 0.298 \pm 0.022$ according to [284] for a standard flat Λ CDM model. More specifically, after the minimization of χ^2 , we extract the H_0 value in each redshift bin, via the *Cobaya* code [340]. To this end, we execute an MCMC using the D'Agostini method to obtain the confidence intervals for H_0 at the 68% and 95% levels, in three bins.

3. The Contribution of BAOs

The environment of relativistic plasma in the early universe was crossed by the sound waves that were generated by cosmological perturbations. At redshift $z_d \sim 1059.3$, which marks the ending of the drag period [341], the recombination of electrons and protons into a neutral gas interrupted the propagation of the sound waves while the photons were able to propagate further [342]. In the period between the formation of the perturbations and the recombination, the different modes produced a sequence of peaks and minima in the anisotropy power spectrum. Given the huge fraction of baryons in the universe, it is expected by cosmological models that the oscillations may affect also the distribution of baryons in the late universe. As a consequence, the BAOs manifest as a local maximum in the correlation function of the galaxies distribution in correspondence of the comoving sound horizon scale at the given redshift z_d , namely $r_s(z_d)$: this is associated with the stopping of the propagation of the acoustic waves.

To use the BAOs data for cosmology, we first need to define the following variables:

$$D_V(z) = \left[\frac{czd_L^2(z)}{(1+z)^2 H(z)} \right]^{1/3}, \quad d_z(z) = \frac{r_s(z_d)}{D_V(z)}. \quad (4)$$

The value of the redshift z_d , which corresponds to the drag era ending and marks the decoupling of the photons, allows estimating the sound horizon scale:

$$(r_d \cdot h)_{fid} = 104.57 \text{ Mpc}, \quad r_s(z_d) = \frac{(r_d \cdot h)_{fid}}{h}, \quad (5)$$

where we use the adimensional ratio $h = H_0/100(\text{km s}^{-1} \text{ Mpc}^{-1})$. To estimate r_s , the following approximated formula [343] can be applied:

$$r_s \approx \frac{55.154 \cdot e^{-72.3(\omega_v+0.0006)^2}}{\omega_{0m}^{0.25351} \omega_b^{0.12807}} \text{ Mpc}, \quad (6)$$

where $\omega_i = \Omega_i \cdot h^2$, and $i = m, v, b$ represent matter, neutrino and baryons. We here assume $\omega_v = 0.00064$ [344] and $\omega_b = 0.02237$ [10]. Given these quantities, we define the χ^2 for BAOs as follows:

$$\chi_{BAO}^2 = \Delta d^T \cdot \mathcal{M}^{-1} \cdot \Delta d, \quad (7)$$

where $\Delta d = d_z^{obs}(z_i) - d_z^{theo}(z_i)$ and \mathcal{M} is the covariance matrix for the BAO $d_z^{obs}(z_i)$ values. In this binned analysis, a subset of the 26 BAO observations set available in [341] will be employed.

4. Multidimensional Binned Analysis with SNe Ia and BAOs

To investigate the H_0 tension through the SNe Ia and BAOs data, we combine the χ^2 Equations (3) and (7) to obtain the total χ^2

$$\chi^2 = \frac{1}{2}\chi_{SN}^2 + \frac{1}{2}\chi_{BAO}^2. \quad (8)$$

In our work, we combine each SNe bin with only 1 BAO data point which has a redshift value within the SNe bin: this approach of using one BAO comes from [18]. In this way we do not have the problem of a different number of BAOs in different bins. Through Equation (8), we investigate if a redshift evolution of $H_0(z)$ is present, obtaining it from the binning of SNe Ia+BAOs considering three bins with the Λ CDM and w_0w_a CDM models. A feasibility study done in [51] performed with different bins selections has highlighted how the maximum number of bins in which the PS should be divided is 3, otherwise the statistical fluctuations would dominate on a multi-dimensional analysis, leading to relatively large uncertainties which would mask any evolving trend, if present. Furthermore, for the same reason, it is not advisable to leave free to vary more than two parameters at the same time, thus in the current section, we will analyze the behavior of H_0 in three bins when it is varied together with a second cosmological parameter. The same considerations make necessary the choice of more tight priors since we are basing the current analysis on the prior knowledge, avoiding the degeneracies among the parameter space, and letting the priors have more weight in the process of posteriors estimation. Differently from [51], for the Λ CDM model, we will let the parameters H_0 and Ω_{0m} vary simultaneously, while in the w_0w_a CDM model the varying parameters are H_0 and w_a . We decided to leave w_a free to vary since, according to the CPL parametrization, w_a gives direct information about the evolution of the $w(z)$ while w_0 is considered a constant in the same model. Concerning the fiducial values and the priors assignment for the MCMC computations, we apply Gaussian priors with mean equal to the central values of $\Omega_{0m} = 0.298 \pm 0.022$ and $H_0 = 70.393 \pm 1.079$ for Ω_{0m} and H_0 , respectively, and with $1\sigma = 2 * 0.022$ and $1\sigma = 2 * 1.079$ for Ω_{0m} and H_0 , respectively. In summary, to draw the Gaussian priors, we consider the mean value of the parameters as the expected one of the Gaussian distribution and we double the σ value which is then considered the new standard deviation for the distribution. Concerning the w_0w_a CDM model, we fix $w_0 = -0.905$ and we consider the priors on w_a with the mean = -0.129 taken from Table 13 of [284], while $1\sigma =$ is the 20% of its central value. Such an assumption with small prior is needed since we need to assume that $w(z) > -1.168$ as the value tabulated in [284]. Besides, since we are here dealing with standard cosmologies, with this constraint we are avoiding some of the phantom Dark Energy models.

After the χ^2 minimization for each bin, we perform a MCMC simulation to draw the mean value of H_0 and its uncertainty. Once H_0 is obtained for each bin, we perform a fit of H_0 using a simple function largely employed to characterize the evolution of many astrophysical objects, such as GRBs and quasars [17,29,31,35,345–349]. More specifically, the fitting of H_0 is given by

$$f(z) = H_0(z) = \frac{\mathcal{H}_0}{(1+z)^\eta}, \quad (9)$$

in which \mathcal{H}_0 and η are the fitting parameters. The former $\mathcal{H}_0 \equiv H_0$ at $z = 0$, while the latter η coefficient describes a possible evolutionary trend of H_0 . We consider the 68% confidence interval at, namely 1σ uncertainty.

In the current treatment, we consider the calibration of the PS with $H_0 = 70$ as provided by [284]. Results are presented in the panels of Table 1. We here stress that the fiducial magnitude value is assumed to be $M = -19.35$ for each SNe bin, thus it will not be mentioned in the same Table. All the uncertainties in the tables in this paper are in 1σ . As reported in the upper half of Table 1, namely with the Λ CDM model, if we do not include the BAOs then the η coefficient is compatible with 0 in 2.0σ for the three bins case. When we introduce the BAOs within the Λ CDM model, we observe again a reduction of the η/σ_η ratio for three bins down to 1.2. Concerning the lower half of Table 1 with the w_0w_a CDM model, when BAOs are not included we have η non compatible with 0 in 5.7σ and, including the BAOs, the compatibility with 0 is given in 5.8σ . The increasing of the ratio η/σ_η is observed when BAOs are added in the case of w_0w_a CDM model in three bins. The results can be visualized in Figure 1. Comparing the η/σ_η ratios with the ones reported in [51] (Table 1) we have that for the Λ CDM model the current η values are compatible in 1σ with the α reported in [51], while the η estimated in the w_0w_a CDM model are compatible in 3σ with the α values in the same reference paper.

Table 1. Upper half. Fit parameters of $H_0(z)$ for three bins (flat Λ CDM model, varying H_0 and Ω_{0m}) in the cases with SNe only and with the SNe + BAOs contribution. The columns are: (1) the number of bins; (2) \mathcal{H}_0 , (3) η ; (4) how many σ s the evolutionary parameter η is compatible with zero (namely, η/σ_η). **Lower half.** Similarly to the upper half, the lower half shows the fit parameters of $H_0(z)$ (flat w_0w_a CDM model, varying H_0 and w_a) without and with the BAOs.

Flat Λ CDM model, without BAOs, varying H_0 and Ω_{0m}			
Bins	\mathcal{H}_0	η	$\frac{\eta}{\sigma_\eta}$
3	70.093 ± 0.102	0.009 ± 0.004	2.0
Flat Λ CDM model, including BAOs, varying H_0 and Ω_{0m}			
Bins	\mathcal{H}_0	η	$\frac{\eta}{\sigma_\eta}$
3	70.084 ± 0.148	0.008 ± 0.006	1.2

Table 1. Cont.

Flat w_0w_a CDM model, without BAOs, varying H_0 and w_a			
Bins	\mathcal{H}_0	η	$\frac{\eta}{\sigma_\eta}$
3	69.847 ± 0.119	0.034 ± 0.006	5.7
Flat w_0w_a CDM model, including BAOs, varying H_0 and w_a			
Bins	\mathcal{H}_0	η	$\frac{\eta}{\sigma_\eta}$
3	69.821 ± 0.126	0.033 ± 0.005	5.8

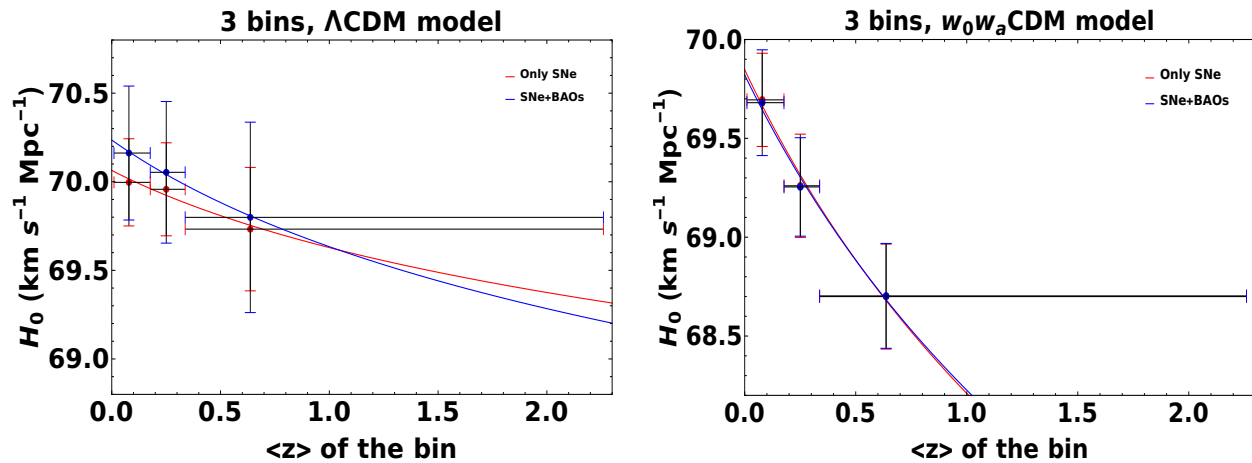


Figure 1. **Left panel** The $H_0(z)$ vs. z with varying also $\Omega_0 M$. The red color indicates the case with only SNe Ia as probes, while the blue refers to the case of SNe + 1 BAO per bin. This color-coded will be applied also in the right panel. **Right.** The same plot for the $w_0 w_a$ CDM model, considering the local fiducial value $H_0 = 70$, where both H_0 and w_a are left free to vary.

5. Perspective of the Future Contribution of GRB-Cosmology in 2030

The discussion of GRBs as possible cosmological tools has been going on for more than two decades [350,351]. The best bet is yet to come since we need first to identify the tightest correlation possible with a solid physical grounding. Among the many correlations proposed [19–23] we here choose to apply the *fundamental plane* (or Dainotti relation) [30,352–354], namely the three-dimensional relation between the end of the plateau emission’s luminosity, L_a , its time in the rest-frame, T_a^* , and the peak luminosity of the GRB, L_{peak} : it is possible to estimate how many GRBs are needed to obtain constraints for the cosmological parameters that are comparable with the ones obtained from the other probes, such as SNe Ia and BAOs. After a selection of the best fundamental plane sample through the trimming of GRBs, a simulation of a sample of 1500 and 2000 GRBs according to the properties of the fundamental plane relation has been performed. The fundamental plane relation can be expressed as the following:

$$\log_{10} L_a = a \times \log_{10} T_a^* + b \times \log_{10} L_{peak} + c, \quad (10)$$

where a, b are the parameters of the plane and c is the normalization constant. It is important to stress that here the variables L_a , T_a^* , and L_{peak} have been corrected for evolutionary effects with redshift applying the Efron and Petrosian method [355]. Based on Equation (10), we perform the maximization of the following log-likelihood for the simulated sample of GRBs:

$$\ln \mathcal{L}_{GRB} = -\frac{1}{2} \left(\ln(\sigma^2 + (a * \delta_{\log_{10} T_a^*})^2 + (b * \delta_{\log_{10} L_{peak}})^2 + \delta_{\log_{10} L_a}^2) \right) - \frac{1}{2} \left(\frac{(\log_{10} L_{a,th} - \log_{10} L_a)^2}{\sigma^2 + (a * \delta_{\log_{10} T_a^*})^2 + (b * \delta_{\log_{10} L_{peak}})^2 + \delta_{\log_{10} L_a}^2} \right), \quad (11)$$

where $L_{a,th}$ is the theoretical luminosity computed through the fundamental plane in Equation (10), σ is the intrinsic scatter of the plane and $\delta_{\log_{10} T_a^*}$, $\delta_{\log_{10} L_{peak}}$, and $\delta_{\log_{10} L_a}$ are the errors on the rest-frame time at the end of the plateau emission, the peak luminosity and the luminosity at the end of the plateau, respectively.

After performing an MCMC analysis using the D’Agostini method [356] and letting vary the parameters $a, b, c, \sigma, \Omega_{0m}$, the results are shown in Figure 2. Through the simulations of 1000

GRBs, with 9500 steps and keeping the same errors (errors undivided) as the ones observed in the fundamental plane ($n = 1$, see the upper left panel of Figure 2) we obtain a value of $\Omega_{0m} = 0.310$ with a symmetrized uncertainty of $\sigma_{\Omega_{0m}} = 0.078$. In the case of 2000 GRBs with 13,000 steps and $n = 1$ (see the upper right panel of Figure 2) instead, we have $\Omega_{0m} = 0.300$, $\sigma_{\Omega_{0m}} = 0.052$. If we consider the division of the errors on the variables of the fundamental plane by a factor 2 (halved errors, $n = 2$) we obtain, in the case of 1500 GRBs with 11100 steps, $\Omega_{0m} = 0.300$, $\sigma_{\Omega_{0m}} = 0.037$ (see the lower-left panel of Figure 2), while through 2000 simulated GRBs in 14,600 steps (still with $n = 2$, see the lower right panel of Figure 2) we have $\Omega_{0m} = 0.310$, $\sigma_{\Omega_{0m}} = 0.034$. The idea of considering halved errors comes from the prospects for improvement in the fitting procedures of GRB light curves. Through this approach, the GRBs have provided constraints on the value of Ω_{0m} that are compatible with the ones of previous samples of SNe Ia: in the $n = 1$ cases, the values of the uncertainties are comparable with the ones from [357], while for the $n = 2$ cases the values are close to the ones found in [358] with 2000 GRBs. Furthermore, the GRBs have proven to be promising standardizable candles and, given the bigger redshift span they can cover if compared with SNe Ia, GRBs will provide more complete information about the structure and the evolution of the early universe after the Big Bang, together with quasars [359,360]. After discussing the potentiality of GRBs as future standard candles, we estimate the frequency of GRBs with a plateau emission over the total number of GRBs observed to date. We can expect that by 2030 we will have reached several GRB observations such that these—as standalone probes that respect the properties of the GRB platinum sample [35]—will give constraints as precise as the ones from [357] in the case of not halved errors. In case of halved errors, we can reach the level of precision of [357] even now. In addition, if we consider a machine learning analysis [361,362] for which we can double the size of the sample we are able to reach the precision of [357] now with the case of $n = 1$. If we consider the case of reconstructing the light curves and thus we have a sample which has the 47% of cases with halved errors we can reach the limit of [357] in 2022 if $n = 1$ and now if $n = 2$.

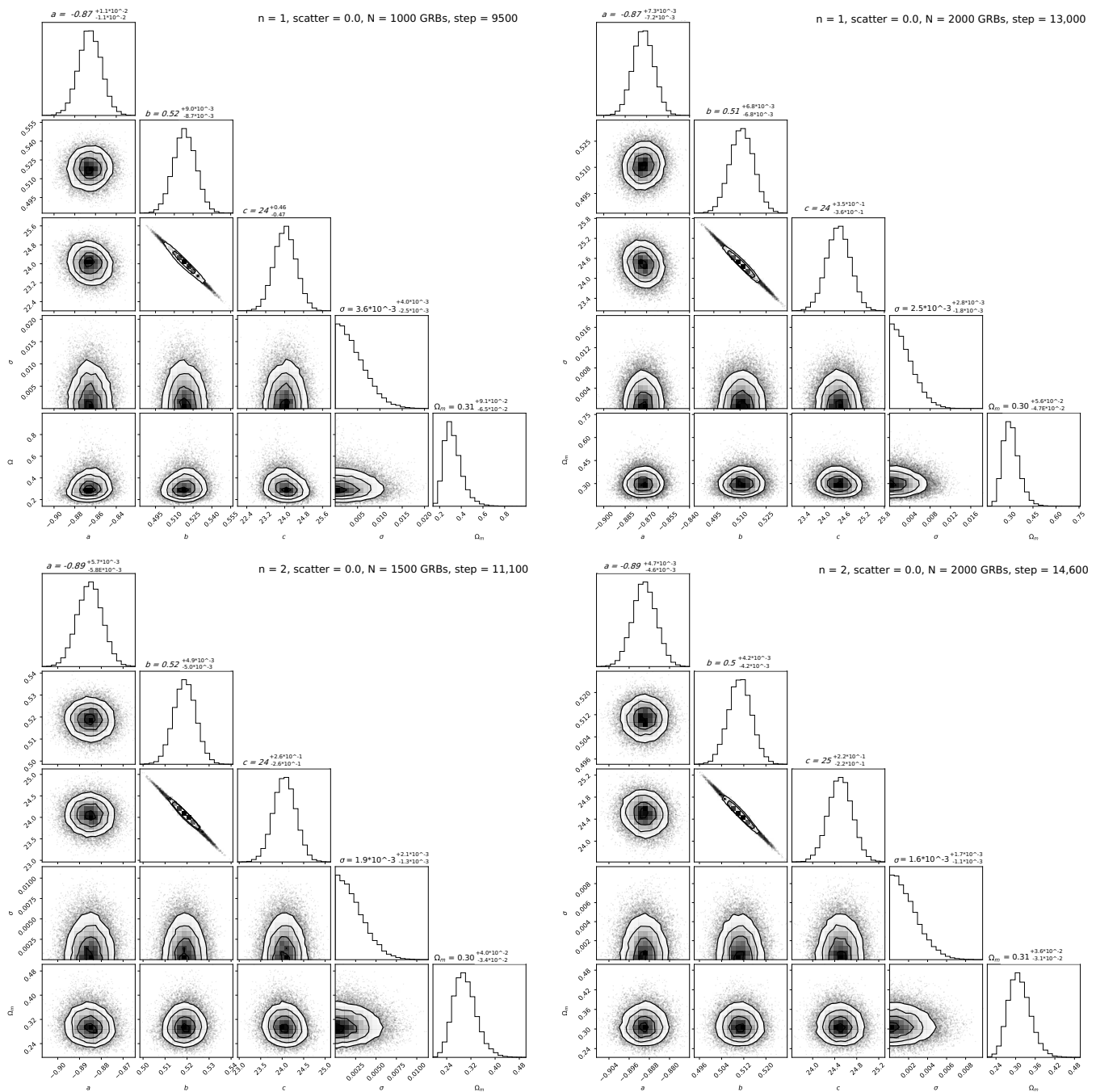


Figure 2. Upper left. An example of 1000 simulated GRBs with the posterior distribution of the fundamental plane parameters a , b , c , and its intrinsic scatter σ together with the total matter density parameter Ω_{0m} . In this case, the steps of the simulation are 9500 and the errors on the variables of the fundamental plane have not been divided by any factor ($n = 1$). **Upper right.** The same case of the upper left panel, but considering 2000 GRBs and a number of steps of 13,000. **Lower left.** The results of 1500 simulated GRBs, dividing by two the errors on the fundamental plane variables (halved errors, $n = 2$): here the steps are 11,100. **Lower right.** The same result of the lower-left panel, considering 2000 GRBs and 14,600 steps instead.

6. Discussions on the Results

Our results can be interpreted because of astrophysical selection biases or theoretical models alternatives to the standard cosmological models.

6.1. Astrophysical Effects

The main effect that has a stake in the SNe Ia luminosity variation is the presence of metallicity and the difference in stellar ages. Indeed, ref. [284] correct the PS with a mass-step contribution (ΔM). Despite this term improving the results, other effects need to be accounted for. Considering the stretch and the color, ref. [363] claim that the Hubble residuals, after being properly corrected according to the stretch and color observations, for SNe Ia in low mass and high mass host galaxies show a difference of 0.077 ± 0.014 mag, compatibly with the result of [284]. SNe Ia age metallicity and age are believed to be responsible for the observed behavior: those can replicate the Hubble residual trends consistent with the ones of [363]. In the PS, to account for the evolutions of stretch (α) and color (β), the parametrization utilized is the following: $\alpha(z) = \alpha_0 + (\alpha_1 \times z)$, $\beta(z) = \beta_0 + (\beta_1 \times z)$. According to [284], there is no clear dependence on the redshift for $\alpha(z)$ and $\beta(z)$, thus α_1 and β_1 are set to zero. Only the selection effect for color is noteworthy and [284] consider the uncertainty on β_1 as a statistical contribution. Concerning the stretch evolution in the PS calibration, it appears to be negligible and is not included at any level.

Conversely, ref. [364] recently studied the SALT2.4 lightcurve stretch and showed that the SN stretch parameter is redshift-dependent. According to their analysis, the asymmetric Gaussian model assumed by [284] for describing the populations of SNe Ia does not take into consideration the redshift drift of the PS, thus leaving a residual evolutionary trend that manifests at higher redshifts. Indeed, the simulations performed by [284] for studying the systematics calibration reach redshifts up to $z = 0.7$: this threshold is present in the third bin of our analysis. The effect from $0.7 \leq z \leq 2.26$ needs additional investigations. It is worth noting that this decreasing trend of H_0 (with a given value of η) found in [51] is consistent in 1σ for the Λ CDM both in the cases of SNe Ia only and SNe+BAOs. When we consider the $w_0 w_a$ CDM, the η values are compatible in 3σ with the ones with SNe Ia only and SNe + BAOs. We here have two cosmological parameters varying at the same time, differently from [51]. Therefore, one of the possible astrophysical reasons behind the observed trend is the residual stretch evolution with redshift. If so, in our work the effect is simply switched from stretch to H_0 . The forthcoming release of the Pantheon+ data [107,365–369] will give the chance to test if these evolutionary effects may be still visible, but this analysis goes far beyond the scope of the current paper. The astrophysical interpretation seems to be favored, but also many theoretical explanations may be possible to describe the outcome of these results.

6.2. Theoretical Interpretations

We now investigate possible theoretical explanations for our results, focusing particular attention on modified gravity models. We first discuss a general scalar-tensor formulation and, then, we concentrate our attention on the so-called metric $f(R)$ gravity.

6.2.1. The Scalar Tensor Theory of Gravity

The action of the scalar tensor theories (STTs) of gravity is given by $S = S^JF + S_m$ [370–374] with the Jordan Frame (JF) action

$$S^JF = \frac{1}{16\pi} \int d^4x \sqrt{-\tilde{g}} \left[\Phi^2 \tilde{R} + 4\omega(\Phi) \tilde{g}^{\mu\nu} \partial_\mu \Phi \partial_\nu \Phi - 4\tilde{V}(\Phi) \right], \quad (12)$$

where \tilde{R} is the Ricci scalar obtained with the physical metric $\tilde{g}_{\mu\nu}$, while the matter fields Ψ_m couple to the metric tensor $\tilde{g}_{\mu\nu}$ and not to Φ , i.e., $S_m = S_m[\Psi_m, \tilde{g}_{\mu\nu}]$.

In this Section we adopt natural units such that $c = 1$ and $G = 1$. Different STTs follow with the appropriate choice of the two functions $\omega(\Phi)$ and $\tilde{V}(\Phi)$: e.g., the Brans–Dicke (BD) theory [375–378] can be obtained for $\omega(\Phi) = \omega(\text{const.})$ and $\tilde{V}(\Phi) = 0$, while the metric $f(R)$ gravity, discussed in the next subsection, would correspond to $\omega \equiv 0$.

The action S^{IF} can be rewritten in the Einstein Frame (EF), where one defines $\tilde{g}_{\mu\nu} \equiv A^2(\varphi)g_{\mu\nu}$, $\Phi^2 \equiv 8\pi M_*^2 A^{-2}(\varphi)$, $V(\varphi) \equiv \frac{A^4(\varphi)}{4\pi} \tilde{V}(\Phi)$, $\gamma(\varphi) \equiv \frac{d \log A(\varphi)}{d\varphi}$, and $\gamma^2(\varphi) = \frac{1}{4\omega(\Phi)+6}$, to get

$$S^{EF} = \frac{M_*^2}{2} \int d^4x \sqrt{-g} \left[R + g^{\mu\nu} \partial_\mu \varphi \partial_\nu \varphi - \frac{2}{M_*^2} V(\varphi) \right]. \quad (13)$$

Matter is coupled to φ only through a purely metric coupling, $S_m = S_m[\Psi_m, A^2(\varphi)g_{\mu\nu}]$ and M_* is the Planck mass.

The physical quantities in the Jordan and Einstein frame are related by $d\tilde{\tau} = A(\varphi)d\tau$, $\tilde{a} = A(\varphi)a$, $\tilde{\rho} = A(\varphi)^{-4}\rho$, $\tilde{p} = A(\varphi)^{-4}p$, where τ is the synchronous time variable. Defining $N \equiv \log \frac{a}{a_0}$, $\lambda \equiv \frac{V(\varphi)}{\rho}$, $w \equiv \frac{p}{\rho}$, and $\varphi' = \frac{d\varphi}{dN} = a \frac{d\varphi}{da}$, the combination of cosmological equations allows to write the equation for φ in the form (for a flat Friedmann–Robertson–Walker geometry) [379]

$$\frac{2}{3} \frac{1 + \lambda}{1 - \varphi'^2/6} \varphi'' + [(1 - w) + 2\lambda]\varphi' = -\sqrt{2} \gamma(\varphi) (1 - 3w) - 2\lambda \frac{V_\varphi(\varphi)}{V}. \quad (14)$$

Moreover, the Jordan- and Einstein-frame Hubble parameters, $\tilde{H} \equiv d \log \tilde{a} / d\tilde{\tau}$ and $H \equiv d \log a / d\tau$, respectively, are related as

$$\tilde{H} = \frac{1 + \gamma(\varphi) \varphi'}{A(\varphi)} H. \quad (15)$$

For our purpose, we consider $A(\varphi) = A_0 e^{c_1 \varphi + c_2 \varphi^2/2}$, which implies $\gamma(\varphi) = c_1 + c_2 \varphi$, where $c_{1,2}$ are constants. Under the following conditions $\varphi''/\varphi \ll 1$, $\varphi'^2/\varphi^2 \ll 1$, and $\frac{V_\varphi(\varphi)}{\varphi V \rho} \ll 1$, the solution of Equation (14) is $\varphi(z) = C(1+z)^K - \frac{c_1}{c_2}$, where $K = \frac{1-3w}{1+w} \sqrt{2} c_2$, and C is an integration constant. We are looking for solutions such that $H = f(\varphi)\tilde{H}_0$, so that $\tilde{H} = \frac{\tilde{H}_0}{(1+z)^\eta}$, where \tilde{H}_0 is constant. These relations and (15) allow to derive $f(\varphi)$ (the expression of $f(\varphi)$ is quite involved, and in the case in which $c_{1,2} \ll 1$, it is a polynomial in φ). The scalar field Φ in the (physical) JF can be cast in the form $\Phi(z) = \Phi_0(1+z)^{\tilde{K}}$, where $\Phi_0 \equiv \frac{\sqrt{8\pi M_*}}{A_0} \left[1 - C \left(c_1 - \frac{C c_2}{c_1} \right) \right]$, $\tilde{K} = -\frac{KC(c_1 + C c_2)}{1 - C(c_1 + \frac{C c_2}{2})}$, and $z < 1$ has been used (note: \tilde{K} is positive for c_1 or c_2 negative). The scalar field Φ reduces to ϕ for $\Phi_0 \rightarrow 1$ and $\tilde{K} \rightarrow 2\eta$.

From the Friedmann Equation [379]

$$\left(\frac{\dot{a}}{a} \right)^2 = \frac{1}{3M_*^2} \left[\rho + \frac{M_*^2}{2} \dot{\varphi}^2 + V(\varphi) \right], \quad (16)$$

with ρ given by matter ($\rho = \rho_{0m}/a^3 = \rho_{0m}(1+z)^3$), and $c_{1,2} \ll 1$, one infers the effective potential

$$\frac{\tilde{V}}{3m^2} = \frac{4\pi M_*^2}{A_0^2} \left[f_0^2 - \frac{1}{\Omega_{0m}} \left(\frac{\Phi}{\Phi_0} \right)^{\frac{3}{2\eta}} - \frac{C^2 K^2 \varphi_0^2}{6\Omega_{0m}} \left(\frac{\Phi}{\Phi_0} \right)^{\frac{K-\eta}{\eta}} \right], \quad (17)$$

where we recall that $\Omega_{0m} = \rho_{0m}/\rho_{cr}$, $\rho_{cr} = 3M_*^2 \tilde{H}_0^2$, $f_0 = f(\varphi = 0)$, and $m^2 = \Omega_{0m} \tilde{H}_0^2$. For redshift $0 \leq z < 0.3$, to which we are interested, the scalar field varies slowly with z , $\Phi \sim \Phi_0$, so that the effective potential behaves like a cosmological constant. We see how the proposed

scalar-tensor formulation has the right degrees of freedom to reproduce, in the JF, the required behavior of the (physical) trend of $H_0(z)$. In the next subsection, we analyze a sub-case of the general paradigm discussed above, which leads to the well-known $f(R)$ gravity, which is among the most popular modified gravity formulations.

6.2.2. Metric $f(R)$ Gravity in the Jordan Frame

The observed decaying behavior of the Hubble constant H_0 with the redshift draws significant attention for an explanation and, if it is not due to selection effects or systematics in the sample data, we need to interpret our results from a physical point of view. As already argued in [380] and [51], the simplest way to account for this unexpected behavior of $H_0(z)$ is that the Einstein constant $\chi = 8\pi G$ (where G denotes the gravitational constant), mediating the gravity-matter interaction, is subjected itself to a slow decaying profile with the redshift. In this Section, we consider $c = 1$ for the speed of light. More specifically, since the critical energy density $\rho_{c0} = 3H_0^2/\chi$ today must be a constant, we need an evolution for $\chi \sim (1+z)^{-2\eta}$, considering the function $H_0(z)$ given by Equation (9). The evolution of $\chi(z)$ is not expected within the cosmological Einsteinian gravity, therefore we are led to think of it as a pure dynamical effect, associated with a modified Lagrangian for the gravitational field beyond the Λ CDM cosmological model. Ref. [143] obtained cosmological constraints within the Brans–Dicke theory considering how the evolution of the gravitational constant G , contained in χ , affects the SNe Ia peak luminosity. The most natural extended framework is the $f(R)$ -gravity proposal [162,163,167,381] which contains only an additional scalar degree of freedom. For instance, Ref. [323] try to alleviate the H_0 tension considering exponential and power-law $f(R)$ models.

The formulation of the $f(R)$ theories in an equivalent scalar-tensor paradigm turns out to be particularly intriguing for our purposes: the function $f(R)$ is restated as a real scalar field ϕ , which is non-minimally coupled to the metric in the JF. The information about the function f turns into the expression of the scalar field potential $V(\phi)$. The relevance of modified gravity models relies on the possibility that this revised scenario for the gravitational field can account for the physics of the so-called “dark universe” component without the need for a cosmological constant. Indeed, the observed cosmic acceleration in the late universe via the SNe Ia data is a pure dynamical effect, i.e., associated with a modification of the Einsteinian gravity at very large scales (in the order of the present Hubble length).

According to the standard literature on this field (which includes a large number of proposals), three specific $f(R)$ models, i.e., the Hu–Sawicki [382], the Starobinsky [383], and Tsujikawa models [384,385], successfully describe the Dark Energy component (say an effective parameter for the Dark Energy $w = w(z) < -1/3$) and overcome all local constraints. The difference in the form of the Lagrangian densities associated with $f(R)$ models is reflected in the morphology of the potential term governing the dynamics of the scalar field. For instance, the scalar field potential related to the Hu–Sawicki $f(R)$ proposal, with the power index $n = 1$, in the JF is given by

$$V(\phi) = \frac{m^2}{c_2} \left[c_1 + 1 - \phi - 2\sqrt{c_1(1 - \phi)} \right], \quad (18)$$

where we have two free parameters c_1 and c_2 , while $m^2 = \chi \rho_{0m}/3$. The scalar-tensor dynamics in the JF for a flat FLRW metric with a matter component is summarized by

$$H^2 = \frac{\chi \rho}{3\phi} - H \frac{\dot{\phi}}{\phi} + \frac{V(\phi)}{6\phi} \quad (19)$$

$$\frac{\ddot{a}}{a} = -\frac{\chi \rho}{3\phi} - \frac{V(\phi)}{6\phi} + \frac{1}{6} \frac{dV}{d\phi} + \frac{\dot{a}\dot{\phi}}{a\phi} \quad (20)$$

$$3\ddot{\phi} - 2V(\phi) + \phi \frac{dV}{d\phi} + 9H\dot{\phi} = \chi \rho, \quad (21)$$

which are the generalized Friedmann equation, the generalized cosmic acceleration equation and the scalar field equation, respectively [167]. We recall that $\phi = \phi(t)$ is a function of the time (or the redshift z) only for an isotropic universe. Considering the first term on the right-hand side of Equation (19), it is possible to recognize that ϕ mediates the gravity-matter coupling, and therefore it mimics a space-time varying Einstein constant. Hence, to account for our observed decay of $H_0(z)$, we have to require that the scalar field assumes a specific behavior with the redshift, i.e.

$$\phi(z) = (1+z)^{2\eta}. \quad (22)$$

Moreover, the remaining terms contained in the gravitational field equations must be negligible. This situation is naturally reached when the potential term is sufficiently slow-varying in a given time interval. We see that the hypothesis of a near-frozen scalar field evolution is a possible assumption, as far as the potential term should provide a dynamical impact, sufficiently close to a cosmological constant term. These simple considerations lead us to claim that this scenario is worth to be investigated for the behavior of $H_0(z)$ here observed.

The specific cosmological models affect the expression of the luminosity distance and this should be the starting point of a careful test of a $f(R)$ theory versus the comprehension of the H_0 tension. A new binned analysis of the PS, using the corrected luminosity distance obtained through a reliable $f(R)$, may in principle shed new light on the observed decaying trend of $H_0(z)$, testing also new physics. This analysis is performed in the next Section.

As a preliminary approach, we try to understand which profile we could expect for the scalar field potential, inferred from the behavior of $H_0(z)$. This is quite different from a standard analysis of $f(R)$ models. Generally, a specific $f(R)$ function is defined a priori, and then the dynamical equations are studied to obtain constraints on the free parameters. Here, instead, starting from the observed decreasing trend of $H_0(z)$ and assuming $\phi(z)$ from Equation (22), we wonder what the scalar field potential would be in a scalar-tensor dynamics. Eventually, we should have a scalar field in near-frozen dynamics, i.e., a slow-roll of the scalar field potential, mimicking a cosmological constant term ($\phi \rightarrow 1$). To this end, we rewrite the generalized Friedmann Equation (19) and calculate $V(\phi)$:

$$V(\phi) = 6(1-2\eta) \left(\frac{dz}{dt} \right)^2 \phi^{1-1/\eta} - 6m^2 \phi^{3/2\eta}, \quad (23)$$

where we have used the standard definition of redshift and the relation (22) for $\phi(z)$. Moreover, we recall that for a matter component $\rho \sim (1+z)^3$. As a final step, we need to calculate the term $\frac{dz}{dt}$. Starting again from the redshift definition, it is well known that

$$\frac{dz}{dt} = -(1+z)H(z). \quad (24)$$

In principle, we would need to compute the Hubble parameter $H(z)$ from the field equations, and then replace $H(z)$ in the term $\frac{dz}{dt}$. However, this procedure is not viable, since we need to fix a well-defined $V(\phi)$ to solve the field equations. Moreover, $H(z)$ appears also in the

right-hand-side of Equation (19), because of the non-minimal coupling with the scalar field. Therefore, we can not calculate exactly $\frac{dz}{dt}$ to get $V(\phi)$ in the JF.

Then, to obtain $V(\phi)$ inferred from the trend of $H_0(z)$, we require that the Hubble function provides the same physical mechanism suggested from our binned analysis in Section 4, i.e., simply replacing H_0 with $H_0(z)$ given by Equation (9) in the standard Friedmann equation in the Λ CDM model. With this new definition of \mathcal{H}_0 , we write the following condition on the Hubble function:

$$H(z) = \frac{\mathcal{H}_0}{(1+z)^\eta} \sqrt{\Omega_{0m}(1+z)^3 + 1 - \Omega_{0m}}. \quad (25)$$

In doing so, using Equations (23), (24) and (25), we determine the form of the scalar field potential

$$\frac{V(\phi)}{m^2} = 6(1-2\eta) \left(\frac{1-\Omega_{0m}}{\Omega_{0m}} \right) - 12\eta \phi^{3/2\eta} \quad (26)$$

inferred from the decreasing trend of $H_0(z)$. In other words, the potential Equ. 26 might provide an effective Hubble constant that evolves with redshift. In the computation, we have used the expression $\Omega_{0m} = m^2/\mathcal{H}_0^2$.

In Figure 3, we plotted this potential profile, observing that, as expected, a flat region consistently appears, validating our guess on the feasibility of $f(R)$ -gravity in the JF to account for the observed behavior of $H_0(z)$. We set $\eta = 0.009$ in Figure 3, according to our binned analysis results for three bins (see Table 1). We stress that the flatness of the potential does not emerge throughout the Pantheon sample redshift range, $0 < z < 2.3$, but it appears only in a narrow region for $0 < z \lesssim z^*$, where $z^* = 0.3$ is the redshift at the Dark Energy and Matter components equivalence of the universe. This form of $V(\phi)$ is reasonable since the Dark Energy contribution, provided by the scalar field in the JF gravity, dominates the matter component only for $0 < z \ll z^*$. It is the weak dependence of H_0 on z that ensures the existence of a flat region of the potential, according to the theoretical scenario argued above.

Finally, we can calculate the form of the $f(R)$ function associated with the potential profile. Recalling the following general relations in the JF [167]:

$$R = \frac{dV}{d\phi}, \quad (27)$$

$$f(R) = R\phi(R) - V(\phi(R)), \quad (28)$$

we can obtain:

$$f(R) = -6m^2 \left[(1-2\eta) \frac{1-\Omega_{0m}}{\Omega_{0m}} + (3-2\eta) \left(-\frac{R}{18m^2} \right)^{\frac{3}{3-2\eta}} \right]. \quad (29)$$

Note that the formula above provides a generalization of the Einstein theory of gravity, as it should be in the context of a $f(R)$ model. Indeed, if $\eta = 0$, then $f(R) \equiv R$ reproduces exactly the Einstein–Hilbert Lagrangian density in GR with a cosmological constant Λ , as soon as you recognize that $\Lambda = 3m^2(1-\Omega_{0m})/\Omega_{0m}$ for a flat geometry, using $m^2 = \mathcal{H}_0^2\Omega_{0m}$. In particular, expanding the function (29) for $\eta \sim 0$, we can see explicitly the deviation from the Einstein–Hilbert term:

$$f(R) \approx \left(R - 6m^2 \frac{1-\Omega_{0m}}{\Omega_{0m}} \right) + \frac{2}{3}\eta \left[R \ln \left(-\frac{R}{m^2} \right) - (1 + \ln 18) R + 18m^2 \frac{1-\Omega_{0m}}{\Omega_{0m}} \right] + O(\eta^2). \quad (30)$$

The first term at the zero-th order in η is exactly the Einstein–Hilbert Lagrangian density, while the linear term in η provides the correction to GR. Therefore, η , in addition to being the

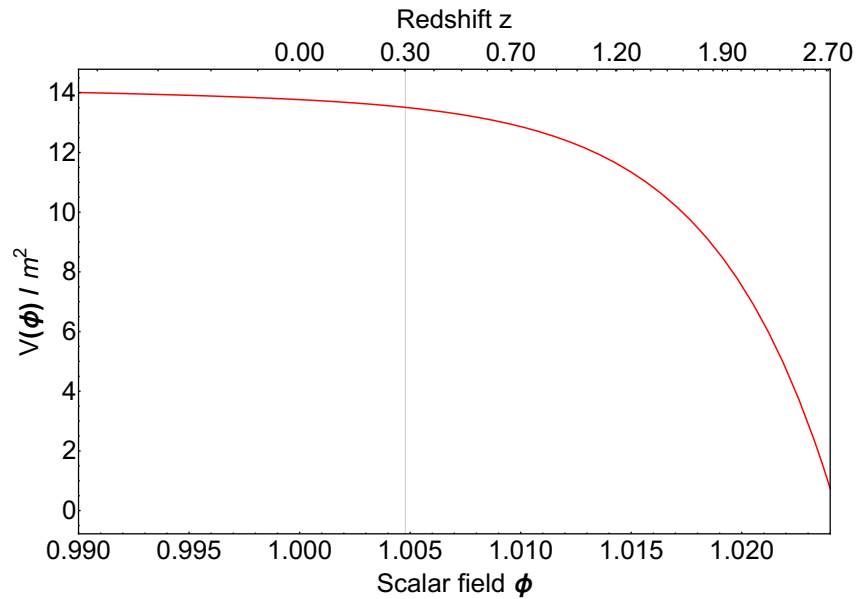


Figure 3. Profile of the scalar field potential $V(\phi)$ in the JF equivalent scalar-tensor formalism of the $f(R)$ modified gravity. The form of $V(\phi)$ is inferred from the behavior of $H_0(z)$ (Equation (9)). Note that $V(\phi)/m^2$ is a dimensionless quantity. A flat profile of $V(\phi)$ occurs only at low redshifts, for $0 < z \lesssim 0.3$ or equivalently $\phi \lesssim 1.005$. Note, also, the non-linearity of the scale for the redshift axis on top, considering the relation (22) between ϕ and z . In this plot, $\eta = 0.009$.

physical parameter that describes the evolution of $H_0(z)$, also denotes the deviation from GR and the standard cosmological model. It is worthwhile to remark that the expression above may not be the final form of the underlying modified theory of gravity, associated with the global universe dynamics, but only its asymptotic form in the late Universe, i.e., as the scalar of curvature approaches the value corresponding to the cosmological constant in the Λ CDM model. In all these computations we do not consider relativistic or radiation components at very high redshifts, but it may be interesting to test this model with other local probes in the late Universe.

In this discussion, we infer that the dependence of H_0 on the redshift points out the necessity of new physics in the description of the universe dynamics and that such a new framework may be identified in the modified gravity, related to metric theories.

7. The Binned Analysis with Modified $f(R)$ Gravity

To try to explain the observed trend of $H_0(z)$, we focus on $f(R)$ theories of gravity, and then we perform the same binned analysis, using the correction for the distance luminosity according to the modified gravity. We start from the gravitational field action [167]:

$$S_g = \frac{1}{2\chi} \int d^4x \sqrt{-g} f(R), \quad (31)$$

where $f(R)$, as a function of the Ricci scalar R , is an extra degree of freedom compared to General Relativity. We rewrite $f(R) = R + F(R)$ to highlight the deviation from the standard gravity. Varying the total action with respect to the metric, we obtain the flat FLRW metric field equations:

$$H^2(1 + F_R) = \frac{\chi\rho}{3} + \left[\frac{R F_R - F}{6} - F^{RR} H \dot{R} \right], \quad (32)$$

where $F_R \equiv \frac{dF(R)}{dR}$. The Ricci scalar R can be cast in the form

$$R = 12H^2 + 6HH', \quad (33)$$

where the Hubble parameter H is expressed as a function of $\gamma \equiv \ln(a)$, and the prime indicates the derivative with respect to γ .

Now, we introduce two dimensionless variables [382]

$$y_H = \frac{H^2}{m^2} - \frac{1}{a^3}, \quad y_R = \frac{R}{m^2} - \frac{3}{a^3}, \quad (34)$$

which denote the deviation of H^2 and R with respect to the matter contribution when compared to the Λ CDM model. We rewrite the modified Friedmann Equation (32) and the Ricci scalar relation (33) in terms of y_H and y_R . Then, we have a set of coupled ordinary differential equations:

$$y_H' = \frac{1}{3}y_R - 4y_H \quad (35)$$

$$y_R' = \frac{9}{a^3} - \frac{1}{y_H + a^{-3}} \frac{1}{m^2 F_{RR}} \left[y_H - F_R \left(\frac{1}{6}y_R - y_H - \frac{a^{-3}}{2} \right) + \frac{1}{6} \frac{F}{m^2} \right]. \quad (36)$$

The solution of this coupled first-order differential equations system above can not be obtained analytically, but can be numerically calculated. We need initial conditions such that this scenario mimics the Λ CDM model in the matter dominated universe at initial redshift $z_i \gg z^*$. Hence, we impose the following conditions for y_H and y_R at the redshift z_i :

$$y_H(z_i) = \frac{\Omega_{0\Lambda}}{\Omega_{0m}} \quad (37)$$

$$y_R(z_i) = 12 \frac{\Omega_{0\Lambda}}{\Omega_{0m}}. \quad (38)$$

The standard Λ CDM model is reached for $z = z_i$ or asymptotically, and we consider a flat geometry, such that $\Omega_{0\Lambda} = 1 - \Omega_{0m}$. Finally, the luminosity distance can be written as

$$d_L(z) = \frac{(1+z)}{H_0} \int_0^z \frac{dz'}{\sqrt{\Omega_{0m} \left(y_H(z') + (1+z')^3 \right)}}, \quad (39)$$

including the solution $y_H(z)$ from Equation (34) [386].

Hu–Sawicki Model

We focus on the Hu–Sawicki model with $n = 1$, considering a late-time gravity modification, described by the following function [382]:

$$f(R) = R + F(R) = R - m^2 \frac{c_1 (R/m^2)^n}{c_2 (R/m^2)^n + 1}, \quad (40)$$

corresponding to the potential $V(\phi)$ in Equation (18). The parameters c_1 and c_2 are fixed by the following conditions [382]

$$\frac{c_1}{c_2} \approx 6 \frac{\Omega_{0\Lambda}}{\Omega_{0m}} \quad (41)$$

$$F_{R0} \approx -\frac{c_1}{c_2^2} \left(\frac{12}{\Omega_{0m}} - 9 \right)^{-2}, \quad (42)$$

where F_{R0} is the value of the field $F_R \equiv dF/dR$ at the present time, and $F(R)$ is the deviation from the Einstein–Hilbert Lagrangian density. Cosmological constraints provide $|F_{R0}| \leq 10^{-7}$ from gravitational lensing and $|F_{R0}| \leq 10^{-3}$ from Solar system [387,388]. We explore several choices of F_{R0} .

To simplify the numerical integration of the modified luminosity distance (39), we approximate the numerical solution y_H , obtained from the system (35), (36), by a polynomial of order 8. This function is an accurate representation of y_H when we restrict the solution to the range of PS (see Figure 4).

As a consequence, we obtain constraints on c_1 and c_2 , according to Equations (41) and (42). Then, we perform the same binned analysis of Section 4 using the Hu–Sawicki model and the modified luminosity distance (39).

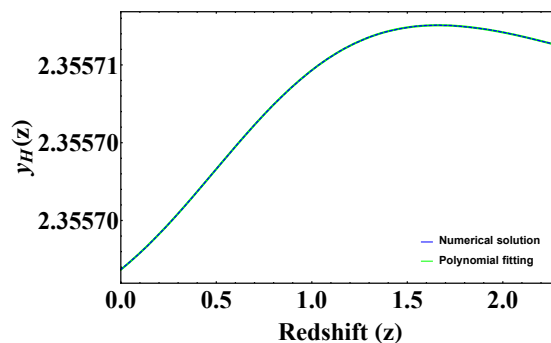


Figure 4. The numerical solution for Equations (35) (36) (blue dashed curve) plotted together with its polynomial fitting (green continuous curve) in the case of $F_{R0} = -10^{-7}$. The assumption of a function of redshift in the form of a order-8 polynomial allows an accurate fit for the numerical values. The same fitting procedure has been used in the $F_{R0} = -10^{-4}$ case.

We here run the analysis both for the case of Ω_{0m} fixed to a fiducial value of 0.298 and for several values of $F_{R0} = -10^{-7}, -10^{-6}, -10^{-5}, -10^{-4}$ (see Table 2 and Figure 5) or we let Ω_{0m} vary with the two values of $F_{R0} = -10^{-7}, -10^{-4}$ (see Table 3 and Figure 6) for the SNe alone and with SNe +BAOs. Note also that the η parameters are all consistent for the several values of F_{R0} in 1σ , as you can see in Table 2, for both SNe Ia and SNe Ia + BAOs. Moreover, the values of η are consistent in 1σ with the ones obtained from the analysis of the Λ CDM model (see also Table 1). We consider the cases $F_{R0} = -10^{-7}, F_{R0} = -10^{-4}$ and, to study how these results may vary according to the different values of Ω_{0m} chosen, we tested the model with four values of $\Omega_{0m} = (0.301, 0.303, 0.305)$ taken from the 1σ from a Gaussian distribution centred around the most probable value of 0.298, see [368].

We show in Figure 6 the comparison between the different applications of the Hu–Sawicki model: in the left panels (upper and lower), we consider SNe Ia only, while in the right panels (upper and lower) we combine SNe Ia+BAOs. We here remind that the assumed values for $|F_{R0}|$ of 10^{-4} and 10^{-7} are well constrained by the $f(T)$ theories. [167,382].

Table 2. Fitting parameters of $H_0(z)$ for three bins within the Hu–Sawicki model, with SNe only and SNe + BAOs with a fixed value of $\Omega_{0m} = 0.298$ and with several values of $F_{R0} : -10^{-4}, -10^{-5}, -10^{-6}, -10^{-7}$. The columns contains: (1) the number of bins; (2) \mathcal{H}_0 , (3) is η , according to Equation (9); (4) how many σ s η is compatible with zero (namely, the ratio η/σ_η); (5) F_{R0} values; (6) the sample used.

Hu–Sawicki Model, Results of the Redshift Binned Analysis					
Bins	\mathcal{H}_0	η	$\frac{\eta}{\sigma_\eta}$	F_{R0}	Sample
3	70.089 ± 0.144	0.008 ± 0.006	1.2	-10^{-4}	SNe
3	70.127 ± 0.128	0.008 ± 0.006	1.4	-10^{-4}	SNe + BAOs
3	70.045 ± 0.052	0.007 ± 0.002	3.0	-10^{-5}	SNe
3	70.062 ± 0.132	0.007 ± 0.005	1.3	-10^{-5}	SNe + BAOs
3	70.125 ± 0.046	0.010 ± 0.002	5.4	-10^{-6}	SNe
3	70.115 ± 0.153	0.008 ± 0.007	12.1	-10^{-6}	SNe + BAOs
3	70.118 ± 0.131	0.011 ± 0.006	1.9	-10^{-7}	SNe
3	70.053 ± 0.150	0.007 ± 0.007	1.1	-10^{-7}	SNe + BAOs

Thus, the existence of this trend is, once again, confirmed, and it remains unexplained also in the modified gravity scenario. Indeed, a suitable modified gravity model which would be able to predict the observed trend of H_0 , would allow observing a flat profile of $H_0(z)$ after a binned analysis. Further analysis must be carried out with other Dark Energy models or other modified gravity theories to investigate this issue in the future, for instance focusing on the proposed model in Section 6.2.2.

Table 3. Fitting parameters of $H_0(z)$ for three bins within the Hu–Sawicki model, with SNe and SNe + BAOs by fixing several values of $\Omega_{0m} = 0.298, 0.303, 0.301, 0.305$ and values of $F_{R0} = -10^{-4}$ and $F_{R0} = -10^{-7}$. The columns are as follows: (1) the Ω_{0m} value; (2) \mathcal{H}_0 , (3) η , according to Equation (9); (4) how many σ s the evolutionary parameter η is compatible with zero (namely, η/σ_η); (5) F_{R0} ; (6) the sample used.

Hu–Sawicki Model, Results of the 3 Bins Analysis					
Ω_{0m}	\mathcal{H}_0	η	$\frac{\eta}{\sigma_\eta}$	F_{R0}	Sample
0.298	70.140 ± 0.045	0.011 ± 0.002	5.1	-10^{-7}	SNe
0.298	70.050 ± 0.126	0.007 ± 0.006	1.2	-10^{-7}	SNe + BAOs
0.303	70.088 ± 0.075	0.012 ± 0.004	3.0	-10^{-7}	SNe
0.303	70.004 ± 0.139	0.009 ± 0.007	1.3	-10^{-7}	SNe + BAOs
0.301	70.054 ± 0.056	0.009 ± 0.003	3.0	-10^{-7}	SNe
0.301	70.072 ± 0.170	0.010 ± 0.008	1.2	-10^{-7}	SNe + BAOs
0.305	70.048 ± 0.034	0.012 ± 0.002	6.0	-10^{-7}	SNe
0.305	70.004 ± 0.140	0.010 ± 0.007	1.4	-10^{-7}	SNe + BAOs
0.298	70.135 ± 0.080	0.009 ± 0.004	2.2	-10^{-4}	SNe
0.298	70.087 ± 0.155	0.009 ± 0.007	1.2	-10^{-4}	SNe + BAOs
0.303	70.096 ± 0.146	0.012 ± 0.007	1.7	-10^{-4}	SNe
0.303	70.044 ± 0.129	0.009 ± 0.006	1.5	-10^{-4}	SNe + BAOs
0.301	70.111 ± 0.158	0.012 ± 0.008	1.5	-10^{-4}	SNe
0.301	70.038 ± 0.170	0.009 ± 0.008	1.1	-10^{-4}	SNe + BAOs
0.305	70.074 ± 0.026	0.016 ± 0.001	16.0	-10^{-4}	SNe
0.305	70.028 ± 0.090	0.011 ± 0.004	2.4	-10^{-4}	SNe + BAOs

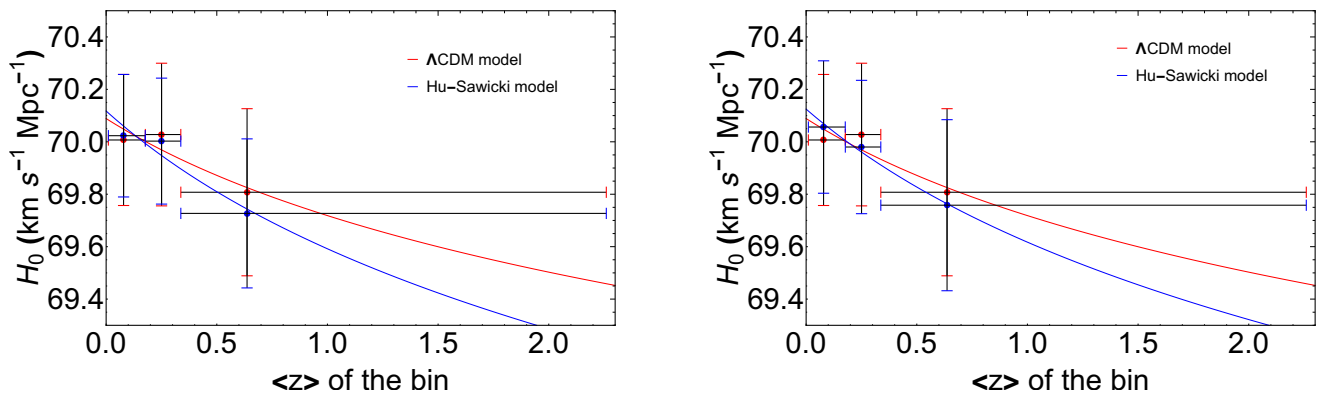


Figure 5. Cont.

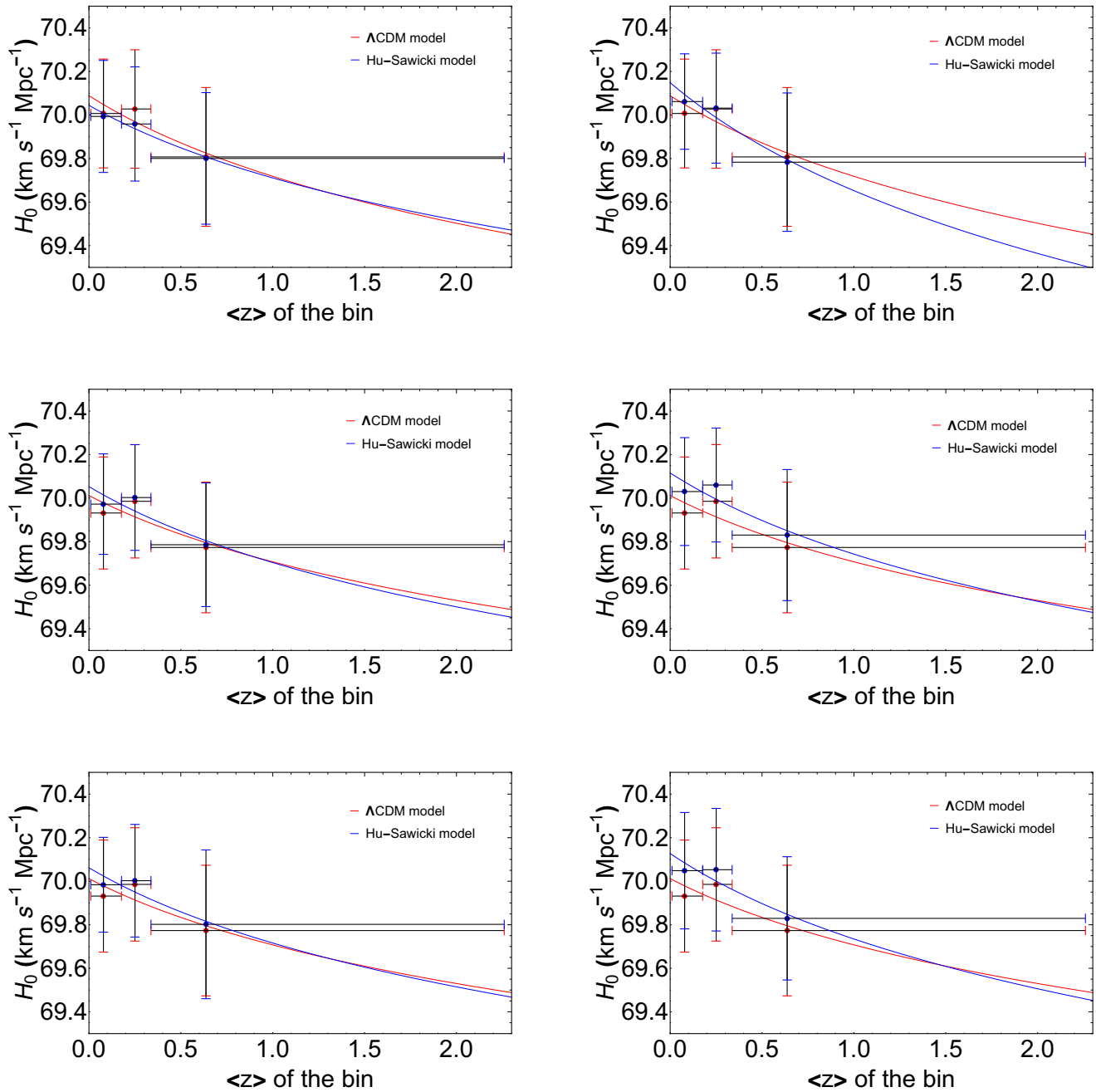


Figure 5. The first four panels deal with H_0 vs. z for SNe, the four bottom panels include BAO measurements for the H-S model. The upper 4 panels show from the left to the right $F_{R0} = -10^{-7}, -10^{-6}, -10^{-5}, -10^{-4}$, respectively. The standard Λ CDM cosmology is shown in red and the Hu-Sawicki model in blue. Analogously, the bottom panels have the same notation about the values of F_{R0} .

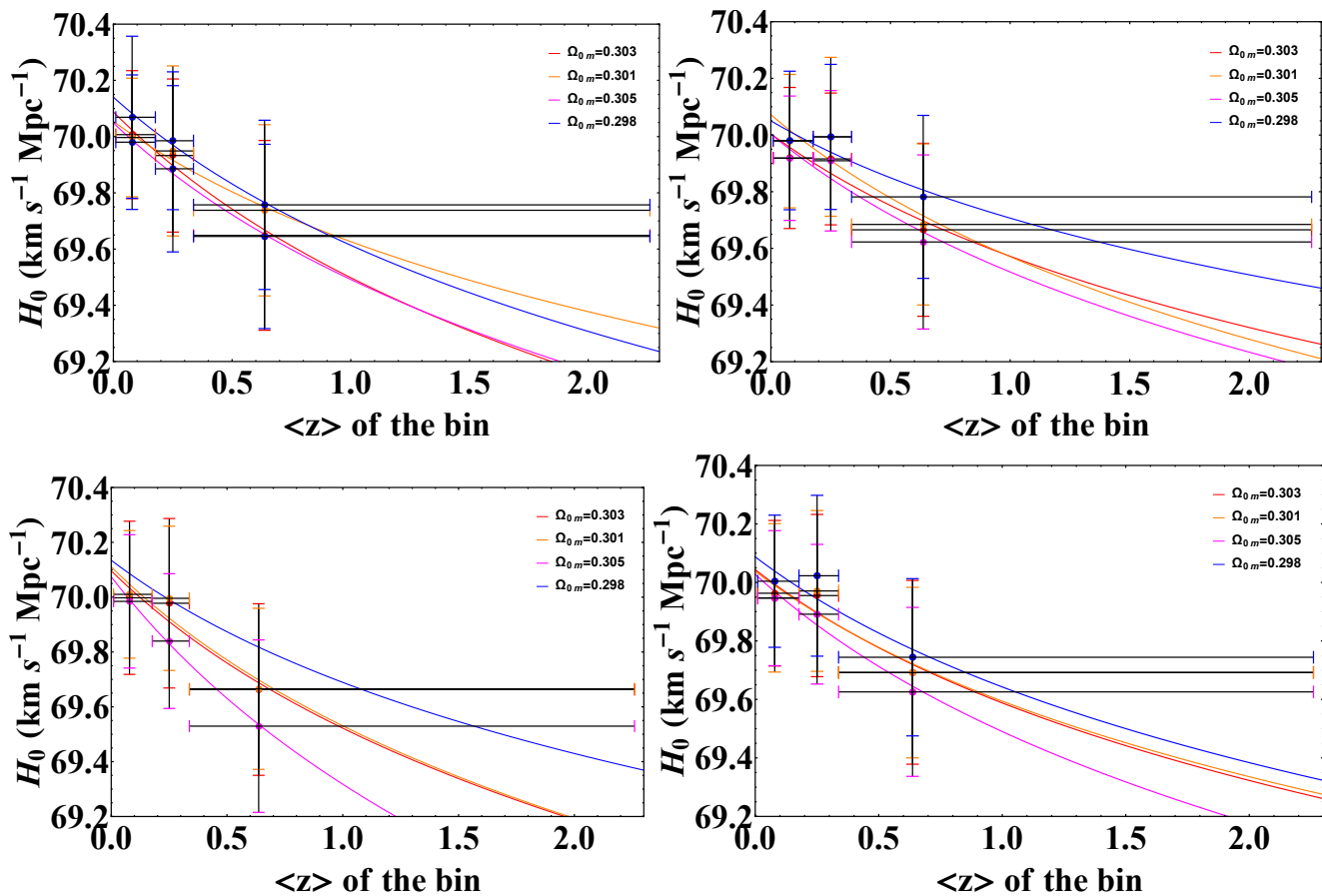


Figure 6. The Hubble constant versus redshift plots for the three bins of SNe Ia only, considering the Hu–Sawicki model. **Upper left panel.** The condition of $F_{R0} = -10^{-7}$ is applied to the case of SNe only, with the different values of $\Omega_{0m} = 0.301, 0.303, 0.305$. **Upper right panel.** The same of the upper left, but with the contribution of BAOs. **Lower left panel.** The SNe only case with the $F_{R0} = -10^{-4}$ condition, considering the different values of $\Omega_{0m} = 0.301, 0.303, 0.305$. **Lower right panel.** The same as the lower left, but with the contribution of BAOs. The orange color refers to $\Omega_{0m} = 0.301$, the red to $\Omega_{0m} = 0.303$, the magenta to $\Omega_{0m} = 0.305$, and the blue to $\Omega_{0m} = 0.298$.

8. Requirements for a Suitable $f(R)$ Model

Since the Hu–Sawicki model seems to be inadequate to account for the observed phenomenon of the decaying $H_0(z)$, in what follows, we provide some general properties that an $f(R)$ model in the JF must possess to induce the necessary scenario of a slowly varying Einstein constant. Now, we consider again the dynamical impact of the scalar field ϕ , related to the $f(R)$ function. Let us observe that the following relation holds in the following way:

$$\frac{d\phi}{dz} = -\frac{1}{1+z} \frac{\dot{\phi}}{H}. \quad (43)$$

In order to get the desired behavior $\phi \simeq (1+z)^{2\eta}$, we must deal with a dynamical regime where the following request is satisfied:

$$\frac{\dot{\phi}}{H} = -2\eta\phi. \quad (44)$$

We consider a slow-rolling evolution of the scalar field ϕ in the late universe, near enough to $\phi \simeq 1$. Then, we consider in Equation (19) $\rho \sim 0$, because we are in the Dark Energy dominated phase, and we consider $H_0 \dot{\phi}$ small with respect to the potential term $V(\phi \simeq 1)$. We neglect, also, the term $\ddot{\phi}$. Under these conditions, Equations (19) and (21) become

$$H^2 = \frac{V}{6\phi} \quad (45)$$

and

$$\frac{\dot{\phi}}{H} = \frac{1}{9H^2} \left(2V - \phi \frac{dV}{d\phi} \right), \quad (46)$$

respectively.

Referring to Equation (45) at $z \sim 0$, we make the identification $H_0^2 \equiv V(\phi \simeq 1)/6$. Hence, in order to reproduce Equation (44), we must require that for $\phi \rightarrow 1$, the following relation holds:

$$\eta = \frac{1}{3V} \left(\phi \frac{dV}{d\phi} - 2V \right). \quad (47)$$

The analysis above states the general features that a $f(R)$ model in the JF has to exhibit to provide a viable candidate to reproduce the observed decay behavior of $H_0(z)$ (Equ. 36). We conclude by observing that the picture depicted above relies on the concept of a slow-rolling phase of the scalar field, when it approaches the value $\phi \simeq 1$ and, in this respect, the potential term should have for such value a limiting dynamics, which remains there confined for a sufficiently long phase. It is just in such a limit that we are reproducing a Λ CDM model, but with the additional feature of a slowly varying Einstein constant. As far as the value of z increases, the deviation of the considered model from General Relativity becomes more important, but this effect is observed mainly in the gravity-matter coupling. In other words, the motion of the photon, as observed in the gravitational lensing, is not directly affected by the considered deviation, since the geodesic trajectories in the space-time do not directly feel the Einstein constant value. This consideration could allow for a large deviation of ϕ from the unity that is expected in studies of the photons' propagation.

8.1. An Example for Low Redshifts

As a viable example for the Dark Energy dominated Universe (slightly different from the traced above), we consider a potential term (and the associated slow-rolling phase) similar to the one adopted in the so-called chaotic inflation [389,390], i.e.:

$$V(\phi) = \delta + 6H_0^2\phi^2, \quad (48)$$

where δ is a positive constant, such that $\delta \ll 6H_0^2$. From Equation (45), we immediately get

$$H^2 \simeq H_0^2\phi \sim H_0^2, \quad (49)$$

where, we recall that we are considering the slow-rolling phase near $\phi \rightarrow 1$. Analogously, from Equation (47), we immediately get:

$$\eta \sim -\frac{\delta}{9H_0^2}. \quad (50)$$

The negative value of η is coherent with the behavior $H^2 \propto \phi$. Hence, we can reproduce the requested behavior of $\phi(z)$ by properly fixing the value of δ to get η as it comes out from the data analysis of Section 4. Specifically, we get $\delta \sim 10^{-3}H_0^2$ to have $\eta \sim 10^{-2}$.

Furthermore, it is easy to check that, for $\phi \rightarrow 1$, Equation (44) and Equation (49), we find the relation

$$\ddot{\phi} \sim |\eta| H_0 \dot{\phi} \ll 3H_0 \dot{\phi}, \quad (51)$$

which ensures that we are dealing with a real slow-rolling phase.

Finally, we compute the $f(R)$ function corresponding to the potential in Equation (48), recalling the relation (28):

$$f(R) = \frac{R^2}{24H_0^2} - \delta. \quad (52)$$

We conclude by observing that this specific model is reliable only as far the universe matter component is negligible, $z < 0.3$. The Einstein constant in front of the matter-energy density ρ would run as $(1+z)^{2\eta}$. The example above confirms that the $f(R)$ gravity in the JF is a possible candidate to account for the observed effect of $H_0(z)$, but the accomplishment of a satisfactory model for the whole Λ CDM phase requires a significant effort in further investigation, especially accounting for the constraints that observations in the local universe provided for modified gravity.

8.2. Discussion

Let us now try to summarize the physical insight that we can get from the analysis above, about the possible theoretical nature of the observed $H_0(z)$ behavior. We can keep as a reliably good starting point the idea that the origin of a modified scaling of the function $H(z)$ with respect to the standard Λ CDM model can be identified in a slowly varying Einstein constant with the redshift. Furthermore, it is a comparably good assumption to search, in the framework of a scalar-tensor formulation of gravity, the natural explanation for such a varying Einstein constant. As shown in Section 6.2, a scalar-tensor formulation can reproduce the required scaling of the function $H(z)$, which we observe as an $H_0(z)$ behavior in the standard Λ CDM model. Hence, we naturally explored one of the most interesting and well-motivated formulations of a scalar-tensor theory, namely the $f(R)$ gravity in the JF. In this respect, in Section 6.2.2, we first evaluated the form of the scalar field potential inferred from the observed decreasing trend of $H_0(z)$, and our data analysis suggested a model described in Equations (26) and (29). Then, we investigated if, one of the most reliable models for reproducing the Dark Energy effect with modified gravity, i.e., the Hu–Sawicki proposal, was able to induce the requested luminosity distance to somehow remove the observed effect, thus accounting for its physical nature. The non-positive result of this investigation leads us to explore theoretically the question of reproducing simultaneously the Dark Energy contribution and the observed $H_0(z)$ effect, by a single $f(R)$ model of gravity in the JF. In Section 8, it has been addressed this theoretical question, by establishing the conditions that a modified gravity model has to satisfy to reach the simultaneous aims mentioned above. Finally, we considered a specific model for the late universe, based on a slow-rolling picture for the scalar field near its today value $\phi \simeq 1$. This model was successful in explaining the Dark Energy contribution and the necessary variation of the Einstein constant, but it seems hard to be reconciled with the earlier Universe behavior, when the role of the matter contribution becomes relevant. Thus, based on this systematic analysis, we can conclude that the explanation for $H_0(z)$ is probably to be attributed to modified gravity dynamics, but it appears more natural to separate its effect from the existence of a Dark Energy contribution. In other words, we are led to believe that what we discovered about the SNe Ia+BAOs binned analysis must be regarded as a modified gravity physics of the scalar-tensor type, but leaving on a standard Universe, well represented by a Λ CDM model a priori.

9. Conclusions

We analyzed the PS together with the BAOs in three bins in both the Λ CDM and w_0w_a CDM models to investigate if an evolutionary trend of H_0 persists also with the contribution of BAOs and by varying two parameters contemporaneously with H_0 (Ω_{0m} and w_a for the Λ CDM and w_0w_a CDM, respectively). The persistence of the trend of H_0 as a function of redshift is also shown in the case of the Hu–Sawicki model. We here stress that the main goal of the current analysis is to highlight the reliability of the trend of $H_0(z)$ and not to further constrain Ω_{0m} or any other cosmological parameters. With the subsequent fitting of H_0 values through the model $g(z) = \mathcal{H}_0/(1+z)^\eta$, we obtain $\eta \sim 10^{-2}$, as in the previous work [51]: those are compatible with zero from 1.2 to 5.8 σ (see Table 1). The multidimensional results could reveal a dependence on the redshift of H_0 , assuming that it is observable at any redshift scale. If this evolution is not caused by statistical effects and other selection biases or hidden evolution of SNe Ia parameters [364], we show how $H_0(z)$ could modify the luminosity distance definition within the modified theory of gravity. If we consider a theoretical interpretation for the observed trend, new cosmological scenarios may explain an evolving Hubble constant with the redshift. For instance, we test in Section 6.2, and Section 7 a simple class of modified gravity theories given by the $f(R)$ models in the equivalent scalar-tensor formalism. In principle, this could be due to an effective varying Einstein constant governed by a slow evolution of a scalar field which mediates the gravity-matter interaction. However, the slow decreasing trend of H_0 has proven to be independent of the Hu–Sawicki model application. Indeed, if this theory had worked we would have observed the trend of the η parameter to be flattened out and be compatible with 0 in 1 σ at any redshift bin. This is not the case, thus new scenarios must be explored within the modified theories of gravity or slightly alternative approaches (see Sec. 8.2). We can state that this evolving trend of H_0 is independent of the starting values of the fitting for H_0 (we here have considered $H_0 = 70$) and, thus, on the fiducial M and on the redshift bins and even when we consider two cosmological parameters changing contemporaneously (Ω_{0m} and w_a in Λ CDM and w_0w_a CDM models, respectively). Thus, we need to further investigate the nature of this trend. In addition, the implementation of GRBs as cosmological probes together with SNe Ia and BAOs has proven to be not only possible in a near future but also necessary since the redshift range that GRBs cover is much larger than the one typical of SNe Ia. This last characteristic will surely allow GRBs to give further information on the nature of the early universe and pose new constraints in the future measurements of H_0 .

Author Contributions: M. G. D. performed the conceptualization of all project, data curation, formal analysis, methodology, writing original draft, validation, supervision, software. B. D. S. performed data curation, visualization, formal analysis, methodology, writing original draft, software. T. S. performed formal analysis, visualization, methodology, writing original draft on $f(R)$ and revised it, G. M. performed a partial conceptualization limited to the theoretical part of the $f(R)$ gravity theory; E. R. edited and review the analysis on $f(R)$ and participated in the general discussion and conceptualization of the paper. G. L. wrote Sec. 6.2.1 and gave suggestions on the cosmological constraints on w . M. B. performed the conceptualization on the priors to answer the referee report. S. U. performed a formal analysis on changing the parameters together with H_0 .

Funding: This research received no external funding.

Institutional Review Board Statement: Not applicable

Informed Consent Statement: Not applicable

Data Availability Statement: Not applicable

Acknowledgments: This work made use of Pantheon sample data [284], which can be found in the GitHub repository: <https://github.com/dscolnic/Pantheon> (accessed on 21 December 2020). This work made use of data supplied by the UK Swift Science Data Centre at the University of Leicester.

We are thankful to V. Nielson, A. Lenart, G. Sarracino, and D. Jyoti for their support on cosmological computations. T. S. is supported in part by INFN under the program TAsP (Theoretical Astroparticle Physics). G. Lambiase and B. De Simone acknowledge the support of INFN. T. S. acknowledges the support of the Department of Physics of the University of Pisa. M. G. Dainotti acknowledges the support from NAOJ and NAOJ—Division of Science.

Conflicts of Interest: The authors declare no conflict of interest.

Notes

¹ <https://github.com/dscolnic/Pantheon> (accessed on 21 December 2020).

² The code is available upon request.

References

1. Riess, A.G.; Filippenko, A.V.; Challis, P.; Clocchiatti, A.; Diercks, A.; Garnavich, P.M.; Gilliland, R.L.; Hogan, C.J.; Jha, S.; Kirshner, R.P.; et al. Observational Evidence from Supernovae for an Accelerating Universe and a Cosmological Constant. *Astron. J.* **1998**, *116*, 1009–1038, doi:10.1086/300499.
2. Perlmutter, S.; Aldering, G.; Goldhaber, G.; Knop, R.A.; Nugent, P.; Castro, P.G.; Deustua, S.; Fabbro, S.; Goobar, A.; Groom, D.E.; et al. Measurements of Ω and Λ from 42 High-Redshift Supernovae. *Astrophys. J.* **1999**, *517*, 565–586, doi:10.1086/307221.
3. Weinberg, S. The cosmological constant problem. *Rev. Mod. Phys.* **1989**, *61*, 1–23. doi:10.1103/RevModPhys.61.1.
4. Peebles, P.J.; Ratra, B. The cosmological constant and dark energy. *Rev. Mod. Phys.* **2003**, *75*, 559–606, doi:10.1103/RevModPhys.75.559.
5. Riess, A.G.; Casertano, S.; Yuan, W.; Macri, L.M.; Scolnic, D. Large Magellanic Cloud Cepheid Standards Provide a 1% Foundation for the Determination of the Hubble Constant and Stronger Evidence for Physics beyond Λ CDM. *Astrophys. J.* **2019**, *876*, 85, doi:10.3847/1538-4357/ab1422.
6. Camarena, D.; Marra, V. Local determination of the Hubble constant and the deceleration parameter. *Phys. Rev. Res.* **2020**, *2*, 013028, doi:10.1103/PhysRevResearch.2.013028.
7. Wong, K.C.; Suyu, S.H.; Chen, G.C.F.; Rusu, C.E.; Millon, M.; Sluse, D.; Bonvin, V.; Fassnacht, C.D.; Taubenberger, S.; Auger, M.W.; et al. H0LiCOW—XIII. A 2.4 per cent measurement of H_0 from lensed quasars: 5.3 σ tension between early- and late-Universe probes. *Mon. Not. R. Astron. Soc.* **2020**, *498*, 1420–1439, doi:10.1093/mnras/stz3094.
8. Gómez-Valent, A.; Amendola, L. H_0 from cosmic chronometers and Type Ia supernovae, with Gaussian Processes and the novel Weighted Polynomial Regression method. *J. Cosmol. Astropart. Phys.* **2018**, *2018*, 051, doi:10.1088/1475-7516/2018/04/051.
9. Reid, M.J.; Pesce, D.W.; Riess, A.G. An Improved Distance to NGC 4258 and Its Implications for the Hubble Constant. *Astrophys. J. Lett.* **2019**, *886*, L27, doi:10.3847/2041-8213/ab552d.
10. Collaboration, P.; Akrami, Y.; Arroja, F.; Ashdown, M.; Aumont, J.; Baccigalupi, C.; Ballardini, M.; Banday, A.J.; Barreiro, R.B.; Bartolo, N.; et al. Planck 2018 results. I. Overview and the cosmological legacy of Planck. *Astron. Astrophys.* **2020**, *641*, A6, doi:10.1051/0004-6361/201833910.
11. Rodney, S.A.; Riess, A.G.; Scolnic, D.M.; Jones, D.O.; Hemmati, S.; Molino, A.; McCully, C.; Mobasher, B.; Strolger, L.G.; Graur, O.; et al. Erratum: “Two SNe Ia at redshift ~ 2 : Improved Classification and redshift determination with medium-band infrared imaging” (2015, AJ, 150, 156). *Astron. J.* **2016**, *151*, 47. doi:10.3847/0004-6256/151/2/47.
12. Cucchiara, A.; Levan, A.J.; Fox, D.B.; Tanvir, N.R.; Ukwatta, T.N.; Berger, E.; Krühler, T.; Yoldaş, A.K.; Wu, X.F.; Toma, K.; et al. A photometric redshift $0.94 < z < 9.4$ for grb 090429B. *Astrophys. J.* **2011**, *736*, 7. doi:10.1088/0004-637x/736/1/7.
13. Wang, F.; Yang, J.; Fan, X.; Hennawi, J.F.; Barth, A.J.; Banados, E.; Bian, F.; Boutsia, K.; Connor, T.; Davies, F.B.; et al. A Luminous Quasar at Redshift 7.642. *Astrophys. J. Lett.* **2021**, *907*, L1. doi:10.3847/2041-8213/abd8c6.
14. Cardone, V.F.; Capozziello, S.; Dainotti, M.G. An updated gamma-ray bursts Hubble diagram. *Mon. Not. R. Astron. Soc.* **2009**, *400*, 775–790, doi:10.1111/j.1365-2966.2009.15456.x.
15. Cardone, V.F.; Dainotti, M.G.; Capozziello, S.; Willingale, R. Constraining cosmological parameters by gamma-ray burst X-ray afterglow light curves. *Mon. Not. R. Astron. Soc.* **2010**, *408*, 1181–1186, doi:10.1111/j.1365-2966.2010.17197.x.
16. Cardone, V.F.; Perillo, M.; Capozziello, S. Systematics in the gamma-ray burst Hubble diagram. *Mon. Not. R. Astron. Soc.* **2011**, *417*, 1672–1683, doi:10.1111/j.1365-2966.2011.19228.x.
17. Dainotti, M.G.; Cardone, V.F.; Piedipalumbo, E.; Capozziello, S. Slope evolution of GRB correlations and cosmology. *Mon. Not. R. Astron. Soc.* **2013**, *436*, 82–88, doi:10.1093/mnras/stt1516.
18. Postnikov, S.; Dainotti, M.G.; Hernandez, X.; Capozziello, S. Nonparametric Study of the Evolution of the Cosmological Equation of State with Snea, Bao, and High-Redshift Grbs. *Astrophys. J.* **2014**, *783*, 126. doi:10.1088/0004-637x/783/2/126.

19. Amati, L.; Frontera, F.; Tavani, M.; i not Zand, J.J.M.; Antonelli, A.; Costa, E.; Feroci, M.; Guidorzi, C.; Heise, J.; Masetti, N.; et al. Intrinsic spectra and energetics of BeppoSAX Gamma-Ray Bursts with known redshifts. *Astron. Astrophys.* **2002**, *390*, 81–89. doi:10.1051/0004-6361:20020722.
20. Yonetoku, D.; Murakami, T.; Nakamura, T.; Yamazaki, R.; Inoue, A.K.; Ioka, K. Gamma-Ray Burst Formation Rate Inferred from the Spectral Peak Energy–Peak Luminosity Relation. *Astrophys. J.* **2004**, *609*, 935–951. doi:10.1086/421285.
21. Ito, H.; Matsumoto, J.; Nagataki, S.; Warren, D.C.; Barkov, M.V.; Yonetoku, D. The photospheric origin of the Yonetoku relation in gamma-ray bursts. *Nat. Commun.* **2019**, *10*. doi:10.1038/s41467-019-09281-z.
22. Liang, E.; Zhang, B. Model-independent Multivariable Gamma-Ray Burst Luminosity Indicator and Its Possible Cosmological Implications. *Astrophys. J.* **2005**, *633*, 611–623. doi:10.1086/491594.
23. Ghirlanda, G.; Nava, L.; Ghisellini, G.. Spectral-luminosity relation within individual Fermi gamma rays bursts. *Astron. Astrophys.* **2010**, *511*, A43. doi:10.1051/0004-6361/200913134.
24. Dainotti, M.G.; Cardone, V.F.; Capozziello, S. A time-luminosity correlation for γ -ray bursts in the X-rays. *Mon. Not. R. Astron. Soc.: Letters* **2008**, *391*, L79–L83, doi:10.1111/j.1745-3933.2008.00560.x.
25. Dainotti, M.G.; Willingale, R.; Capozziello, S.; Cardone, V.F.; Ostrowski, M. Discovery of a Tight Correlation for Gamma-Ray Burst Afterglows with “Canonical” Light Curves. *Astrophys. J. Lett.* **2010**, *722*, L215–L219. doi:10.1088/2041-8205/722/2/L215.
26. Dainotti, M.G.; Cardone, V.F.; Capozziello, S.; Ostrowski, M.; Willingale, R. Study of possible systematics in the $L^*X - Ta^*$ correlation of Gamma Ray Bursts. *Astrophys. J.* **2011**, *730*, 135. doi:10.1088/0004-637x/730/2/135.
27. Dainotti, M.G.; Petrosian, V.; Singal, J.; Ostrowski, M. Determination of the intrinsic luminosity time correlation in the X-ray afterglows of gamma-ray bursts. *Astrophys. J.* **2013**, *774*, 157. doi:10.1088/0004-637x/774/2/157.
28. Dainotti, M.G.; Vecchio, R.D.; Shigehiro, N.; Capozziello, S. Selection effects in Gamma-Ray Burst Correlations: Consequences on the Ratio Between Gamma-Ray Burst And Star Formation rates. *Astrophys. J.* **2015**, *800*, 31. doi:10.1088/0004-637x/800/1/31.
29. Dainotti, M.; Petrosian, V.; Willingale, R.; O’Brien, P.; Ostrowski, M.; Nagataki, S. Luminosity–time and luminosity–luminosity correlations for GRB prompt and afterglow plateau emissions. *Mon. Not. R. Astron. Soc.* **2015**, *451*, 3898–3908, doi:10.1093/mnras/stv1229.
30. Dainotti, M.G.; Postnikov, S.; Hernandez, X.; Ostrowski, M. A fundamental Plane for Long Gamma-Ray Bursts with X-Ray plateaus. *Astrophys. J. Lett.* **2016**, *825*, L20. doi:10.3847/2041-8205/825/2/L20.
31. Dainotti, M.G.; Nagataki, S.; Maeda, K.; Postnikov, S.; Pian, E. A study of gamma ray bursts with afterglow plateau phases associated with supernovae. *Astron. Astrophys.* **2017**, *600*, A98. doi:10.1051/0004-6361/201628384.
32. Dainotti, M.G.; Hernandez, X.; Postnikov, S.; Nagataki, S.; O’Brien, P.; Willingale, R.; Striegel, S. A Study of the Gamma-Ray Burst Fundamental Plane. *Astrophys. J.* **2017**, *848*, 88. doi:10.3847/1538-4357/aa8a6b.
33. Dainotti, M.G.; Amati, L. Gamma-ray Burst Prompt Correlations: Selection and Instrumental Effects. *Astrophys. J.* **2018**, *130*, 051001. doi:10.1088/1538-3873/aaa8d7.
34. Dainotti, M.G.; Del Vecchio, R.; Tarnopolski, M. Gamma-Ray Burst Prompt Correlations. *Adv. Astron.* **2018**, *2018*, 1–31. doi:10.1155/2018/4969503.
35. Dainotti, M.G.; Lenart, A.L.; Sarracino, G.; Nagataki, S.; Capozziello, S.; Fraija, N. The X-Ray Fundamental Plane of the Platinum Sample, the Kilonovae, and the SNe Ib/c Associated with GRBs. *Astrophys. J.* **2020**, *904*, 97. doi:10.3847/1538-4357/abbe8a.
36. Dainotti, M.G.; Omodei, N.; Srinivasaragavan, G.P.; Vianello, G.; Willingale, R.; O’Brien, P.; Nagataki, S.; Petrosian, V.; Nuygen, Z.; Hernandez, X.; et al. On the Existence of the Plateau Emission in High-energy Gamma-Ray Burst Light Curves Observed by Fermi-LAT. *Astrophys. J. Suppl. Ser.* **2021**, *255*, 13. doi:10.3847/1538-4365/abfe17.
37. Dainotti, M.; Levine, D.; Fraija, N.; Chandra, P. Accounting for Selection Bias and Redshift Evolution in GRB Radio Afterglow Data. *Galaxies* **2021**, *9*, 95. doi:10.3390/galaxies9040095.
38. Del Vecchio, R.; Dainotti, M.G.; Ostrowski, M. Study of Grb Light-Curve Decay Indices in the Afterglow phase. *Astrophys. J.* **2016**, *828*, 36. doi:10.3847/0004-637x/828/1/36.
39. Duncan, R.C. Gamma-ray bursts from extragalactic Magnetar Flares. *AIP Conf. Proc.* **2001**. doi:10.1063/1.1419599.
40. Dall’Osso, S.; Granot, J.; Piran, T. Magnetic field decay in neutron stars: from soft gamma repeaters to “weak-field magnetars”. *Mon. Not. R. Astron. Soc.* **2012**, *422*, 2878–2903. doi:10.1111/j.1365-2966.2012.20612.x.
41. Rowlinson, A.; Gompertz, B.P.; Dainotti, M.; O’Brien, P.T.; Wijers, R.A.M.J.; van der Horst, A.J. Constraining properties of GRB magnetar central engines using the observed plateau luminosity and duration correlation. *Mon. Not. R. Astron. Soc.* **2014**, *443*, 1779–1787, doi:10.1093/mnras/stu1277.
42. Rea, N.; Gullón, M.; Pons, J.A.; Perna, R.; Dainotti, M.G.; Miralles, J.A.; Torres, D.F. Constraining The Grb-Magnetar Model By Means Of The Galactic Pulsar Population. *Astrophys. J.* **2015**, *813*, 92. doi:10.1088/0004-637x/813/2/92.
43. Stratta, G.; Dainotti, M.G.; Dall’Osso, S.; Hernandez, X.; Cesare, G.D. On the Magnetar Origin of the GRBs Presenting X-Ray Afterglow Plateaus. *Astrophys. J.* **2018**, *869*, 155. doi:10.3847/1538-4357/aadd8f.
44. Amati, L.; D’Agostino, R.; Luongo, O.; Muccino, M.; Tantalò, M. Addressing the circularity problem in the $E_p - E_{iso}$ correlation of gamma-ray bursts. *Mon. Not. R. Astron. Soc. Lett.* **2019**, *486*, L46–L51, doi:10.1093/mnrasl/slz056.

45. Liao, K.; Shafieloo, A.; Keeley, R.E.; Linder, E.V. A Model-independent Determination of the Hubble Constant from Lensed Quasars and Supernovae Using Gaussian Process Regression. *Astrophys. J. Lett.* **2019**, *886*, L23, doi:10.3847/2041-8213/ab5308.
46. Keeley, R.E.; Shafieloo, A.; Hazra, D.K.; Souradeep, T. Inflation wars: A new hope. *J. Cosmol. Astropart. Phys.* **2020**, *2020*, 055, doi:10.1088/1475-7516/2020/09/055.
47. Risaliti, G.; Lusso, E. Cosmological Constraints from the Hubble Diagram of Quasars at High Redshifts. *Nat. Astron.* **2019**, *3*, 272–277, doi:10.1038/s41550-018-0657-z.
48. Freedman, W.L.; Madore, B.F.; Hatt, D.; Hoyt, T.J.; Jang, I.S.; Beaton, R.L.; Burns, C.R.; Lee, M.G.; Monson, A.J.; Neeley, J.R.; et al. The Carnegie-Chicago Hubble Program. VIII. An Independent Determination of the Hubble Constant Based on the Tip of the Red Giant Branch. *Astrophys. J.* **2019**, *882*, 34, doi:10.3847/1538-4357/ab2f73.
49. Dutta, K.; Roy, A.; Ruchika.; Sen, A.A.; Sheikh-Jabbari, M.M. Cosmology with low-redshift observations: No signal for new physics. *Phys. Rev. D* **2019**, *100*, 103501, doi:10.1103/PhysRevD.100.103501.
50. Yang, T.; Banerjee, A.; Ó Colgáin, E. Cosmography and flat Λ CDM tensions at high redshift. *Phys. Rev. D* **2020**, *102*, 123532, doi:10.1103/PhysRevD.102.123532.
51. Dainotti, M.G.; De Simone, B.; Schiavone, T.; Montani, G.; Rinaldi, E.; Lambiase, G. On the Hubble Constant Tension in the SNe Ia Pantheon Sample. *Astrophys. J.* **2021**, *912*, 150, doi:10.3847/1538-4357/abeb73.
52. Ingram, A.; Mastroserio, G.; van der Klis, M.; Nathan, E.; Connors, R.; Dauser, T.; García, J.A.; Kara, E.; König, O.; Lucchini, M.; et al.
53. Agrawal, P.; Cyr-Racine, F.Y.; Pinner, D.; Randall, L. Rock ‘n’ Roll Solutions to the Hubble Tension. *arXiv* **2019**, arXiv:1904.01016, On measuring the Hubble constant with X-ray reverberation mapping of active galactic nuclei. *arXiv* **2021**, arXiv:2110.15651.
54. Arjona, R.; Espinosa-Portales, L.; García-Bellido, J.; Nesseris, S. A GREAT model comparison against the cosmological constant. *arXiv* **2021**, arXiv:2111.13083.
55. Fernandez-Martinez, E., Pierre, M., Pinsard, E. & Rosauro-Alcaraz, S. Inverse Seesaw, dark matter and the Hubble tension. *The European Physical Journal C.* **81** (2021,10), <http://dx.doi.org/10.1140/epjc/s10052-021-09760-y>
56. Ghose, S. & Bhadra, A. Is non-particle dark matter equation of state parameter evolving with time?. *The European Physical Journal C.* **81** (2021,8), <http://dx.doi.org/10.1140/epjc/s10052-021-09490-1>
57. Hart, L. & Chluba, J. Varying fundamental constants principal component analysis: additional hints about the Hubble tension. *Monthly Notices Of The Royal Astronomical Society.* **510**, 2206–2227 (2021,10), <http://dx.doi.org/10.1093/mnras/stab2777>
58. Beltrán Jiménez, J., Bettoni, D., Figueruelo, D., Teppa Pannia, F. & Tsujikawa, S. Probing elastic interactions in the dark sector and the role of S8. *Physical Review D.* **104** (2021,11), <http://dx.doi.org/10.1103/PhysRevD.104.103503>
59. Rezaei, M., Peracaula, J. & Malekjani, M. Cosmographic approach to Running Vacuum dark energy models: New constraints using BAOs and Hubble diagrams at higher redshifts. *Monthly Notices Of The Royal Astronomical Society.* (2021,11), <http://dx.doi.org/10.1093/mnras/stab3117>
60. Shah, P., Lemos, P. & Lahav, O. A buyer’s guide to the Hubble constant. *The Astronomy And Astrophysics Review.* **29** (2021,12), <http://dx.doi.org/10.1007/s00159-021-00137-4>
61. Firouzjahi, H. Cosmological constant problem on the horizon. (2022)
62. Banihashemi, A.; Khosravi, N.; Shafieloo, A. Dark energy as a critical phenomenon: a hint from Hubble tension. *J. Cosmol. Astropart. Phys.* **2021**, *2021*, 003. doi:10.1088/1475-7516/2021/06/003.
63. Ballardini, M.; Finelli, F.; Sapone, D. Cosmological constraints on Newton’s gravitational constant. *arXiv* **2021**, arXiv:2111.09168.
64. Corona, M.A.; Murgia, R.; Cadeddu, M.; Archidiacono, M.; Gariazzo, S.; Giunti, C.; Hannestad, S. Pseudoscalar sterile neutrino self-interactions in light of Planck, SPT and ACT data. *arXiv* **2021**, arXiv:astro-ph.CO/2112.00037.
65. Cyr-Racine, F.Y.; Ge, F.; Knox, L. A Symmetry of Cosmological Observables, and a High Hubble Constant as an Indicator of a Mirror World Dark Sector. *arXiv* **2021**, arXiv:astro-ph.CO/2107.13000.
66. Di Valentino, E.; Gariazzo, S.; Giunti, C.; Mena, O.; Pan, S.; Yang, W. Minimal dark energy: key to sterile neutrino and Hubble constant tensions? *arXiv* **2021**, arXiv:astro-ph.CO/2110.03990.
67. Di Valentino, E.; Melchiorri, A. Neutrino Mass Bounds in the era of Tension Cosmology. *arXiv* **2021**, arXiv:astro-ph.CO/2112.02993.
68. Drees, M.; Zhao, W. $U(1)_{L_\mu-L_\tau}$ for Light Dark Matter, $g_\mu - 2$, the 511 keV excess and the Hubble Tension. *arXiv* **2021**, arXiv:hep-ph/2107.14528.
69. Gu, Y.; Wu, L.; Zhu, B. Axion Dark Radiation and Late Decaying Dark Matter in Neutrino Experiment. *arXiv* **2021**, arXiv:hep-ph/2105.07232.
70. Khalifeh, A.R.; Jimenez, R. Using Neutrino Oscillations to Measure H_0 . *arXiv* **2021**, arXiv:astro-ph.CO/2111.15249.
71. Li, J.; Zhou, Y.; Xue, X. Spatial Curvature and Large Scale Lorentz Violation. *arXiv* **2021**, [arXiv:gr-qc/2112.02364.
72. Lulli, M.; Marciano, A.; Shan, X. Stochastic Quantization of General Relativity à la Ricci-Flow. *arXiv* **2021**, arXiv:gr-qc/2112.01490.
73. Mawas, E.; Street, L.; Gass, R.; Wijewardhana, L.C.R. Interacting dark energy axions in light of the Hubble tension. *arXiv* **2021**, arXiv:astro-ph.CO/2108.13317.
74. Moreno-Pulido, C.; Peracaula, J.S. Renormalized ρ_{vac} without m^4 terms. *arXiv* **2021**, arXiv:gr-qc/2110.08070.

75. Naidoo, K.; Massara, E.; Lahav, O. Cosmology and neutrino mass with the Minimum Spanning Tree. *arXiv* **2021**, arXiv:astro-ph.CO/2111.12088.
76. Niedermann, F.; Sloth, M.S. Hot New Early Dark Energy: Towards a Unified Dark Sector of Neutrinos, Dark Energy and Dark Matter. *arXiv* **2021**, arXiv:hep-ph/2112.00759.
77. Nilsson, N.A.; Park, M.I. Tests of Standard Cosmology in Horava Gravity. *arXiv* **2021**, arXiv:hep-th/2108.07986.
78. Ray, P.P.; Tarai, S.; Mishra, B.; Tripathy, S.K. Cosmological models with Big rip and Pseudo rip Scenarios in extended theory of gravity. *arXiv* **2021**, arXiv:gr-qc/2107.04413.
79. Schöneberg, N.; Abellán, G.F.; Sánchez, A.P.; Witte, S.J.; Poulin, V.; Lesgourgues, J. The H_0 Olympics: A fair ranking of proposed models. *arXiv* **2021**, arXiv:astro-ph.CO/2107.10291.
80. Trott, E.; Huterer, D. Challenges for the statistical gravitational-wave method to measure the Hubble constant. *arXiv* **2021**, arXiv:astro-ph.CO/2112.00241.
81. Ye, G.; Zhang, J.; Piao, Y.S. Resolving both H_0 and S_8 tensions with AdS early dark energy and ultralight axion. *arXiv* **2021**, arXiv:astro-ph.CO/2107.13391.
82. Zhou, Z.; Liu, G.; Xu, L. Can late dark energy restore the Cosmic concordance? *arXiv* **2021**, arXiv:astro-ph.CO/2105.04258.
83. Zhu, L.G.; Xie, L.H.; Hu, Y.M.; Liu, S.; Li, E.K.; Napolitano, N.R.; Tang, B.T.; Dong Zhang, J.; Mei, J. Constraining the Hubble constant to a precision of about 1% using multi-band dark standard siren detections. *arXiv* **2021**, arXiv:astro-ph.CO/2110.05224.
84. Alestas, G.; Perivolaropoulos, L.; Tanidis, K. Constraining a late time transition of G_{eff} using low- z galaxy survey data. *arXiv* **2022**, arXiv:astro-ph.CO/2201.05846.
85. Cea, P. The Ellipsoidal Universe and the Hubble tension. *arXiv* **2022**, arXiv:astro-ph.CO/2201.04548.
86. Gurzadyan, V.G.; Fimin, N.N.; Chechetkin, V.M. On the origin of cosmic web. *Eur. Phys. J. Plus* **2022**, *137*. doi:10.1140/epjp/s13360-022-02373-8.
87. Rashkovetskyi, M.; Muñoz, J.; Eisenstein, D. & Dvorkin, C. Small-scale clumping at recombination and the Hubble tension. *Physical Review D*. **104** (2021,11), <http://dx.doi.org/10.1103/PhysRevD.104.103517>
88. Das, A. Self-interacting neutrinos as a solution to the Hubble tension?. (2021)
89. Karwal, T. & Kamionkowski, M. Dark energy at early times, the Hubble parameter, and the string axiverse. *Physical Review D*. **94**, e103523 (2016,11)
90. Yang, W.; Pan, S.; Di Valentino, E.; Nunes, R.C.; Vagnozzi, S.; Mota, D.F. Tale of stable interacting dark energy, observational signatures, and the H_0 tension. *J. Cosmol. Astropart. Phys.* **2018**, *2018*, 019, doi:10.1088/1475-7516/2018/09/019.
91. Di Valentino, E.; Linder, E.V.; Melchiorri, A. Vacuum phase transition solves the H_0 tension. *Phys. Rev. D* **2018**, *97*, 043528, doi:10.1103/PhysRevD.97.043528.
92. Di Valentino, E.; Ferreira, R.Z.; Visinelli, L.; Danielsson, U. Late time transitions in the quintessence field and the H_0 tension. *Phys. Dark Univ.* **2019**, *26*, 100385, doi:10.1016/j.dark.2019.100385.
93. Pan, S.; Yang, W.; Di Valentino, E.; Shafieloo, A.; Chakraborty, S. Reconciling H_0 tension in a six parameter space? *J. Cosmol. Astropart. Phys.* **2020**, *2020*, 062, doi:10.1088/1475-7516/2020/06/062.
94. Di Valentino, E.; Anchordoqui, L.A.; Akarsu, O.; Ali-Haimoud, Y.; Amendola, L.; Arendse, N.; Asgari, M.; Ballardini, M.; Basilakos, S.; Battistelli, E.; et al. Snowmass2021 - Letter of interest cosmology intertwined I: Perspectives for the next decade. *Astropart. Phys.* **2021**, *131*, 102606. doi:10.1016/j.astropartphys.2021.102606.
95. Di Valentino, E.; Anchordoqui, L.A.; Akarsu, O.; Ali-Haimoud, Y.; Amendola, L.; Arendse, N.; Asgari, M.; Ballardini, M.; Basilakos, S.; Battistelli, E.; et al. Snowmass2021—Letter of interest cosmology intertwined II: The hubble constant tension. *Astropart. Phys.* **2021**, *131*, 102605. doi:10.1016/j.astropartphys.2021.102605.
96. Di Valentino, E.; Anchordoqui, L.A.; Akarsu, O.; Ali-Haimoud, Y.; Amendola, L.; Arendse, N.; Asgari, M.; Ballardini, M.; Basilakos, S.; Battistelli, E.; et al. Cosmology Intertwined III: $f\sigma_8$ and S_8 *Astropart. Phys.* **2021**, *131*, 102604. doi:10.1016/j.astropartphys.2021.102604.
97. Di Valentino, E.; Anchordoqui, L.A.; Akarsu, O.; Ali-Haimoud, Y.; Amendola, L.; Arendse, N.; Asgari, M.; Ballardini, M.; Basilakos, S.; Battistelli, E.; et al. Snowmass2021—Letter of interest cosmology intertwined IV: The age of the universe and its curvature. *Astropart. Phys.* **2021**, *131*, 102607. doi:10.1016/j.astropartphys.2021.102607.
98. Di Valentino, E.; Boehm, C.; Hivon, E.; Bouchet, F.R. Reducing the H_0 and σ_8 tensions with dark matter-neutrino interactions. *Phys. Rev. D* **2018**, *97*, 043513, doi:10.1103/PhysRevD.97.043513.
99. Di Valentino, E.; Pan, S.; Yang, W.; Anchordoqui, L.A. Touch of neutrinos on the vacuum metamorphosis: Is the H_0 solution back? *Phys. Rev. D* **2021**, *103*, 123527, doi:10.1103/PhysRevD.103.123527.
100. Anchordoqui, L.A.; Di Valentino, E.; Pan, S.; Yang, W. Dissecting the H_0 and S_8 tensions with Planck + BAO + supernova type Ia in multi-parameter cosmologies. *J. High Energy Astrophys.* **2021**, *32*, 28–64, doi:10.1016/j.jheap.2021.08.001.
101. Di Valentino, E.; Mukherjee, A.; Sen, A.A. Dark Energy with Phantom Crossing and the H_0 Tension. *Entropy* **2021**, *23*, 404, doi:10.3390/e23040404.
102. Di Valentino, E.; Linder, E.V.; Melchiorri, A. H_0 ex machina: Vacuum metamorphosis and beyond H_0 . *Phys. Dark Univ.* **2020**, *30*, 100733, doi:10.1016/j.dark.2020.100733.

103. Di Valentino, E.; Melchiorri, A.; Silk, J. Planck evidence for a closed Universe and a possible crisis for cosmology. *Nat. Astron.* **2020**, *4*, 196–203, doi:10.1038/s41550-019-0906-9.
104. Allali, I.J.; Hertzberg, M.P.; Rompineve, F. Dark sector to restore cosmological concordance. *Phys. Rev. D* **2021**, *104*, doi:10.1103/physrevd.104.1081303.
105. Anderson, R.I. Relativistic corrections for measuring Hubble's constant to 1% using stellar standard candles. *arXiv* **2021**, arXiv:astro-ph.CO/2108.09067.
106. Asghari, M.; Sheykhi, A. Observational constraints of the modified cosmology through Barrow entropy. *arXiv* **2021**, arXiv:gr-qc/2110.00059.
107. Brownsberger, S.; Brout, D.; Scolnic, D.; Stubbs, C.W.; Riess, A.G. The Pantheon+ Analysis: Dependence of Cosmological Constraints on Photometric-Zeropoint Uncertainties of Supernova Surveys. *arXiv* **2021**, arXiv:astro-ph.CO/2110.03486.
108. Cyr-Racine, F.Y. Cosmic Expansion: A mini review of the Hubble-Lemaitre tension. *arXiv* **2021**, arXiv:astro-ph.CO/2105.09409.
109. Khosravi, N.; Farhang, M. Phenomenological Gravitational Phase Transition: Early and Late Modifications. *arXiv* **2021**, arXiv:astro-ph.CO/2109.10725.
110. Mantz, A.B.; Morris, R.G.; Allen, S.W.; Canning, R.E.A.; Baumont, L.; Benson, B.; Bleem, L.E.; Ehlert, S.R.; Floyd, B.; Herbonnet, R.; et al. Cosmological constraints from gas mass fractions of massive, relaxed galaxy clusters. *Mon. Not. R. Astron. Soc.* **2021**, *510*, 131–145. doi:10.1093/mnras/stab3390.
111. Mortsell, E.; Goobar, A.; Johansson, J.; Dhawan, S. The Hubble Tension Bites the Dust: Sensitivity of the Hubble Constant Determination to Cepheid Color Calibration. *arXiv* **2021**, arXiv:astro-ph.CO/2105.11461.
112. Mortsell, E.; Goobar, A.; Johansson, J.; Dhawan, S. The Hubble Tension Revisited: Additional Local Distance Ladder Uncertainties. *arXiv* **2021**, arXiv:astro-ph.CO/2106.09400.
113. Theodoropoulos, A.; Perivolaropoulos, L. The Hubble Tension, the M Crisis of Late Time H(z) Deformation Models and the Reconstruction of Quintessence Lagrangians. *Universe* **2021**, *7*, 300, doi:10.3390/universe7080300.
114. Gómez-Valent, A. Measuring the sound horizon and absolute magnitude of SNIa by maximizing the consistency between low-redshift data sets. *arXiv* **2022**, arXiv:astro-ph.CO/2111.15450.
115. Pol, A.R.; Caprini, C.; Neronov, A.; Semikoz, D. The gravitational wave signal from primordial magnetic fields in the Pulsar Timing Array frequency band. *arXiv* **2022**, arXiv:astro-ph.CO/2201.05630.
116. Wong, J.H.W.; Shanks, T.; Metcalfe, N. The Local Hole: a galaxy under-density covering 90% of sky to 200 Mpc. *arXiv* **2022**, arXiv:astro-ph.CO/2107.08505.
117. Romaniello, M.; Riess, A.; Mancino, S.; Anderson, R.I.; Freudling, W.; Kudritzki, R.P.; Macri, L.; Mucciarelli, A.; Yuan, W. The iron and oxygen content of LMC Classical Cepheids and its implications for the Extragalactic Distance Scale and Hubble constant. *arXiv* **2021**, arXiv:astro-ph.CO/2110.08860.
118. Luu, H.N. Axi-Higgs cosmology: Cosmic Microwave Background and cosmological tensions. *arXiv* **2021**, arXiv:astro-ph.CO/2111.01347.
119. Alestas, G.; Kazantzidis, L.; Perivolaropoulos, L. w -M phantom transition at $z_t < 0.1$ as a resolution of the Hubble tension. *Phys. Rev. D* **2021**, *103*, 083517, doi:10.1103/PhysRevD.103.083517.
120. Sakr, Z.; Sapone, D. Can varying the gravitational constant alleviate the tensions? *arXiv* **2021**, arXiv:astro-ph.CO/2112.14173.
121. Wang, Y.Y.; Tang, S.P.; Li, X.Y.; Jin, Z.P.; Fan, Y.Z. Prospects of calibrating afterglow modeling of short GRBs with gravitational wave inclination angle measurements and resolving the Hubble constant tension with a GW/GRB association event. *arXiv* **2021**, arXiv:astro-ph.HE/2111.02027.
122. Safari, Z.; Rezazadeh, K.; Malekolkalami, B. Structure Formation in Dark Matter Particle Production Cosmology. *arXiv* **2022**, arXiv:astro-ph.CO/2201.05195.
123. Roth, M.M.; Jacoby, G.H.; Ciardullo, R.; Davis, B.D.; Chase, O.; Weilbacher, P.M. Towards Precision Cosmology With Improved PNLF Distances Using VLT-MUSE I. Methodology and Tests. *Astrophys. J.* **2021**, *916*, 21, doi:10.3847/1538-4357/ac02ca.
124. Gutiérrez-Luna, E.; Carvente, B.; Jaramillo, V.; Barranco, J.; Escamilla-Rivera, C.; Espinoza, C.; Mondragón, M.; Núñez, D. Scalar field dark matter with two components: Combined approach from particle physics and cosmology. *arXiv* **2021**, arXiv:astro-ph.CO/2110.10258.
125. Chang, C. Imprint of early dark energy in stochastic gravitational wave background. *Physical Review D.* **105** (2022,1), <http://dx.doi.org/10.1103/PhysRevD.105.023508>
126. Liu, S., Zhu, L., Hu, Y., Zhang, J. & Ji, M. Capability for detection of GW190521-like binary black holes with TianQin. *Physical Review D.* **105** (2022,1), <http://dx.doi.org/10.1103/PhysRevD.105.023019>
127. Farrugia, C., Sultana, J. & Mifsud, J. Spatial curvature in f(R) gravity. *Physical Review D.* **104** (2021,12), <http://dx.doi.org/10.1103/PhysRevD.104.123503>
128. Lu, W. & Qin, Y. New constraint of the Hubble constant by proper motions of radio components observed in AGN twin-jets. *Research In Astronomy And Astrophysics.* **21**, 261 (2021,11), <http://dx.doi.org/10.1088/1674-4527/21/10/261>
129. Greene, K. & Cyr-Racine, F. Hubble distancing: Focusing on distance measurements in cosmology, arXiv 2021, arXiv:2112.11567.

130. Borghi, N., Moresco, M. & Cimatti, A. Towards a Better Understanding of Cosmic Chronometers: A new measurement of $H(z)$ at $z \sim 0.7.$, arXiv 2021, arXiv:2110.04304.
131. Asencio, E.; Banik, I.; Kroupa, P. A massive blow for Λ CDM - the high redshift, mass, and collision velocity of the interacting galaxy cluster El Gordo contradicts concordance cosmology. *Mon. Not. R. Astron. Soc.* **2021**, *500*, 5249–5267, doi:10.1093/mnras/staa3441.
132. Javanmardi, B.; Mérand, A.; Kervella, P.; Breuval, L.; Gallenne, A.; Nardetto, N.; Gieren, W.; Pietrzyński, G.; Hocdé, V.; Borgniet, S. Inspecting the Cepheid Distance Ladder: the Hubble Space Telescope Distance to the SN Ia Host Galaxy NGC 5584. *Astrophys. J.* **2021**, *911*, 12, doi:10.3847/1538-4357/abe7e5.
133. Zhao, D.; Xia, J.Q. Constraining the anisotropy of the Universe with the X-ray and UV fluxes of quasars. *arXiv* **2021**, arXiv:2105.03965,
134. Thakur, R.K.; Singh, M.; Gupta, S.; Nigam, R. Cosmological Analysis using Panstarrs data: Hubble Constant and Direction Dependence. *arXiv* **2021**, arXiv:2105.14514,
135. Sharov, G.S.; Sinyakov, E.S. Cosmological models, observational data and tension in Hubble constant. *arXiv* **2020**, arXiv:2002.03599.
136. Vagnozzi, S.; Pacucci, F.; Loeb, A. Implications for the Hubble tension from the ages of the oldest astrophysical objects. *arXiv* **2021**, arXiv:2105.10421.
137. Staicova, D. Hints of the $H_0 - r_d$ tension in uncorrelated Baryon Acoustic Oscillations dataset. *arXiv* **2021**, arXiv:astro-ph.CO/2111.07907.
138. Krishnan, C.; Mohayaee, R.; Colgain, E.O.; Sheikh-Jabbari, M.M.; Yin, L. Hints of FLRW Breakdown from Supernovae. *arXiv* **2021**, arXiv:astro-ph.CO/2106.02532.
139. Li, B.; Shapiro, P.R. Precision cosmology and the stiff-amplified gravitational-wave background from inflation: NANOGrav, Advanced LIGO-Virgo and the Hubble tension. *J. Cosmol. Astropart. Phys.* **2021**, *2021*, 024. doi:10.1088/1475-7516/2021/10/024.
140. Mozzon, S.; Ashton, G.; Nuttall, L.K.; Williamson, A.R. Does non-stationary noise in LIGO and Virgo affect the estimation of H_0 ? *arXiv* **2021**, arXiv:astro-ph.CO/2110.11731.
141. Abbott, T.C.; Buffaz, E.; Vieira, N.; Cabero, M.; Haggard, D.; Mahabal, A.; McIver, J. GWSkyNet-Multi: A Machine Learning Multi-Class Classifier for LIGO-Virgo Public Alerts. *arXiv* **2021**, arXiv:astro-ph.IM/2111.04015.
142. Mehrabi, A.; Basilakos, S.; Tsiapi, P.; Plionis, M.; Terlevich, R.; Terlevich, E.; Moran, A.L.G.; Chavez, R.; Bresolin, F.; Arenas, D.F.; et al. Using our newest VLT-KMOS HII Galaxies and other cosmic tracers to test the Λ CDM tension. *Mon. Not. R. Astron. Soc.* **2021**, stab2915, doi:10.1093/mnras/stab2915.
143. Li, J.X.; Wu, F.Q.; Li, Y.C.; Gong, Y.; Chen, X.L. Cosmological constraint on Brans–Dicke Model. *Res. Astron. Astrophys.* **2015**, *15*, 2151–2163. doi:10.1088/1674-4527/15/12/003.
144. Freedman, W.L. Measurements of the Hubble Constant: Tensions in Perspective. *Astrophys. J.* **2021**, *919*, 16. doi:10.3847/1538-4357/ac0e95.
145. Wu, Q.; Zhang, G.Q.; Wang, F.Y. An 8% Determination of the Hubble Constant from localized Fast Radio Bursts. *arXiv* **2021**, arXiv:astro-ph.CO/2108.00581.
146. Perivolaropoulos, L.; Skara, F. Hubble tension or a transition of the Cepheid Sn Ia calibrator parameters? *arXiv* **2021**, arXiv:astro-ph.CO/2109.04406.
147. Horstmann, N.; Pietschke, Y.; Schwarz, D.J. Inference of the cosmic rest-frame from supernovae Ia. *arXiv* **2021**, arXiv:astro-ph.CO/2111.03055.
148. Ferree, N.C.; Bunn, E.F. Constraining H_0 Via Extragalactic Parallax. *arXiv* **2021**, arXiv:astro-ph.CO/2109.07529.
149. Luongo, O.; Muccino, M.; Colgáin, E.O.; Sheikh-Jabbari, M.M.; Yin, L. On Larger H_0 Values in the CMB Dipole Direction. *arXiv* **2021**, arXiv:astro-ph.CO/2108.13228.
150. de Souza, J.M.S.; Sturani, R.; Alcaniz, J. Cosmography with Standard Sirens from the Einstein Telescope. *arXiv* **2021**, arXiv:gr-qc/2110.13316.
151. Fang, Y.; Yang, H. Orbit Tomography of Binary Supermassive Black Holes with Very Long Baseline Interferometry. *arXiv* **2021**, arXiv:gr-qc/2111.00368.
152. Palmese, A.; Bom, C.R.; Mucesh, S.; Hartley, W.G. A standard siren measurement of the Hubble constant using gravitational wave events from the first three LIGO/Virgo observing runs and the DESI Legacy Survey. *arXiv* **2021**, arXiv:astro-ph.CO/2111.06445.
153. Yang, T.; Lee, H.M.; Cai, R.G.; Gil Choi, H.; Jung, S. Space-borne Atom Interferometric Gravitational Wave Detections II: Dark Sirens and Finding the One. *arXiv* **2021**, arXiv:gr-qc/2110.09967.
154. Gray, R.; Messenger, C.; Veitch, J. A Pixelated Approach to Galaxy Catalogue Incompleteness: Improving the Dark Siren Measurement of the Hubble Constant. *arXiv* **2021**, arXiv:astro-ph.CO/2111.04629.
155. Moresco, M.; et al. Unveiling the Universe with Emerging Cosmological Probes. *arXiv* **2022**, arXiv:astro-ph.CO/2201.07241.
156. Collaboration, T.L.S.; the Virgo Collaboration.; the KAGRA Collaboration.; Abbott, R.; Abe, H.; Acernese, F.; Ackley, K.; Adhikari, N.; et al.. Constraints on the cosmic expansion history from GWTC-3. *arXiv* **2021**, arXiv:2111.03604.
157. Nunes, R.C.; Pan, S.; Saridakis, E.N.; Abreu, E.M. New observational constraints on $f(R)$ gravity from cosmic chronometers. *J. Cosmol. Astropart. Phys.* **2017**, *2017*, 005–005. doi:10.1088/1475-7516/2017/01/005.

158. Nunes, R.C. Structure formation in $f(T)$ gravity and a solution for H_0 tension. *J. Cosmol. Astropart. Phys.* **2018**, *2018*, 052–052. doi:10.1088/1475-7516/2018/05/052.
159. Benetti, M.; Capozziello, S.; Lambiase, G. Updating constraints on $f(T)$ teleparallel cosmology and the consistency with big bang nucleosynthesis. *Mon. Not. R. Astron. Soc.* **2020**, *500*, 1795–1805, doi:10.1093/mnras/staa3368.
160. Räsänen, S. Light propagation in statistically homogeneous and isotropic dust universes. *J. Cosmol. Astropart. Phys.* **2009**, *2009*, 011. doi:10.1088/1475-7516/2009/02/011.
161. Räsänen, S. Light propagation in statistically homogeneous and isotropic universes with general matter content. *J. Cosmol. Astropart. Phys.* **2010**, *2010*, 018. doi:10.1088/1475-7516/2010/03/018.
162. Sotiriou, T.P. $f(R)$ gravity and scalar tensor theory. *Class. Quantum Gravity* **2006**, *23*, 5117–5128, doi:10.1088/0264-9381/23/17/003.
163. Nojiri, S.; Odintsov, S.D. Introduction to modified gravity and gravitational alternative for dark energy. *Int. J. Geom. Methods Mod. Phys.* **2007**, *04*, 115–145, doi:10.1142/S0219887807001928.
164. Koksang, S.M. Towards statistically homogeneous and isotropic perfect fluid universes with cosmic backreaction. *Class. Quantum Gravity* **2019**, *36*, 185004. doi:10.1088/1361-6382/ab376c.
165. Koksang, S. Another look at redshift drift and the backreaction conjecture. *J. Cosmol. Astropart. Phys.* **2019**, *2019*, 036. doi:10.1088/1475-7516/2019/10/036.
166. Koksang, S.M. Observations in statistically homogeneous, locally inhomogeneous cosmological toy-models without FLRW backgrounds. *arXiv* **2020**, arXiv:astro-ph.CO/2008.07108.
167. Sotiriou, T.P.; Faraoni, V. $f(R)$ theories of gravity. *Rev. Mod. Phys.* **2010**, *82*, 451–497. doi:10.1103/RevModPhys.82.451.
168. Odderskov, I.; Koksang, S.; Hannestad, S. The local value of H_0 in an inhomogeneous universe. *J. Cosmol. Astropart. Phys.* **2016**, *2016*, 001. doi:10.1088/1475-7516/2016/02/001.
169. Nájera, A.; Fajardo, A. Testing $f(Q, T)$ gravity models that have Λ CDM as a submodel. *arXiv* **2021**, arXiv:2104.14065.
170. Nájera, A.; Fajardo, A. Fitting $f(Q, T)$ gravity models with a Λ CDM limit using $H(z)$ and Pantheon data. *Phys. Dark Univ.* **2021**, *34*, 100889. doi:10.1016/j.dark.2021.100889.
171. Nájera, A.; Fajardo, A. Cosmological Perturbation Theory in $f(Q, T)$ Gravity. *arXiv* **2021**, arXiv:gr-qc/2111.04205.
172. Linares Cedeño, F.X.; Nucamendi, U. Revisiting cosmological diffusion models in Unimodular Gravity and the H_0 tension. *Phys. Dark Univ.* **2021**, *32*, 100807, doi:10.1016/j.dark.2021.100807.
173. Fung, L.W.; Li, L.; Liu, T.; Luu, H.N.; Qiu, Y.C.; Tye, S.H.H. The Hubble Constant in the Axi-Higgs Universe. *arXiv* **2021**, arXiv:astro-ph.CO/2105.01631.
174. Shokri, M.; Sadeghi, J.; Setare, M.R.; Capozziello, S. Nonminimal coupling inflation with constant slow roll. *arXiv* **2021**, arXiv:2104.00596.
175. Castellano, A.; Font, A.; Herraes, A.; Ibáñez, L.E. A Gravitino Distance Conjecture. *arXiv* **2021**, arXiv:2104.10181.
176. Tomita, K. Cosmological renormalization of model parameters in second-order perturbation theory. *Prog. Theor. Exp. Phys.* **2017**, *2017*, 053E01, doi:10.1093/ptep/ptx049.
177. Tomita, K. Cosmological models with the energy density of random fluctuations and the Hubble-constant problem. *Prog. Theor. Exp. Phys.* **2017**, *2017*, 083E04, doi:10.1093/ptep/ptx117.
178. Tomita, K. Super-horizon second-order perturbations for cosmological random fluctuations and the Hubble-constant problem. *Prog. Theor. Exp. Phys.* **2018**, *2018*, 021E01, doi:10.1093/ptep/pty015.
179. Tomita, K. Hubble constants and luminosity distance in the renormalized cosmological models due to general-relativistic second-order perturbations. *arXiv* **2019**, arXiv:1906.09519.
180. Tomita, K. Cosmological renormalization of model parameters in the second-order perturbation theory. *Prog. Theor. Exp. Phys.* **2020**, *2020*, 019202. doi:10.1093/ptep/ptz162.
181. Belgacem, E.; Prokopec, T. Quantum origin of dark energy and the Hubble tension. *arXiv* **2021**, arXiv:astro-ph.CO/2111.04803.
182. Bernardo, R.C.; Grandón, D.; Said, J.L.; Cárdenas, V.H. Parametric and nonparametric methods hint dark energy evolution. *arXiv* **2022**, arXiv:astro-ph.CO/2111.08289.
183. Ambjorn, J.; Watabiki, Y. Easing the Hubble constant tension? *arXiv* **2021**, arXiv:gr-qc/2111.05087.
184. Di Bari, P.; Marfatia, D.; Zhou, Y.L. Gravitational waves from first-order phase transitions in Majoron models of neutrino mass. *arXiv* **2021**, arXiv:2106.00025.
185. Duan, W.F.; Li, S.P.; Li, X.Q.; Yang, Y.D. Linking $R_{K^{(*)}}$ anomalies to H_0 tension via Dirac neutrino. *arXiv* **2021**, arXiv:hep-ph/2111.05178.
186. Ghosh, D. Explaining the R_K and R_{K^*} anomalies. *Eur. Phys. J. C* **2017**, *77*. doi:10.1140/epjc/s10052-017-5282-y.
187. Burgess, C.P.; Dineen, D.; Quevedo, F. Yoga Dark Energy: Natural Relaxation and Other Dark Implications of a Supersymmetric Gravity Sector. *arXiv* **2021**, arXiv:hep-th/2111.07286.
188. Jiang, J.Q.; Piao, Y.S. Testing AdS early dark energy with Planck, SPTpol and LSS data. *arXiv* **2021**, arXiv:astro-ph.CO/2107.07128.
189. Karwal, T.; Raveri, M.; Jain, B.; Khoury, J.; Trodden, M. Chameleon Early Dark Energy and the Hubble Tension. *arXiv* **2021**, arXiv:astro-ph.CO/2106.13290.

190. Nojiri, S.; Odintsov, S.D.; Sáez-Chillón Gómez, D.; Sharov, G.S. Modeling and testing the equation of state for (Early) dark energy. *Phys. Dark Univ.* **2021**, *32*, 100837. <https://doi.org/10.1016/j.dark.2021.100837>.
191. Tian, S.X.; Zhu, Z.H. Early dark energy in k-essence. *Phys. Rev. D* **2021**, *103*, 043518, doi:10.1103/PhysRevD.103.043518.
192. Linares Cedeño, F.X.; Roy, N.; Ureña-López, L.A. Tracker phantom field and a cosmological constant: dynamics of a composite dark energy model. *arXiv* **2021**, arXiv:2105.07103.
193. Hernández-Almada, A.; Leon, G.; Magaña, J.; García-Aspeitia, M.A.; Motta, V.; Saridakis, E.N.; Yesmakhanova, K. Kaniadakis holographic dark energy: observational constraints and global dynamics. *arXiv* **2021**, arXiv:astro-ph.CO/2111.00558.
194. Hernández-Almada, A.; García-Aspeitia, M.A.; Rodríguez-Meza, M.A.; Motta, V. A hybrid model of viscous and Chaplygin gas to tackle the Universe acceleration. *Eur. Phys. J. C* **2021**, *81*, 295, doi:10.1140/epjc/s10052-021-09104-w.
195. Abchouyeh, M.A.; van Putten, M.H.P.M. Late-time Universe, H_0 -tension, and unparticles. *Phys. Rev. D* **2021**, *104*, 083511. doi:10.1103/PhysRevD.104.083511.
196. Wang, D. Dark energy constraints in light of Pantheon SNe Ia, BAO, cosmic chronometers and CMB polarization and lensing data. *Phys. Rev. D* **2018**, *97*, 123507, doi:10.1103/PhysRevD.97.123507.
197. Ye, G.; Hu, B.; Piao, Y.S. Implication of the Hubble tension for the primordial Universe in light of recent cosmological data. *Phys. Rev. D* **2021**, *104*, 063510. doi:10.1103/PhysRevD.104.063510.
198. Nguyen, H. Analyzing Pantheon SNe Ia data in the context of Barrow's variable speed of light. *arXiv* **2020**, arXiv:2010.10292.
199. Barrow, J.D. Cosmologies with varying light speed. *Phys. Rev. D* **1999**, *59*, 043515, doi:10.1103/PhysRevD.59.043515.
200. Artymowski, M.; Ben-Dayan, I.; Kumar, U. More on Emergent Dark Energy from Unparticles. *arXiv* **2021**, arXiv:astro-ph.CO/2111.09946.
201. Yang, W.; Di Valentino, E.; Pan, S.; Shafieloo, A.; Li, X. Generalized Emergent Dark Energy Model and the Hubble Constant Tension. *arXiv* **2021**, arXiv:2103.03815.
202. Adil, S.A.; Gangopadhyay, M.R.; Sami, M.; Sharma, M.K. Late time acceleration due to generic modification of gravity and Hubble tension. *arXiv* **2021**, arXiv:2106.03093.
203. Vagnozzi, S. Consistency tests of Λ CDM from the early ISW effect: implications for early-time new physics and the Hubble tension. *arXiv* **2021**, arXiv:2105.10425.
204. Alestas, G.; Kazantzidis, L.; Perivolaropoulos, L. H_0 tension, phantom dark energy, and cosmological parameter degeneracies. *Phys. Rev. D* **2020**, *101*, 123516, doi:10.1103/PhysRevD.101.123516.
205. Kazantzidis, L.; Koo, H.; Nesseris, S.; Perivolaropoulos, L.; Shafieloo, A. Hints for possible low redshift oscillation around the best-fitting Λ CDM model in the expansion history of the Universe. *Mon. Not. R. Astron. Soc.* **2021**, *501*, 3421–3426, doi:10.1093/mnras/staa3866.
206. Martín, M.S.; Rubio, C. Hubble tension and matter inhomogeneities: A theoretical perspective. *arXiv* **2021**, arXiv:astro-ph.CO/2107.14377.
207. Buchert, T. On Average Properties of Inhomogeneous Fluids in General Relativity: Dust Cosmologies. *Gen. Relativ. Gravit.* **2000**, *32*, 105–125. doi:10.1023/a:1001800617177.
208. Gasperini, M.; Marozzi, G.; Veneziano, G. Gauge invariant averages for the cosmological backreaction. *J. Cosmol. Astropart. Phys.* **2009**, *2009*, 011–011. doi:10.1088/1475-7516/2009/03/011.
209. Gasperini, M.; Marozzi, G.; Nugier, F.; Veneziano, G. Light-cone averaging in cosmology: formalism and applications. *J. Cosmol. Astropart. Phys.* **2011**, *2011*, 008–008. doi:10.1088/1475-7516/2011/07/008.
210. Fanizza, G.; Gasperini, M.; Marozzi, G.; Veneziano, G. Generalized covariant prescriptions for averaging cosmological observables. *J. Cosmol. Astropart. Phys.* **2020**, *2020*, 017–017. doi:10.1088/1475-7516/2020/02/017.
211. Ben-Dayan, I.; Gasperini, M.; Marozzi, G.; Nugier, F.; Veneziano, G. Average and dispersion of the luminosity-redshift relation in the concordance model. *J. Cosmol. Astropart. Phys.* **2013**, *2013*, 002–002. doi:10.1088/1475-7516/2013/06/002.
212. Fleury, P.; Clarkson, C.; Maartens, R. How does the cosmic large-scale structure bias the Hubble diagram? *J. Cosmol. Astropart. Phys.* **2017**, *2017*, 062–062. doi:10.1088/1475-7516/2017/03/062.
213. Adamek, J.; Clarkson, C.; Coates, L.; Durrer, R.; Kunz, M. Bias and scatter in the Hubble diagram from cosmological large-scale structure. *Phys. Rev. D* **2019**, *100*, 021301. doi:10.1103/PhysRevD.100.021301.
214. Amendola, L.; Appleby, S.; Avgoustidis, A.; Bacon, D.; Baker, T.; Baldi, M.; Bartolo, N.; Blanchard, A.; Bonvin, C.; Borgani, S.; et al. Cosmology and fundamental physics with the Euclid satellite. *Living Rev. Relativ.* **2018**, *21*. doi:10.1007/s41114-017-0010-3.
215. Fanizza, G. Precision Cosmology and Hubble tension in the era of LSS survey. *arXiv* **2021**, arXiv:astro-ph.CO/2110.15272.
216. Andreoni, I.; Margutti, R.; Salafia, O.S.; Parazin, B.; Villar, V.A.; Coughlin, M.W.; Yoachim, P.; Mortensen, K.; Brethauer, D.; Smartt, S.J.; et al. Target of Opportunity Observations of Gravitational Wave Events with Vera C. Rubin Observatory. *arXiv* **2021**, arXiv:astro-ph.HE/2111.01945.
217. Ben-Dayan, I.; Durrer, R.; Marozzi, G.; Schwarz, D.J. Value of H_0 in the Inhomogeneous Universe. *Phys. Rev. Lett.* **2014**, *112*, 221301, doi:10.1103/PhysRevLett.112.221301.

218. Fanizza, G.; Fiorini, B.; Marozzi, G. Cosmic variance of H_0 in light of forthcoming high-redshift surveys. *Phys. Rev. D* **2021**, *104*, 083506. doi:10.1103/PhysRevD.104.083506.
219. Haslbauer, M.; Banik, I.; Kroupa, P. The KBC void and Hubble tension contradict Λ CDM on a Gpc scale—Milgromian dynamics as a possible solution. *Mon. Not. R. Astron. Soc.* **2020**, *499*, 2845–2883, doi:10.1093/mnras/staa2348.
220. Perivolaropoulos, L. Large Scale Cosmological Anomalies and Inhomogeneous Dark Energy. *arXiv* **2014**, arXiv:astro-ph.CO/1401.5044.
221. Castello, S.; Höggås, M.; Mörtzell, E. A Cosmological Underdensity Does Not Solve the Hubble Tension. *arXiv* **2021**, arXiv:astro-ph.CO/2110.04226.
222. Banik, I.; Zhao, H. From galactic bars to the Hubble tension—Weighing up the astrophysical evidence for Milgromian gravity. *arXiv* **2021**, arXiv:astro-ph.CO/2110.06936.
223. Alestas, G.; Perivolaropoulos, L. Late-time approaches to the Hubble tension deforming $H(z)$, worsen the growth tension. *Mon. Not. R. Astron. Soc.* **2021**, *504*, 3956–3962, doi:10.1093/mnras/stab1070.
224. Normann, B.D.; Brevik, I.H. Can the Hubble tension be resolved by bulk viscosity? *Mod. Phys. Lett. A* **2021**, *36*, 2150198, doi:10.1142/S0217732321501984.
225. Bernal, J.L.; Verde, L.; Jimenez, R.; Kamionkowski, M.; Valcin, D.; Wandelt, B.D. Trouble beyond H_0 and the new cosmic triangles. *Phys. Rev. D* **2021**, *103*, 103533, doi:10.1103/PhysRevD.103.103533.
226. Thiele, L.; Guan, Y.; Hill, J.C.; Kosowsky, A.; Spergel, D.N. Can small-scale baryon inhomogeneities resolve the Hubble tension? An investigation with ACT DR4. *arXiv* **2021**, arXiv:2105.03003.
227. Grande, J.; Perivolaropoulos, L. Generalized Lemaitre-Tolman-Bondi model with inhomogeneous isotropic dark energy: Observational constraints. *Phys. Rev. D* **2011**, *84*, 023514, doi:10.1103/PhysRevD.84.023514.
228. Dinda, B.R. Cosmic expansion parametrization: Implication for curvature and H_0 tension. *arXiv* **2021**, arXiv:2106.02963.
229. Marra, V.; Perivolaropoulos, L. Rapid transition of G_{eff} at $z_t \approx 0.01$ as a possible solution of the Hubble and growth tensions. *Phys. Rev. D* **2021**, *104*, doi:10.1103/physrevd.104.1021303.
230. Krishnan, C.; Colgáin, E.Ó.; Ruchika, Sen, A.A.; Sheikh-Jabbari, M.M.; Yang, T. Is there an early Universe solution to Hubble tension? *Phys. Rev. D* **2020**, *102*, 103525, doi:10.1103/PhysRevD.102.103525.
231. Krishnan, C.; O Colgain, E.; Sheikh-Jabbari, M.M.; Yang, T. Running Hubble tension and a H_0 diagnostic. *Phys. Rev. D* **2021**, *103*, 103509. doi:10.1103/PhysRevD.103.103509.
232. Krishnan, C.; Mohayaee, R.; Colgáin, E.Ó.; Sheikh-Jabbari, M.M.; Yin, L. Does Hubble Tension Signal a Breakdown in FLRW Cosmology? *arXiv* **2021**, arXiv:2105.09790..
233. Robertson, H.P. Kinematics and World-Structure. *Astrophys. J.* **1935**, *82*, 284. doi:10.1086/143681.
234. Gerardi, F.; Feeney, S.M.; Alsing, J. Unbiased likelihood-free inference of the Hubble constant from light standard sirens. *arXiv* **2021**, arXiv:2104.02728.
235. Escamilla-Rivera, C.; Levi Said, J.; Mifsud, J. Performance of Non-Parametric Reconstruction Techniques in the Late-Time Universe. *arXiv* **2021**, arXiv:2105.14332.
236. Sun, W.; Jiao, K.; Zhang, T.J. Influence of the Bounds of the Hyperparameters on the Reconstruction of Hubble Constant with Gaussian Process. *arXiv* **2021**, arXiv:astro-ph.CO/2105.12618.
237. Renzi, F.; Silvestri, A. A look at the Hubble speed from first principles. *arXiv* **2020**, arXiv:astro-ph.CO/2011.10559.
238. Gurzadyan, V.G.; Stepanian, A. Hubble tension vs. two flows. *Eur. Phys. J. Plus* **2021**, *136*, doi:10.1140/epjp/s13360-021-01229-x.
239. Geng, C.Q.; Hsu, Y.T.; Lu, J.R.; Yin, L. A Dark Energy model from Generalized Proca Theory. *Phys. Dark Univ.* **2021**, *32*, 100819, doi:10.1016/j.dark.2021.100819.
240. Reyes, M.; Escamilla-Rivera, C. Improving data-driven model-independent reconstructions and updated constraints on dark energy models from Horndeski cosmology. *arXiv* **2021**, arXiv:2104.04484. doi:10.1088/1475-7516/2021/07/048.
241. Petronikolou, M.; Basilakos, S.; Saridakis, E.N. Alleviating H_0 tension in Horndeski gravity. *arXiv* **2021**, arXiv:gr-qc/2110.01338.
242. Alestas, G.; Antoniou, I.; Perivolaropoulos, L. Hints for a Gravitational Transition in Tully–Fisher Data. *Universe* **2021**, *7*, 366. doi:10.3390/universe7100366.
243. Benisty, D.; Staicova, D. A preference for Dynamical Dark Energy? *arXiv* **2021**, arXiv:astro-ph.CO/2107.14129.
244. Ó Colgáin, E.; Sheikh-Jabbari, M.; Yin, L. Can dark energy be dynamical? *Phys. Rev. D* **2021**, *104*, doi:10.1103/physrevd.104.023510.
245. Chevallier, M.; Polarski, D. Accelerating Universes with Scaling Dark Matter. *Int. J. Mod. Phys. D* **2001**, *10*, 213–223, doi:10.1142/S0218271801000822.
246. Linder, E.V. Exploring the Expansion History of the Universe. *Phys. Rev. Lett.* **2003**, *90*, 091301, doi:10.1103/PhysRevLett.90.091301.
247. Aloni, D.; Berlin, A.; Joseph, M.; Schmaltz, M.; Weiner, N. A Step in Understanding the Hubble Tension. *arXiv* **2021**, arXiv:astro-ph.CO/2111.00014.
248. Ghosh, S.; Kumar, S.; Tsai, Y. Free-streaming and Coupled Dark Radiation Isocurvature Perturbations: Constraints and Application to the Hubble Tension. *arXiv* **2021**, arXiv:astro-ph.CO/2107.09076.
249. Shrivastava, P.; Khan, A.J.; Goswami, G.K.; Yadav, A.K.; Singh, J.K. The simplest parametrization of equation of state parameter in the scalar field Universe. *arXiv* **2021**, arXiv:astro-ph.CO/2107.05044.

250. Pereira, S.H. An unified cosmological model driven by a scalar field nonminimally coupled to gravity. *arXiv* **2021**, arXiv:astro-ph.CO/2111.00029.
251. Bag, S.; Sahni, V.; Shafieloo, A.; Shtanov, Y. Phantom braneworld and the Hubble tension. *arXiv* **2021**, arXiv:astro-ph.CO/2107.03271.
252. Franchino-Viñas, S.A.; Mosquera, M.E. The cosmological lithium problem, varying constants and the H_0 tension. *arXiv* **2021**, arXiv:astro-ph.CO/2107.02243.
253. Palle, D. Einstein–Cartan cosmology and the high-redshift Universe. *arXiv* **2021**, arXiv:physics.gen-ph/2106.08136.
254. Liu, W.; Anchordoqui, L.A.; Di Valentino, E.; Pan, S.; Wu, Y.; Yang, W. Constraints from High-Precision Measurements of the Cosmic Microwave Background: The Case of Disintegrating Dark Matter with Λ or Dynamical Dark Energy. *arXiv* **2021**, arXiv:astro-ph.CO/2108.04188.
255. Blinov, N.; Krnjaic, G.; Li, S.W. Towards a Realistic Model of Dark Atoms to Resolve the Hubble Tension. *arXiv* **2021**, arXiv:hep-ph/2108.11386.
256. Galli, S.; Pogosian, L.; Jedamzik, K.; Balkenhol, L. Consistency of Planck, ACT and SPT constraints on magnetically assisted recombination and forecasts for future experiments. *arXiv* **2021**, arXiv:astro-ph.CO/2109.03816.
257. Liu, X.H.; Li, Z.H.; Qi, J.Z.; Zhang, X. Galaxy-Scale Test of General Relativity with Strong Gravitational Lensing. *arXiv* **2021**, arXiv:astro-ph.CO/2109.02291.
258. Hou, S.; Fan, X.L.; Zhu, Z.H. Constraining cosmological parameters from strong lensing with DECIGO and B-DECIGO sources. *Mon. Not. R. Astron. Soc.* **2021**, *507*, 761–771, doi:10.1093/mnras/stab2221.
259. Sola, J. Running vacuum interacting with dark matter or with running gravitational coupling. Phenomenological implications. *arXiv* **2021**, arXiv:gr-qc/2109.12086.
260. Cuesta, A.J.; Gómez, M.E.; Illana, J.I.; Masip, M. Cosmology of an Axion-Like Majoron. *arXiv* **2021**, arXiv:hep-ph/2109.07336.
261. González-López, M. Neutrino Masses and Hubble Tension via a Majoron in MFV. *arXiv* **2021**, arXiv:hep-ph/2110.15698.
262. Prat, J.; Hogan, C.; Chang, C.; Frieman, J. Vacuum Energy Density Measured from Cosmological Data. *arXiv* **2021**, arXiv:astro-ph.CO/2111.08151.
263. Joseph, A.; Saha, R. Dark energy with oscillatory tracking potential: Observational Constraints and Perturbative effects. *arXiv* **2021**, arXiv:astro-ph.CO/2110.00229.
264. Aghababaei, S.; Moradpour, H.; Vagenas, E.C. Hubble tension bounds the GUP and EUP parameters. *Eur. Phys. J. Plus* **2021**, *136*, doi:10.1140/epjp/s13360-021-02007-5.
265. Bansal, S.; Kim, J.H.; Kolda, C.; Low, M.; Tsai, Y. Mirror Twin Higgs Cosmology: Constraints and a Possible Resolution to the H_0 and S_8 Tensions. *arXiv* **2021**, arXiv:hep-ph/2110.04317.
266. Dialektopoulos, K.; Said, J.L.; Mifsud, J.; Sultana, J.; Adami, K.Z. Neural Network Reconstruction of Late-Time Cosmology and Null Tests. *arXiv* **2021**, arXiv:astro-ph.CO/2111.11462.
267. Alestas, G.; Camarena, D.; Di Valentino, E.; Kazantzidis, L.; Marra, V.; Nesseris, S.; Perivolaropoulos, L. Late-transition vs. smooth $H(z)$ deformation models for the resolution of the Hubble crisis. *arXiv* **2021**, arXiv:astro-ph.CO/2110.04336.
268. Parnovsky, S. Possible Modification of the Standard Cosmological Model to Resolve a Tension with Hubble Constant Values. *Ukr. J. Phys.* **2021**, *66*, 739. doi:10.15407/ujpe66.9.739.
269. Zhang, P.; D’Amico, G.; Senatore, L.; Zhao, C.; Cai, Y. BOSS Correlation Function Analysis from the Effective Field Theory of Large-Scale Structure. *arXiv* **2021**, arXiv:astro-ph.CO/2110.07539.
270. Hansen, S.H. Accelerated expansion induced by dark matter with two charges. *Mon. Not. R. Astron. Soc. Lett.* **2021**, *508*, 22–25, doi:10.1093/mnrasl/slab103.
271. Gariazzo, S.; Di Valentino, E.; Mena, O.; Nunes, R.C. Robustness of non-standard cosmologies solving the Hubble constant tension. *arXiv* **2021**, arXiv:astro-ph.CO/2111.03152.
272. Ruiz-Zapatero, J.; Stölzner, B.; Joachimi, B.; Asgari, M.; Bilicki, M.; Dvornik, A.; Giblin, B.; Heymans, C.; Hildebrandt, H.; Kannawadi, A.; et al. Geometry versus growth—Internal consistency of the flat model with KiDS-1000. *Astron. Astrophys.* **2021**, *655*, A11. doi:10.1051/0004-6361/202141350.
273. Cai, R.G.; Guo, Z.K.; Wang, S.J.; Yu, W.W.; Zhou, Y. A No-Go guide for the Hubble tension. *arXiv* **2021**, arXiv:astro-ph.CO/2107.13286.
274. Mehrabi, A.; Vazirnia, M. Non-parametric modeling of the cosmological data, base on the χ^2 distribution. *arXiv* **2021**, arXiv:astro-ph.CO/2107.11539.
275. Parnovsky, S.L. Bias of the Hubble constant value caused by errors in galactic distance indicators. *arXiv* **2021**, arXiv:astro-ph.CO/2109.09645.
276. Baldwin, D.; Schechter, P.L. A Malmquist-like bias in the inferred areas of diamond caustics and the resulting bias in inferred time delays for gravitationally lensed quasars. *arXiv* **2021**, arXiv:astro-ph.CO/2110.06378.
277. Huber, S.; Suyu, S.H.; Ghoshdastidar, D.; Taubenberger, S.; Bonvin, V.; Chan, J.H.H.; Kromer, M.; Noebauer, U.M.; Sim, S.A.; Leal-Taixé, L. HOLISMOKES—VII. Time-delay measurement of strongly lensed SNe Ia using machine learning. *arXiv* **2021**, arXiv:astro-ph.CO/2108.02789.

278. Mercier, C. A New Physics Would Explain What Looks Like an Irreconcilable Tension between the Values of Hubble Constants and Allows H_0 to Be Calculated Theoretically Several Ways. *J. Mod. Phys.* **2021**, *12*, 1656–1707. doi:10.4236/jmp.2021.1212098.
279. Ren, X.; Wong, T.H.T.; Cai, Y.F.; Saridakis, E.N. Data-driven reconstruction of the late-time cosmic acceleration with $f(T)$ gravity. *Phys. Dark Univ.* **2021**, *32*, 100812. <https://doi.org/10.1016/j.dark.2021.100812>.
280. Hryczuk, A.; Jodłowski, K. Self-interacting dark matter from late decays and the H_0 tension. *Phys. Rev. D* **2020**, *102*. doi:10.1103/physrevd.102.043024.
281. Di Valentino, E.; Mena, O.; Pan, S.; Visinelli, L.; Yang, W.; Melchiorri, A.; Mota, D.F.; Riess, A.G.; Silk, J. In the realm of the Hubble tension—A review of solutions. *Class. Quantum Gravity* **2021**, *38*, 153001, doi:10.1088/1361-6382/ac086d.
282. Perivolaropoulos, L.; Skara, F. Challenges for Λ CDM: An update. *arXiv* **2021**, arXiv:2105.05208.
283. Saridakis, E.N.; Lazkoz, R.; Salzano, V.; Vargas Moniz, P.; Capozziello, S.; Beltrán Jiménez, J.; De Laurentis, M.; Olmo, G.J.; Akrami, Y.; Bahamonde, S.; et al. Modified Gravity and Cosmology: An Update by the CANTATA Network. *arXiv* **2021**, arXiv:2105.12582.
284. Scolnic, D.M.; Jones, D.O.; Rest, A.; Pan, Y.C.; Chornock, R.; Foley, R.J.; Huber, M.E.; Kessler, R.; Narayan, G.; Riess, A.G.; et al. The Complete Light-curve Sample of Spectroscopically Confirmed SNe Ia from Pan-STARRS1 and Cosmological Constraints from the Combined Pantheon Sample. *Astrophys. J.* **2018**, *859*, 101, doi:10.3847/1538-4357/aab9bb.
285. Weinberg, S. *Cosmology*; Oxford University Press: Oxford, UK, 2008.
286. Guy, J.; Sullivan, M.; Conley, A.; Regnault, N.; Astier, P.; Balland, C.; Basa, S.; Carlberg, R.G.; Fouchez, D.; Hardin, D.; et al. The Supernova Legacy Survey 3-year sample: Type Ia supernovae photometric distances and cosmological constraints. *Astron. Astrophys.* **2010**, *523*, A7, doi:10.1051/0004-6361/201014468.
287. Chotard, N.; Gangler, E.; Aldering, G.; Antilogus, P.; Aragon, C.; Bailey, S.; Baltay, C.; Bongard, S.; Buton, C.; Canto, A.; et al. The reddening law of type Ia supernovae: Separating intrinsic variability from dust using equivalent widths. *Astron. Astrophys.* **2011**, *529*, L4, doi:10.1051/0004-6361/201116723.
288. Kenworthy, W.D.; Scolnic, D.; Riess, A. The Local Perspective on the Hubble Tension: Local Structure Does Not Impact Measurement of the Hubble Constant. *Astrophys. J.* **2019**, *875*, 145, doi:10.3847/1538-4357/ab0ebf.
289. Deng, H.K.; Wei, H. Null signal for the cosmic anisotropy in the Pantheon supernovae data. *Eur. Phys. J. C* **2018**, *78*, 755, doi:10.1140/epjc/s10052-018-6159-4.
290. Akarsu, Ö.; Kumar, S.; Sharma, S.; Tedesco, L. Constraints on a Bianchi type I spacetime extension of the standard Λ CDM model. *Phys. Rev. D* **2019**, *100*, 023532, doi:10.1103/PhysRevD.100.023532.
291. Shafieloo, A.; L’Huillier, B.; Starobinsky, A.A. Falsifying Λ CDM : Model-independent tests of the concordance model with eBOSS DR14Q and Pantheon. *Phys. Rev. D* **2018**, *98*, 083526, doi:10.1103/PhysRevD.98.083526.
292. Hossienkhani, H.; Azimi, N.; Zarei, Z. Probing the anisotropy effects on the CPL parametrizations from light-curve SNIa, BAO and OHD datasets. *Int. J. Geom. Methods Mod. Phys.* **2019**, *16*, 1950177–L5. doi:10.1142/S0219887819501779.
293. L’Huillier, B.; Shafieloo, A.; Linder, E.V.; Kim, A.G. Model independent expansion history from supernovae: Cosmology versus systematics. *Mon. Not. R. Astron. Soc.* **2019**, *485*, 2783–2790, doi:10.1093/mnras/stz589.
294. Lusso, E.; Piedipalumbo, E.; Risaliti, G.; Paolillo, M.; Bisogni, S.; Nardini, E.; Amati, L. Tension with the flat Λ CDM model from a high-redshift Hubble diagram of supernovae, quasars, and gamma-ray bursts. *Astron. Astrophys.* **2019**, *628*, L4, doi:10.1051/0004-6361/201936223.
295. Ma, Y.B.; Cao, S.; Zhang, J.; Qi, J.; Liu, T.; Liu, Y.; Geng, S. Testing Cosmic Opacity with the Combination of Strongly Lensed and Unlensed Supernova Ia. *Astrophys. J.* **2019**, *887*, 163, doi:10.3847/1538-4357/ab50c4.
296. Sadri, E. Observational constraints on interacting Tsallis holographic dark energy model. *Eur. Phys. J. C* **2019**, *79*, 762, doi:10.1140/epjc/s10052-019-7263-9.
297. Sadri, E.; Khurshudyan, M. An interacting new holographic dark energy model: Observational constraints. *Int. J. Mod. Phys. D* **2019**, *28*, 1950152–26, doi:10.1142/S0218271819501529.
298. Wagner, J.; Meyer, S. Generalized model-independent characterization of strong gravitational lenses V: reconstructing the lensing distance ratio by supernovae for a general Friedmann universe. *Mon. Not. R. Astron. Soc.* **2019**, *490*, 1913–1927, doi:10.1093/mnras/stz2717.
299. Zhai, Z.; Wang, Y. Robust and model-independent cosmological constraints from distance measurements. *J. Cosmol. Astropart. Phys.* **2019**, *2019*, 005, doi:10.1088/1475-7516/2019/07/005.
300. Zhao, D.; Zhou, Y.; Chang, Z. Anisotropy of the Universe via the Pantheon supernovae sample revisited. *Mon. Not. R. Astron. Soc.* **2019**, *486*, 5679–5689, doi:10.1093/mnras/stz1259.
301. Abdullah, M.H.; Klypin, A.; Wilson, G. Cosmological Constraints on Ω_m and σ_8 from Cluster Abundances Using the GalWCat19 Optical-spectroscopic SDSS Catalog. *Astrophys. J.* **2020**, *901*, 90, doi:10.3847/1538-4357/aba619.
302. Al Mamon, A.; Saha, S. The logotropic dark fluid: Observational and thermodynamic constraints. *Int. J. Mod. Phys. D* **2020**, *29*, 2050097, doi:10.1142/S0218271820500972.
303. Anagnostopoulos, F.K.; Basilakos, S.; Saridakis, E.N. Observational constraints on Barrow holographic dark energy. *Eur. Phys. J. C* **2020**, *80*, 826, doi:10.1140/epjc/s10052-020-8360-5.

304. Brout, D.; Hinton, S.R.; Scolnic, D. Binning is Sinning (Supernova Version): The Impact of Self-calibration in Cosmological Analyses with Type Ia Supernovae. *Astrophys. J. Lett.* **2021**, *912*, L26, doi:10.3847/2041-8213/abf4db.
305. Cai, R.G.; Ding, J.F.; Guo, Z.K.; Wang, S.J.; Yu, W.W. Do the observational data favor a local void? *Phys. Rev. D* **2021**, *103*, 123539, doi:10.1103/PhysRevD.103.123539.
306. Chang, Z.; Zhao, D.; Zhou, Y. Constraining the anisotropy of the Universe with the Pantheon supernovae sample. *Chin. Phys. C* **2019**, *43*, 125102, doi:10.1088/1674-1137/43/12/125102.
307. D'Amico, G.; Senatore, L.; Zhang, P. Limits on Λ CDM from the EFTofLSS with the PyBird code. *J. Cosmol. Astropart. Phys.* **2021**, *2021*, 006, doi:10.1088/1475-7516/2021/01/006.
308. Di Valentino, E.; Gariazzo, S.; Mena, O.; Vagnozzi, S. Soundness of dark energy properties. *J. Cosmol. Astropart. Phys.* **2020**, *2020*, 045, doi:10.1088/1475-7516/2020/07/045.
309. Gao, C.; Chen, Y.; Zheng, J. Investigating the relationship between cosmic curvature and dark energy models with the latest supernova sample. *Res. Astron. Astrophys.* **2020**, *20*, 151, doi:10.1088/1674-4527/20/9/151.
310. Garcia-Quintero, C.; Ishak, M.; Ning, O. Current constraints on deviations from General Relativity using binning in redshift and scale. *J. Cosmol. Astropart. Phys.* **2020**, *2020*, 018, doi:10.1088/1475-7516/2020/12/018.
311. Geng, S.; Cao, S.; Liu, T.; Biesiada, M.; Qi, J.; Liu, Y.; Zhu, Z.H. Gravitational-wave Constraints on the Cosmic Opacity at $z \sim 5$: Forecast from Space Gravitational-wave Antenna DECIGO. *Astrophys. J.* **2020**, *905*, 54. doi:10.3847/1538-4357/abc076.
312. Ghaffari, S.; Sadri, E.; Ziaie, A.H. Tsallis holographic dark energy in fractal universe. *Mod. Phys. Lett. A* **2020**, *35*, 2050107, doi:10.1142/S0217732320501072.
313. Hu, J.P.; Wang, Y.Y.; Wang, F.Y. Testing cosmic anisotropy with Pantheon sample and quasars at high redshifts. *Astron. Astrophys.* **2020**, *643*, A93, doi:10.1051/0004-6361/202038541.
314. Huang, Z. Supernova Magnitude Evolution and Page Approximation. *Astrophys. J. Lett.* **2020**, *892*, L28, doi:10.3847/2041-8213/ab8011.
315. Çamlıbel, A.K.; Semiz, İ.; Feyizoğlu, M.A. Pantheon update on a model-independent analysis of cosmological supernova data. *Class. Quantum Gravity* **2020**, *37*, 235001, doi:10.1088/1361-6382/abba48.
316. Liao, K.; Shafieloo, A.; Keeley, R.E.; Linder, E.V. Determining Model-independent H_0 and Consistency Tests. *Astrophys. J. Lett.* **2020**, *895*, L29, doi:10.3847/2041-8213/ab8dbb.
317. Koo, H.; Shafieloo, A.; Keeley, R.E.; L'Huillier, B. Model selection and parameter estimation using the iterative smoothing method. *J. Cosmol. Astropart. Phys.* **2021**, *2021*, 034, doi:10.1088/1475-7516/2021/03/034.
318. Li, E.K.; Du, M.; Xu, L. General cosmography model with spatial curvature. *Mon. Not. R. Astron. Soc.* **2020**, *491*, 4960–4972, doi:10.1093/mnras/stz3308.
319. Luković, V.V.; Haridasu, B.S.; Vittorio, N. Exploring the evidence for a large local void with supernovae Ia data. *Mon. Not. R. Astron. Soc.* **2020**, *491*, 2075–2087, doi:10.1093/mnras/stz3070.
320. Luongo, O.; Muccino, M. Kinematic constraints beyond $z \simeq 0$ using calibrated GRB correlations. *Astron. Astrophys.* **2020**, *641*, A174, doi:10.1051/0004-6361/202038264.
321. Micheletti, S.M.R. Quintessence and tachyon dark energy in interaction with dark matter: Observational constraints and model selection. *Int. J. Mod. Phys. D* **2020**, *29*, 2050057, doi:10.1142/S0218271820500571.
322. Mishra, R.K.; Dua, H. Phase transition of cosmological model with statistical techniques. *Astrophys. Space Sci.* **2020**, *365*, 131. doi:10.1007/s10509-020-03843-0.
323. Odintsov, S.D.; Sáez-Chillón Gómez, D.; Sharov, G.S. Analyzing the H_0 tension in $F(R)$ gravity models. *Nucl. Phys. B* **2021**, *966*, 115377, doi:10.1016/j.nuclphysb.2021.115377.
324. Prasad, R.; Singh, M.; Yadav, A.K.; Beesham, A. An exact solution of the observable universe in Bianchi V space-time. *Int. J. Mod. Phys. A* **2021**, *36*, 2150044, doi:10.1142/S0217751X21500445.
325. Rezaei, M.; Pour-Ojaghi, S.; Malekjani, M. A Cosmography Approach to Dark Energy Cosmologies: New Constraints Using the Hubble Diagrams of Supernovae, Quasars, and Gamma-Ray Bursts. *Astrophys. J.* **2020**, *900*, 70, doi:10.3847/1538-4357/aba517.
326. Ringermacher, H.I.; Mead, L.R. Reaffirmation of cosmological oscillations in the scale factor from the Pantheon compilation of 1048 Type Ia supernovae. *Mon. Not. R. Astron. Soc.* **2020**, *494*, 2158–2165, doi:10.1093/mnras/staa872.
327. Tang, L.; Li, X.; Lin, H.N.; Liu, L. Model-independently Calibrating the Luminosity Correlations of Gamma-Ray Bursts Using Deep Learning. *Astrophys. J.* **2021**, *907*, 121, doi:10.3847/1538-4357/abcd92.
328. Wang, K.; Chen, L. Constraints on Newton's constant from cosmological observations. *Eur. Phys. J. C* **2020**, *80*, 570, doi:10.1140/epjc/s10052-020-8137-x.
329. Wei, J.J.; Melia, F. Cosmology-independent Estimate of the Hubble Constant and Spatial Curvature using Time-delay Lenses and Quasars. *Astrophys. J.* **2020**, *897*, 127, doi:10.3847/1538-4357/ab959b.
330. Zhang, X.; Huang, Q.G. Measuring H_0 from low- z datasets. *Sci. China Phys. Mech. Astron.* **2020**, *63*, 290402, doi:10.1007/s11433-019-1504-8.

331. Baxter, E.J.; Sherwin, B.D. Determining the Hubble constant without the sound horizon scale: measurements from CMB lensing. *Mon. Not. R. Astron. Soc.* **2021**, *501*, 1823–1835, doi:10.1093/mnras/staa3706.
332. Camarena, D.; Marra, V. On the use of the local prior on the absolute magnitude of Type Ia supernovae in cosmological inference. *Mon. Not. R. Astron. Soc.* **2021**, *504*, 5164–5171, doi:10.1093/mnras/stab1200.
333. Cao, S.; Ryan, J.; Ratra, B. Using Pantheon and DES supernova, baryon acoustic oscillation, and Hubble parameter data to constrain the Hubble constant, dark energy dynamics, and spatial curvature. *Mon. Not. R. Astron. Soc.* **2021**, *504*, 300–310, doi:10.1093/mnras/stab942.
334. Heisenberg, L.; Bartelmann, M.; Brandenberger, R.; Refregier, A. Model independent analysis of supernova data, dark energy, trans-Planckian censorship and the swampland. *Phys. Lett. B* **2021**, *812*, 135990, doi:10.1016/j.physletb.2020.135990.
335. Jesus, J.F.; Valentim, R.; Moraes, P.H.R.S.; Malheiro, M. Kinematic constraints on spatial curvature from supernovae Ia and cosmic chronometers. *Mon. Not. R. Astron. Soc.* **2021**, *500*, 2227–2235, doi:10.1093/mnras/staa3426.
336. Lee, S. Constraints on the time variation of the speed of light using Pantheon dataset. *arXiv* **2021**, arXiv:2101.09862.
337. Montiel, A.; Cabrera, J.I.; Hidalgo, J.C. Improving sampling and calibration of gamma-ray bursts as distance indicators. *Mon. Not. R. Astron. Soc.* **2021**, *501*, 3515–3526. doi:10.1093/mnras/staa3926.
338. Mukherjee, P.; Banerjee, N. Non-parametric reconstruction of the cosmological jerk parameter. *Eur. Phys. J. C* **2021**, *81*, 36, doi:10.1140/epjc/s10052-021-08830-5.
339. Wang, G.J.; Ma, X.J.; Xia, J.Q. Machine learning the cosmic curvature in a model-independent way. *Mon. Not. R. Astron. Soc.* **2021**, *501*, 5714–5722, doi:10.1093/mnras/staa4044.
340. Torrado, J.; Lewis, A. Cobaya: Code for Bayesian Analysis of hierarchical physical models. *JCAP* **2021**, *05*, 057, doi:10.1088/1475-7516/2021/05/057.
341. Sharov, G.S.; Vasiliev, V.O. How predictions of cosmological models depend on Hubble parameter data sets. *Math. Model. Geom.* **2018**, *6*, doi:10.26456/mmg/2018-611.
342. Eisenstein, D.J.; Zehavi, I.; Hogg, D.W.; Scoccimarro, R.; Blanton, M.R.; Nichol, R.C.; Scranton, R.; Seo, H.J.; Tegmark, M.; Zheng, Z.; et al. Detection of the Baryon Acoustic Peak in the Large-Scale Correlation Function of SDSS Luminous Red Galaxies. *Astrophys. J.* **2005**, *633*, 560–574, doi:10.1086/466512.
343. Cuceu, A.; Farr, J.; Lemos, P.; Font-Ribera, A. Baryon Acoustic Oscillations and the Hubble constant: past, present and future. *J. Cosmol. Astropart. Phys.* **2019**, *2019*, 044, doi:10.1088/1475-7516/2019/10/044.
344. Aubourg, É.; Bailey, S.; Bautista, J.E.; Beutler, F.; Bhardwaj, V.; Bizyaev, D.; Blanton, M.; Blomqvist, M.; Bolton, A.S.; Bovy, J.; et al. Cosmological implications of baryon acoustic oscillation measurements. *Phys. Rev. D* **2015**, *92*, 123516, doi:10.1103/PhysRevD.92.123516.
345. Singal, J.; Petrosian, V.; Lawrence, A.; Stawarz, Ł. On the Radio and Optical Luminosity Evolution of Quasars. *Astrophys. J.* **2011**, *743*, 104, doi:10.1088/0004-637X/743/2/104.
346. Singal, J.; Petrosian, V.; Stawarz, Ł.; Lawrence, A. The Radio and Optical Luminosity Evolution of Quasars. II. The SDSS Sample. *Astrophys. J.* **2013**, *764*, 43, doi:10.1088/0004-637X/764/1/43.
347. Petrosian, V.; Kitanidis, E.; Kocevski, D. Cosmological Evolution of Long Gamma-Ray Bursts and the Star Formation Rate. *Astrophys. J.* **2015**, *806*, 44, doi:10.1088/0004-637X/806/1/44.
348. Lloyd, N.M.; Petrosian, V. Synchrotron Radiation as the Source of Gamma-Ray Burst Spectra. *Astrophys. J.* **2000**, *543*, 722–732, doi:10.1086/317125.
349. Dainotti, M.G.; Petrosian, V.; Bowden, L. Cosmological Evolution of the Formation Rate of Short Gamma-Ray Bursts with and without Extended Emission. *Astrophys. J.* **2021**, *914*, L40. doi:10.3847/2041-8213/abf5e4.
350. Atteia, J.L. Gamma-ray bursts: towards a standard candle luminosity. *Astron. Astrophys.* **1997**, *328*, L21–L24.
351. Atteia, J.L. Choosing a measure of GRB brightness that approaches a standard candle. In *Gamma-Ray Bursts, 4th Huntsville Symposium*; American Institute of Physics Conference Series; Meegan, C.A., Preece, R.D., Koshut, T.M., Eds.; American Institute of Physics: College Park, MD, USA, 1998; Volume 428, pp. 92–96. doi:10.1063/1.55422.
352. De Simone, B.; Nielson, V.; Rinaldi, E.; Dainotti, M.G. A new perspective on cosmology through Supernovae Ia and Gamma Ray Bursts. *arXiv* **2021**, arXiv:astro-ph.CO/2110.11930.
353. Cao, S.; Dainotti, M.; Ratra, B. Standardizing Platinum Dainotti-correlated gamma-ray bursts, and using them with standardized Amati-correlated gamma-ray bursts to constrain cosmological model parameters. *arXiv* **2022**, arXiv:astro-ph.CO/2201.0524.
354. Cao, S.; Khadka, N.; Ratra, B. Standardizing Dainotti-correlated gamma-ray bursts, and using them with standardized Amati-correlated gamma-ray bursts to constrain cosmological model parameters. *MNRAS* **2022**, doi:10.1093/mnras/stab3559.
355. Efron, B.; Petrosian, V. A simple test of independence for truncated data with applications to redshift surveys. *Astrophys. J.* **1992**, *399*, 345–352.
356. D’Agostini, G. A multidimensional unfolding method based on Bayes’ theorem. *Nucl. Instrum. Methods Phys. Res. A* **1995**, *362*, 487–498. doi:10.1016/0168-9002(95)00274-X.

357. Conley, A.; Guy, J.; Sullivan, M.; Regnault, N.; Astier, P.; Ballew, C.; Basa, S.; Carlberg, R.G.; Fouchez, D.; Hardin, D.; et al. Supernova constraints and systematic uncertainties from the first three years of the supernova legacy survey. *Astrophys. J. Suppl. Ser.* **2010**, *192*, 1. doi:10.1088/0067-0049/192/1/1.
358. Betoule, M.; Kessler, R.; Guy, J.; Mosser, J.; Hardin, D.; Biswas, R.; Astier, P.; El-Hage, P.; Konig, M.; Kuhlmann, S.; et al. Improved cosmological constraints from a joint analysis of the SDSS-II and SNLS supernova samples. *Astron. Astrophys.* **2014**, *568*, A22. doi:10.1051/0004-6361/201423413.
359. Bargiacchi, G., Benetti, M., Capozziello, S., Lusso, E., Risaliti, G. & Signorini, M. Quasar cosmology: dark energy evolution and spatial curvature. arXiv 2021, arXiv:2111.02420.
360. Bargiacchi, G., Risaliti, G., Benetti, M., Capozziello, S., Lusso, E., Saccardi, A. & Signorini, M. Cosmography by orthogonalized logarithmic polynomials. *Astronomy & Astrophysics*. **649** pp. A65 (2021,5), <http://dx.doi.org/10.1051/0004-6361/202140386>
361. Dainotti, M.G.; Bogdan, M.; Narendra, A.; Gibson, S.J.; Miasojedow, B.; Liodakis, I.; Pollo, A.; Nelson, T.; Wozniak, K.; Nguyen, Z.; et al. Predicting the Redshift of γ -Ray-loud AGNs Using Supervised Machine Learning. *Astrophys. J.* **2021**. *920*, 118. doi:10.3847/1538-4357/ac1748.
362. Dainotti, M.; Petrosian, V.; Bogdan, M.; Miasojedow, B.; Nagataki, S.; Hastie, T.; Nuyngen, Z.; Gilda, S.; Hernández, X.; Krol, D. Gamma-ray Bursts as distance indicators through a machine learning approach. *arXiv* **2019**, arXiv:1907.05074.
363. Childress, M.; Aldering, G.; Antilogus, P.; Aragon, C.; Bailey, S.; Baltay, C.; Bongard, S.; Buton, C.; Canto, A.; Cellier-Holzem, F.; et al. Host Galaxies of Type Ia Supernovae from the Nearby Supernova Factory. *Astrophys. J.* **2013**, *770*, 107, doi:10.1088/0004-637X/770/2/107.
364. Nicolas, N.; Rigault, M.; Copin, Y.; Graziani, R.; Aldering, G.; Briday, M.; Kim, Y.L.; Nordin, J.; Perlmutter, S.; Smith, M. Redshift evolution of the underlying type Ia supernova stretch distribution. *Astron. Astrophys.* **2021**, *649*, A74, doi:10.1051/0004-6361/202038447.
365. Brout, D.; Taylor, G.; Scolnic, D.; Wood, C.M.; Rose, B.M.; Vincenzi, M.; Dwomoh, A.; Lidman, C.; Riess, A.; Ali, N.; et al. The Pantheon+ Analysis: SuperCal-Fragilistic Cross Calibration, Retrained SALT2 Light Curve Model, and Calibration Systematic Uncertainty. *arXiv* **2021**, arXiv:astro-ph.CO/2112.03864.
366. Carr, A.; Davis, T.M.; Scolnic, D.; Said, K.; Brout, D.; Peterson, E.R.; Kessler, R. The Pantheon+ Analysis: Improving the Redshifts and Peculiar Velocities of Type Ia Supernovae Used in Cosmological Analyses. *arXiv* **2021**, arXiv:astro-ph.CO/2112.01471.
367. Popovic, B.; Brout, D.; Kessler, R.; Scolnic, D. The Pantheon+ Analysis: Forward-Modeling the Dust and Intrinsic Colour Distributions of Type Ia Supernovae, and Quantifying their Impact on Cosmological Inferences. *arXiv* **2021**, arXiv:astro-ph.CO/2112.04456.
368. Scolnic, D.; Brout, D.; Carr, A.; Riess, A.G.; Davis, T.M.; Dwomoh, A.; Jones, D.O.; Ali, N.; Charvu, P.; Chen, R.; et al. The Pantheon+ Type Ia Supernova Sample: The Full Dataset and Light-Curve Release. *arXiv* **2021**, arXiv:astro-ph.CO/2112.03863.
369. Riess, A.G.; Yuan, W.; Macri, L.M.; Scolnic, D.; Brout, D.; Casertano, S.; Jones, D.O.; Murakami, Y.; Breuval, L.; Brink, T.G.; et al. A Comprehensive Measurement of the Local Value of the Hubble Constant with 1 km/s/Mpc Uncertainty from the Hubble Space Telescope and the SH0ES Team. *arXiv* **2022**, arXiv:astro-ph.CO/2112.04510.
370. Damour, T.; Nordtvedt, K. Tensor-scalar cosmological models and their relaxation toward general relativity. *Phys. Rev. D* **1993**, *48*, 3436–3450. doi:10.1103/PhysRevD.48.3436.
371. Damour, T.; Polyakov, A.M. The string dilation and a least coupling principle. *Nucl. Phys. B* **1994**, *423*, 532–558, doi:10.1016/0550-3213(94)90143-0.
372. Damour, T. Gravitation, experiment and cosmology. Les Houches Summer School on Gravitation and Quantizations, Session 57. *arXiv* **1996**, arXiv:gr-qc/gr-qc/9606079.
373. Boisseau, B.; Esposito-Farèse, G.; Polarski, D.; Starobinsky, A.A. Reconstruction of a Scalar-Tensor Theory of Gravity in an Accelerating Universe. *Phys. Rev. Lett.* **2000**, *85*, 2236–2239, doi:10.1103/PhysRevLett.85.2236.
374. Esposito-Farèse, G.; Polarski, D. Scalar-tensor gravity in an accelerating universe. *Phys. Rev. D* **2001**, *63*, 063504, doi:10.1103/PhysRevD.63.063504.
375. Jordan, P. *Schwerkraft und Weltall: Grundlagen der theoretischen Kosmologie*; Die Wissenschaft: Braunschweig, Germany, 1955.
376. Fierz, M. On the physical interpretation of P. Jordan's extended theory of gravitation. *Helv. Phys. Acta* **1956**, *29*, 128–134.
377. Brans, C.; Dicke, R.H. Mach's Principle and a Relativistic Theory of Gravitation. *Phys. Rev.* **1961**, *124*, 925–935. doi:10.1103/PhysRev.124.925.
378. Singh, C.P.; Peracaula, J.S. Friedmann cosmology with decaying vacuum density in Brans–Dicke theory. *arXiv* **2021**, arXiv:gr-qc/2110.12411.
379. Catena, R.; Fornengo, N.; Masiero, A.; Pietroni, M.; Rosati, F. Dark matter relic abundance and scalar-tensor dark energy. *Phys. Rev. D* **2004**, *70*, 063519, doi:10.1103/PhysRevD.70.063519.
380. Kazantzidis, L.; Perivolaropoulos, L. Hints of a local matter underdensity or modified gravity in the low z Pantheon data. *Phys. Rev. D* **2020**, *102*, 023520, doi:10.1103/PhysRevD.102.023520.
381. Capozziello, S.; de Laurentis, M. Extended Theories of Gravity. *Physics Reports* **2011**, *509*, 167–321, doi:10.1016/j.physrep.2011.09.003.
382. Hu, W.; Sawicki, I. Models of $f(R)$ cosmic acceleration that evade solar system tests. *Phys. Rev. D* **2007**, *76*, 064004, doi:10.1103/PhysRevD.76.064004.
383. Starobinsky, A.A. Disappearing cosmological constant in $f(R)$ gravity. *Soviet Journal of Experimental and Theoretical Physics Letters* **2007**, *86*, 157–163, doi:10.1134/S0021364007150027.

384. Amendola, L.; Gannouji, R.; Polarski, D.; Tsujikawa, S. Conditions for the cosmological viability of $f(R)$ dark energy models. *Phys. Rev. D* **2007**, *75*, 083504, doi:10.1103/PhysRevD.75.083504.
385. Tsujikawa, S. Observational signatures of $f(R)$ dark energy models that satisfy cosmological and local gravity constraints. *Phys. Rev. D* **2008**, *77*, 023507, doi:10.1103/PhysRevD.77.023507.
386. Martinelli, M.; Melchiorri, A.; Amendola, L. Cosmological constraints on the Hu-Sawicki modified gravity scenario. *Phys. Rev. D* **2009**, *79*, 123516, doi:10.1103/PhysRevD.79.123516.
387. Burrage, C.; Sakstein, J. Tests of chameleon gravity. *Living Rev. Relativ.* **2018**, *21*, 1, doi:10.1007/s41114-018-0011-x.
388. Liu, T.; Zhang, X.; Zhao, W. Constraining $f(R)$ gravity in solar system, cosmology and binary pulsar systems. *Phys. Lett. B* **2018**, *777*, 286–293, doi:10.1016/j.physletb.2017.12.051.
389. Linde, A.D. Chaotic inflation. *Phys. Lett. B* **1983**, *129*, 177–181. doi:10.1016/0370-2693(83)90837-7.
390. Riotto, A. Inflation and the Theory of Cosmological Perturbations. *ICTP Lect. Notes Ser.* **2003**, *14*, 317–413.